A COMPARATIVE STUDY BETWEEN TWO-DIMENSIONAL AND AXISYMMETRICAL TURBULENT BOUNDARY LAYERS WITH RESPECT TO THE LAW OF THE WALL, THE VELOCITY DEFECT LAW, AND THE AVERAGE SHEAR COEFFICIENT

Joseph Hulet

A Dissertation

in

The Faculty

of

Engineering

Presented in Partial Fulfillment of the Requirements

for the Degree of Master of Engineering at

Concordia University

Montreal, Quebec, Canada

April 1981

ABSTRACT

A COMPARATIVE STUDY BETWEEN TWO-DIMENSIONAL AND AXISYMMETRICAL TURBULENT BOUNDARY LAYERS WITH RESPECT TO THE LAW OF THE WALL, THE VELOCITY DEFECT LAW, AND THE AVERAGE SHEAR COEFFICIENT

Joseph Hulet

The objective of this dissertation is to enable selection of the optimum method for solution of axisymmetrical boundary layer problems for turbulent flow with respect to the law of the wall, the velocity defect law, and the average shear coefficient. No consensus presently exists on the appropriate similarity laws for axisymmetrical flow. The competing axisymmetrical hypotheses previously proposed by various authors are analyzed and compared with the accepted classical two-dimensional similarity laws. Each similarity law hypothesis is examined with respect to its accuracy of prediction in comparision to published experimental results, its range of application, and the constraints existing on its respective utilization.

An experimental and theoretical analysis of axisymmetrical average shear coefficients for a circular thread subjected to a steady jet of water discharging from a conical annular nozzle is performed. The experimentally based axisymmetrical shear coefficients are compared with theoretical average shear coefficients derived utilizing the classical two-dimensional equations and an axisymmetrical approximation approach. The experimentally based average jet velocity at the end of the conical annulus is compared with theoretical values derived using an integral momentum method and a macroscopic energy balance method. The various parameters affecting the conical annular nozzle performance are discussed.

ACKNOWLEDGEMENTS

The author wishes to express his appreciation to Dr. M.P. duPlessis for the initiation of this project, Dr. S. Katz for his guidance in the preparation of the final version of this dissertation, and Dr. T.S. Sankar for his aid and patience which enabled its completion.

TABLE OF CONTENTS

		PAGE
ABSTRACT		i
ACKNOWLEDGEMENTS		ii
LIST OF FIGURES		vii
LIST OF TABLES		x
NOMENCLATURE		xi
INTRODUCTION		xvi
CHAPTER 1 - THE LAW OF THE WALL		
1.1.0	INTRODUCTION	1
1.1.1	Literature Search for Six Competing Hypotheses	2
1.2.0	DERIVATION OF COMPETING HYPOTHESES	6
1.2.1	Derivation of Planar Hypothesis	6
	1.2.1.a Derivation of Mixing Length	9
	1.2.1.b Two-Dimensional Law of the Wall	12
	1.2.1.c Comparison of Sublayer and Transition Region Equations	13
	1.2.1.d Van Driest's Relation	17
1.2.2	Axisymmetrical Equations of Motion	19
1.2.3	Derivation of Rao's Method	19
1.2.4	Derivation of Richmond's Streamline Method	21
1.2.5	Derivation of the Local Similarity Method	22
1.3.0	DISCUSSION OF COMPETING HYPOTHESES	23
1.3.1	Two-Dimensional Hypothesis	23
1.3.2	Richmond's Streamline Hypothesis	24
1.3.3	Rao's Hypothesis	26

PAGE

1.3.3.a Validity of Rao's Hypothesis for Transpiration Flow..... 27

1.3.4 Local Similarity Hypothesis..... 28

1.3.5 Derivative Hypothesis..... 30

1.3.6 Comparison of Competing Hypotheses with Experimental Results..... 30

1.4.0 EFFECTS OF TRANSVERSE CURVATURE..... 33

1.4.1 Influence of Wall Law..... 33

1.4.2 Relaminarizetion..... 35

1.4.3 Variation in the Viscous Damping Constant..... 37

1.4.4 Reduction in Turbulent Eddies Size..... 40

1.4.5 Intensity of Turbulence..... 41

1.5.0 CONCLUSIONS..... 42

CHAPTER 2 THE VELOCITY DEFECT LAW AND THE LAW OF THE WAKE

2.1.0 INTRODUCTION..... 46

2.2.0 DISCUSSION OF COMPETING HYPOTHESES..... 48

2.2.1 Two-Dimensional Velocity Defect Law..... 48

2.2.1.a Chin's Application..... 52

2.2.2 Yu's Hypothesis..... 53

2.2.3 Willmarth and Yang's Hypothesis 55

2.2.3.a Willmarth et al's Application..... 57

2.2.3.b Afzal and Narasimha's Application..... 57

2.2.3.c Afzal and Singh's Application..... 62

2.2.4 Rao and Keshaven's Hypothesis..... 64

2.3.0 AXISYMMETRIC WAKE..... 66

		PAGE
2.3.1	Existence of Axisymmetrical Wake	66
2.3.2	Negative Wake and Marginal Profiles	71
2.4.0	ALTERNATE OUTER LAYER VELOCITY EQUATION	72
2.5.0	CONCLUSIONS	76
CHAPTER 3	COMPARISON OF EXPERIMENTAL AND THEORETICAL TURBULENT SHEAR COEFFICIENTS AND AVERAGE CONICAL ANNULUS EXIT VELOCITY	
3.1.0	INTRODUCTION	81
3.1.1	Fundamentals of Shuttleless Jet Loom Operation With Conical Annular Nozzles	82
3.1.2	Literature Search for Previous Work	84
	3.1.2.a Review on Flow From a Conical Annulus	84
	3.1.2.b Review on Experimental Data for Flow Along Cylinders	85
3.2.0	EQUATION FORMULATION	87
3.2.1	Average Exit Velocity From an Annulus and Average Shear Coefficient Along a Circular Cylinder Using Experimental Data	87
3.2.2	White's Axisymmetric Shear Coefficients	89
3.2.3	Two Theoretical Methods for Calculation of Average Exit Velocity at the End of a Conical Annulus	91
	3.2.3.a Method 1 - Based on Integral Momentum Equations.	91
	3.2.3.b Method 2 - Based on Head Loss Equations	93
3.3.0	EXPERIMENTAL INVESTIGATION	95
3.3.1	Experimental Apparatus	95
3.3.2	Experimental Procedure	96
3.4.0	EXPERIMENTAL RESULTS	97
3.4.1	Comparison of Experimental and Theoretical Results	97

PAGE

3.5.0 DISCUSSION OF VARIOUS PARAMETERS AFFECTING NOZZLE PERFORMANCE 108

3.5.1 Creation of an Air Pocket 108

3.5.1.a Effect of Nozzle Angle 108

3.5.1.b Effect of Water Vortices and Air Pocket Shape ... 110

3.5.2 Entrainment of Air 110

3.5.2.a Effect of Nozzle Protrusion 111

3.5.3 Choice of Co-ordinate Axis 111

3.6.0 CONCLUSIONS AND SUGGESTIONS FOR FURTHER WORK 113

3.6.1 Conclusions 113

3.6.2 Suggestions for Further Work 114

GENERAL CONCLUSIONS 115

BIBLIOGRAPHY 118

APPENDIX A Calculation of Angle α 123

APPENDIX B Calculation of Clearance c 124

APPENDIX C Calculation of Hydraulic Diameter D_H 125

LIST OF FIGURES

FIGURE		PAGE
	CHAPTER 1	
1.1	Notation for Mixing Length Theory	11
1.2	Graph of y^+ versus ℓ^+ (Two-Dimensional)	15
1.3	Graph of $\overline{u^+}$ versus ℓ^+ (Two-Dimensional)	16
1.4	Definition Sketch for Thick Boundary Layer Along Cylinder	19
1.5	Comparison of Streamline and Rao's Hypotheses (Ref. 19)	25
1.6	Mean Velocity Profiles for Competing Hypotheses (Ref. 23)	25
1.7	Mean Velocity Profiles for Competing Hypotheses (Ref. 9).	31
1.8	Mean Velocity Profiles for Competing Hypotheses (Ref. 9).	31
1.9	Velocity Profiles for Two Cylinders (Ref. 35)	34
1.10	Influence of Transverse Curvature on the Law of the Wall (Ref. 24)	34
1.11	Graph of A^+ versus $-\{\partial\tau^+/\partial y^+\}$ (Ref. 18)	39
1.12	Comparison of Mean Velocity Profiles (Ref. 17)	41
	CHAPTER 2	
2.1	Mean Velocity Distribution (Ref. 46)	51
2.2	Velocity Defect Law Plot (Ref. 46)	51
2.3	Velocity Defect Law Plot (Ref. 47)	52
2.4	Velocity Defect Law Plot (Ref. 11)	54
2.5	Velocity Defect Law Plot (Ref. 10)	54
2.6	Velocity Defect Law Plot (Ref. 10)	56
2.7	Velocity Defect Law Plot (Ref. 10)	56
2.8	Influence of Transverse Curvature (Ref. 14)	58
2.9	Velocity Defect Law Plot (Ref. 14)	58

FIGURE		PAGE
2.10	Velocity Defect Law Plot (Ref. 12).....	60
2.11	Velocity Defect Law Plot (Ref. 12).....	60
2.12	Velocity Defect Law Plot (Ref. 12).....	61
2.13	Velocity Defect Additive Term (Ref. 12).....	61
2.14	Velocity Defect Law Plot (Ref. 13).....	63
2.15	Velocity Defect Additive Term (Ref. 13).....	63
2.16	Velocity Defect versus r^* (Ref. 20).....	65
2.17	Velocity Defect versus r^* (Ref. 20).....	65
2.18	Profile Parameter II versus r^* (Ref. 46).....	67
2.19	Mean Velocity Showing Wake (Ref. 46).....	67
2.20	Velocity Profile Comparison (Ref. 35).....	70
2.21	Marginal Values r^* versus R_a.....	70
2.22	Critical R_θ versus R_a.....	73
2.23	Radial Distance at Which Outer Region Departs from the Logarithmic Line.....	73
	CHAPTER 3	
3.1	Perspective View of Shuttleless Fluid Jet Loom (Ref. 54).	83
3.2	Definition Sketch for Conical Annulus (Ref. 52).....	91
3.3	Schematic of Test Setup.....	94
3.4	Water Jet Nozzle (Ref. 52).....	94
3.5	Average Shear Coefficient versus Reynolds' Number When Supply Pressure Has a Value of 206.85 kPa.....	101
3.6	Average Shear Coefficient versus Reynolds' Number When Supply Pressure Has a Value of 206.85 kPa.....	101
3.7	Average Shear Coefficient versus Reynolds' Number When Supply Pressure Has a Value of 206.85 kPa.....	101

FIGURE		PAGE
3.8	Average Shear Coefficient versus Reynolds' Number, R_x, With R_a Equal to 2,693 and P Equal to 275.80 kPa.....	102
3.9	Average Shear Coefficient versus Reynolds' Number, R_x, With R_a Equal to 2,922 and P Equal to 275.80 kPa.....	102
3.10	Average Shear Coefficient versus Reynolds' Number, R_x, With R_a Equal to 3,085 and P Equal to 275.80 kPa.....	102
3.11	Average Shear Coefficient versus Reynolds' Number, R_x, With R_a Equal to 2,862 and P Equal to 344.75 kPa.....	103
3.12	Average Shear Coefficient versus Reynolds' Number, R_x, With R_a Equal to 3,260 and P Equal to 344.75 kPa.....	103
3.13	Average Shear Coefficient versus Reynolds' Number, R_x, With R_a Equal to 3,428 and P Equal to 344.75 kPa.....	103
3.14	Average Shear Coefficient versus Reynolds' Number, R_x, With R_a Equal to 3,198 and P Equal to 413.70 kPa.....	104
3.15	Average Shear Coefficient versus Reynolds' Number, R_x, With R_a Equal to 3,822 and P Equal to 413.70 kPa.....	104
3.16	Average Shear Coefficient versus Reynolds' Number, R_x, With R_a Equal to 3,942 and P Equal to 413.70 kPa.....	104
3.17	Average Shear Coefficient versus Reynolds' Number, R_x, With R_a Equal to 4,040 and P Equal to 482.65 kPa.....	105
3.18	Average Shear Coefficient versus Reynolds' Number, R_x, With R_a Equal to 4,046 and P Equal to 482.65 kPa.....	105
3.19	Average Shear Coefficient versus Reynolds' Number, R_x, With R_a Equal to 4,285 and P Equal to 482.65 kPa.....	105
3.20	Annular Flow versus Supply Pressure.....	106
3.21	Air Pocket Surrounding Thread.....	109
3.22	Air Pocket Surrounding Thread at Lower Pressure.....	109

LIST OF TABLES

TABLE		PAGE
	CHAPTER 1	
1.1	Five Modern Hypotheses For Fully Developed Turbulent Flow	4
1.2	Variations on the Two-Dimensional Hypothesis	5
1.3	Various Laws of the Wall	7
1.4	Composite Correction Terms for the Two-Dimensional Sublayer and Transition Region	14
	CHAPTER 2	
2.1	Various Hypotheses for the Velocity Defect Law in Functional Form	47
2.2	Velocity Defect Laws	49
	CHAPTER 3	
3.1	Previous and Present Work for Flow Along a Circular Cylinder	86
3.2	Force-Pressure Relationships	99
3.3	Force-Pressure Relationships	100

NOMENCLATURE

SYMBOL		UNITS
A	constant	-
A_N	annular area	m^2
A_{TS}	thread surface area	m^2
A_1	constant	-
A_2	constant	-
a	cylinder radius	m
a^+	dimensionless radius $u_* a/\nu$	-
B	constant	-
B_1	constant	-
B_2	constant	-
b	constant	-
b_1	constant	-
c	clearance	-
C_f	average shear coefficient	-
C_{fs}	average shear coefficient with shifted axis	-
D	B_2	-
D_H	hydraulic diameter	cm
D_I	inner nozzle diameter (minimum value of D_{IN})	cm
D_{IN}	inner nozzle diameter with protrusion	cm
D_O	outer nozzle diameter	cm
D_1	nozzle diameter as defined in Fig.3.2	cm
$D_{1,II}$	nozzle diameter as defined in Fig.3.2	cm
F	experimental average shear force	g
f	function	-

SYMBOL		UNITS
G	gap between $D_{IN}/2$ and $D_0/2$	cm
g	gravitational acceleration	m/s^2
H	shape factor δ^*/θ	-
h_L	head loss	kPa
J_1	constant	-
K	constant	-
k	constant	-
L	length as defined in Fig. 3.2	cm
L_0	length as defined in Fig. 3.2	cm
P	pressure	kPa
P_I	pressure at section I	kPa
P_{II}	pressure at section II	kPa
Q	flow of water	lpm
R_a	Reynolds number based on a	-
R_D	Reynolds number based on D_H	-
R_x	Reynolds number based on x	-
R_{XT}	Reynolds number based on laminar-turbulent transition point	-
R_θ	Reynolds number based on θ	-
r	radius /+a	cm
r_1	inner radius at axial location z in Fig. 3.2	cm
r_2	outer radius at axial location z c sin in Fig. 3.2	cm
r_*	radius parameter ru_*/ν	-
r^+	r_*	-
R	velocity correlation coefficient	-
T	time	-

SYMBOL		UNITS
U	free stream velocity	m/s
U_{jet}	velocity of water jet	m/s
U_I	velocity at section I	m/s
U_{II}	velocity at section II	m/s
u	local velocity parallel to the wall	m/s
$\bar{u}$	mean local velocity parallel to the wall	m/s
u_e	velocity at boundary layer edge	m/s
u_*	friction velocity	m/s
u_τ	u_*	m/s
u_∞	free stream velocity	m/s
u'	velocity fluctuations parallel to flow	m/s
u^+	velocity ratio $\bar{u}/u_*$	-
V	mean flow velocity at any position z	m/s
V_w	injection or suction velocity	m/s
v	local velocity normal to wall	m/s
$\bar{v}$	mean local velocity normal to wall	m/s
v'	velocity fluctuations normal to flow	m/s
v_{II}	mean jet velocity at exit	m/s
w	wake component variable	-
x	length scale along wall	cm
x	thread length from end of nozzle protusion	cm
x_D	distance between x_T and x_{NT}	cm
x_N	nozzle protrusion length	cm
x_{Nmax}	maximum nozzle protrusion length	cm
x_p	maximum length of air pocket with thread including effect of vortices	cm

SYMBOL		UNITS
x_T	maximum length of air pocket with thread.....	cm
x_{TOT}	total length of x_{NT} plus x_N.....	cm
x_V	maximum length of air pocket with thread including effect of vortices.....	cm
x_{WT}	maximum length of air pocket without thread.....	cm
Y^+	length parameter $a^+ \ln (r^+/a^+)$.....	-
y	length scale normal to wall.....	cm
y^+	coordinat ratio $u_* y/\nu$.....	-
z	length coordinate as defined in Fig. 3.2.....	-

SYMBOL		UNITS
α	angle	o
β	constant	-
δ	displacement thickness	cm
ε	eddy viscosity coefficient	m^2/s
γ	intermittency factor	-
ρ_A	density of air	kg/m^3
ρ_W	density of water	kg/m^3
τ	shear stress	N/m^2
τ_s	shear stress at shifted axis	N/m^2
τ_w	shear stress at wall	N/m^2
τ^+	shear stress ratio τ/τ_w	-
μ	dynamic viscosity	Ns/m^2
ν	kinematic viscosity	m^2/s
λ	constant	-
θ	momentum thickness	-
σ	velocity ratio U/u_*	-
η	parameter $(u_e/x)^{\frac{1}{2}}y$	-
Π	constant	-
Ω	constant	-
ψ	stream function	-

INTRODUCTION

The earliest studies on the boundary layer properties for axial flow along cylinders revealed that they were sufficiently different in comparision with the two-dimensional flat-plate values to warrant a separate theoretical analysis which would take into account the effects of the transverse curvature. When compared to a flat plate for the same R_x, the Reynolds number based on the distance from the leading edge, these first cylindrical studies reported that the shear coefficients and the momentum thickness values were higher and that the displacement thickness values were less. These transverse curvature effects have been confirmed by all subsequent reports. Disagreement still exists on the various theoretical methods of solution of axisymmetrical boundary layer problems with respect to the similarity laws. The previous axisymmetrical studies, which are based on modification of the the arguments of the similarity function and variation in the empirical constants of the classical two-dimensional velocity laws, are classified according to six hypotheses for the law of the wall and four hypotheses for the velocity defect law. The merits and drawbacks of each theoretical axisymmetrical approach are evaluated and comparision is given to the two-dimensional laws. Three semi-empirical composite correction terms for the eddy viscosity and the mixing length for the sublayer and transition flow regions are examined. The effects of transverse curvature on the size of the turbulent eddies, relaminarisation, and the division of mean flow properties into a wall and wake region are investigated.

A series of experimental tests are performed on a circular thread subjected to a steady jet of water discharging from a conical annular

nozzle utilized in the textile industry in shuttleless fluid jet looms for weaving fabric. The test parameters which are varied include the supply pressure, the water flow rate, the thread length, and the clearance between the inner and outer radii for the annular nozzle. Experimentally based shear coefficients for the thread are compared with the theoretical values derived from the two-dimensional equations for the average shear coefficient and White's axisymmetrical approximation average shear coefficient equation. Two theoretical methods are used for comparision with the experimentally based average jet velocity at the end of the conical annular nozzle. The first method is based on the integral momentum equations for the inner and outer boundary layers of the conical annulus. The second is based on a macroscopic energy balance between the annulus entrance and exit while incorporating a head loss to account for the friction loss for flow in the nozzle passage. The various parameters affecting nozzle performance are examined, including the entrainment of air, the effect of water vortices, and choice of nozzle protrusion length.

CHAPTER 1

THE LAW OF THE WALL

1.1.0 Introduction

No agreement presently exists regarding the appropriate similarity laws for the mean flow along cylinders, as some discrepancies still remain between reported experimental results and the various theoretical predictions, especially when both the cylinder radius and the free stream velocity are small. In this chapter it will be shown that all previous cylindrical studies for mean velocity can be classified into one of six major approaches. The first was based on the assumption of a power law velocity profile. This has been long abandoned due to its inaccuracy and therefore, will not be examined. The five remaining modern methods are based on modification of the classical two-dimensional velocity law, with various proposals of alteration of the argument of the similarity function of the two-dimensional wall law and variation in the empirical constants. Each of the five methods will be examined with respect to their prediction accuracy in comparision with experimental results and also to see if any constraints exist on their usage and, if so, under what conditions the various parameters control these limitations. Discussion will include the justification of the various authors for their selection of one method over another and thier criticisms of the various competing methods not chosen. Because of the vast amount of disagreement on the choice of the appropriate similarity laws ,this chapter will staft with basic brief derivations of the two-dimensional law of the wall and the later axisymetric alterations to it proposed by each method, to examine any constraints on application due to the definition of the derivations.

Several of the studies in the various five methods include the sublayer and transition flow regions as well as the fully turbulent zone through the use of one of three different semi-empirical composite correction terms for eddy viscosity and mixing length, those by Deissler (1), Van Driest (2), and a recently proposed method by Landweber and Porch presented by Patel (3). These three correction terms will be examined and a comparision will be made with previous experimental results.

1.1.1 Literature Search of Six Competing Hypotheses

The first attempts at cylinder flow theories all utilized the assuption of a power law velocity profile: Millikan (4), Landweber (5), Eckert (6), Karhan (7), and Sakiadis (8). These power laws were presented in the form

$$u^+ = A_1 (y^+)^{1/n} \tag{1.1}$$

where u^+ was the dimensionless velocity ratio, y^+ was the dimensionless coordinate ratio and where A_1 and n were constants which had the values of 8.74 and 7.0 respectively for the two-dimensional case but were modified for axisymmetric flow. Their drawbacks were the limited Reynolds number range of application and predicted transverse curvature effects which were too small by an order of magnitude.

Presently five modern methods are in use for the study for the mean velocity profile without a pressure gradient along a cylindrical body for turbulent flow. One of these assumes that the classical two-dimensional law of the wall is valid under certain conditions. The five competing hypotheses for mean velocity in a functional form as

suggested by Chase (9) are shown in Table 1.1. Their respective eddy viscosities and actual wall laws, except for the derivative wall law, are also shown. Chase(9) only presented the derivative law in a functional form.

The first of the modern hypotheses was the assumption of the classical two-dimensional law of the wall which is

$$u^+ = A_1 \ln y^+ + A_2 \qquad (1.2)$$

where A_1 and A_2 are constants. This planar hypothesis approach was taken by Yu (10), Chin et al (11), Afzal and Narasimha (12), Afzal and Singh (13) and Willmarth et al (14). However as Table 1.2 shows they disagreed on their respective values for A_1 and A_2. Several authors found A_1 and A_2 were functions of either R_a, the Reynolds number based on radius a, or the radius based parameter a^+. Also shown in Table 1.2 is the range over which a specified parameter was varied.

The streamline hypothesis proposed by Richmond (15) is based on an alteration of the argument of the similarity function of the two-dimensional wall law for axisymmetric flow so that the mean velocity is in the form

$$u^+ = A_1 \ln (y^+ (1 + \frac{y^+}{2a^+})) + A_2 \qquad (1.3)$$

Also using this method were Yasuhara (16), Willmarth and Yang (17), and Huffman and Bradshaw (18) as shown in Table 1.3.

An alternate hypothesis proposal was submitted by Rao (19) that the axisymmetric wall variable is the one that will preserve the linear form of the law of the wall in the viscous sublayer so that the equation is

HYPOTHESIS		ε	u^+
Planar	$f(y^+, \frac{y^+}{a^+}) = f(y^+, 0)$	ku_*y	$A_1 \ln y^+ + A_2$
Streamline	$f(y^+, \frac{y^+}{a^+}) = f(y^+ 1+ \frac{y^+}{a^+}, 0)$	$ku_*y\frac{(1+\frac{y}{2a})}{(1+\frac{y}{a})^2}$	$A_1 \ln(y^+(1+\frac{y^+}{2a^+}) + A_2$
Rao	$f(y^+, \frac{y^+}{a^+}) = f(a^+ \ln(1+\frac{y^+}{a^+}, 0)$	$ku_*a \ln(1+\frac{y}{a})$	$A_1 \ln(a^+ \ln(1+ \frac{y^+}{a^+})) + A_2$
Derivative	$\frac{df}{dy^+}(y^+, \frac{y^+}{a^+}) = (1+\frac{y^+}{a^+})^{-1} \frac{df(y^+, 0)}{dy^+}$	ku_*y	
Local Similarity	$f(y^+, \frac{y^+}{a^+}) = f(y^+ (1+\frac{y^+}{a^+})^{-\frac{1}{2}}, 0)$	$ku_*\frac{y}{(1+\frac{y}{a})^{\frac{1}{2}}}$	$A_1 \ln(y^+ \frac{4}{(1+(1+y^+/a^+)^{\frac{1}{2}})^2}) + A_2$

Table 1.1 Five Modern Hypotheses for Fully Developed Turbulent Flow

PROPOSED LAW	AUTHOR (REF.)	CONSTANT		VARIABLE RANGE	TRANSITION ℓ^+ OR ϵ
		A_1	A_2		
PLANAR	YU (10)	2.57	$f(R_a)$	R_a - 15,250 to 45,000	
$u^+ = A_1 \ln y^+ + A_2$	CHIN ET AL (11)	1.95	5.3		
	AFZAL AND NARASIMHA (12)	2.44	$f(\frac{1}{a^+})$ 5.0 if $a^+ >> 1.0$	R_a - 825 to 134,000 x - 7.62 to 975.36 cm	
	AFZAL AND SINGH (13)	2.44	$f(\frac{1}{a^+})$ 5.0 if $a^+ >> 1.0$	R_a - 14,200 $\frac{x}{a}$ - 54 to 150	
	WILLMARTH ET AL (14)	2.44	5.0	a - 0.0254 to 2.54 cm $\frac{\delta}{a}$ - 1.8 to 37.5	

Table 1.2 Variations on the Planar Hypothesis

$$u^+ = A_1 \ln \{ a^+ \ln (1 + \frac{y^+}{a^+}) \} + A_2 \qquad (1.4)$$

Later, Rao and Keshaven (20) showed that A_1 and A_2 were not constants but functions of R_a and a^+ (see Table 1.3). Other cylindrical studies using Rao's method were also conducted by White (21), (22), and Chase (9), (23).

The local similarity hypothesis used by Patel (24) and Patel and Bradshaw (25) in the form

$$u^+ = A_1 \ln \{ 4y^+ / (1 + (1 + \frac{y^+}{a^+})^{\frac{1}{2}})^2 \} + A_2 \qquad (1.5)$$

and is shown in Table 1.3. Sparrow et al (26) and Ginevski and Solokin (27) also used this method.

The derivative hypothesis corresponds to an eddy viscosity, at a given y and friction velocity $u_* = \sqrt{\tau_w/\rho}$, that is independent of cylinder radius. Only two authors have used this hypothesis, Cebeci (28) and later on, Chase (9) and (23) who only used it in showing the superiority of another method.

1.2.0 DERIVATION OF COMPETING HYPOTHESES

1.2.1 Derivation of Planar Hypothesis

In order to express the momentum shear stresses in terms of mean velocities, Prandtl introduced the concept of a mixing length. In a gas one molecule, before striking another, travels an average distance known as the mean free path of the gas. Using this as an analogy, Prandlt conceived the mixing length theory with the assumption that a particle of fluid is displaced a certain distance before its momentum is changed by the new environment. In this section, a brief review of the

PROPOSED LAW	AUTHOR (REF.)	CONSTANT		VARIABLE RANGE	TRANSITION ℓ^+ OR ε
		A_1	A_2		
STREAMLINE $u^+ = A_1 \ln\{y(1+\frac{y^+}{2a^+})\} + A_2$	RICHMOND (15)	2.5	5.0	R_a - 93.8 to 40,870	
	WILLMARTH AND YANG (17)	2.55	5.10	R_a - 70,200 to 134,000 u_∞ - 100 to 200	
$u^+ = \int\{\frac{(1+4\ell^{+2})^{\frac{1}{2}}-1}{2\ell^{+2}}\}dy^+$	HUFFMAN AND BRADSHAW (18)	2.44	$f(\frac{1}{a^+})$	a^+ - 17 and 1500 $(\frac{\partial\tau^+}{\partial y^+})$ - -0.016 and -0.00062	$\ell^+ = ky^+\{1-\exp\frac{-\tau^{+\frac{1}{2}}y^+}{A^+}\}$ k =0.41 A^+=27 and 29
LOCAL SIMILARITY $u^+ = A_1 \ln\{(4a^+)\frac{(1+y^+/a^+)^{\frac{1}{2}}-1}{(1+y^+/a^+)^{\frac{1}{2}}+1}\} + A_2$	PATEL (24)	2.39	$f(a^+)$	R_a - 93.8 to 70,200 a^+ - 6.0 to 2600	$\ell^+ = ky^+\{\tanh(\lambda^2 y^{+2})\}^{\frac{1}{2}}$ k =0.418 λ =0.02749
	PATEL AND BRADSHAW (25)	2.39	$f(a^+)$		$\ell^+ = ky^+\{\tanh(\lambda^2 y^{+2})\}^{\frac{1}{2}}$ k =0.418 λ =0.02749
$y_i^+ = \int(1+\frac{y^+}{a^+})(1+n^2u^+y^+)du^+$ $y^+ = \int\frac{2}{3}ka^+\{(1+\frac{y^+}{a^+})^{\frac{3}{2}}-1\}du^+$	SPARROW ET AL (26)			a^+ - 51 to 32,000	$\frac{\varepsilon_{m_i}}{\nu} = n^2u^+y^+$ $\frac{\varepsilon_{m_o}}{\nu} = k^2\frac{(du^+/dy^+)^3}{(d^2u^+/du^{+2})^2}$

Table 1.3a Various Laws of the Wall

PROPOSED LAW	AUTHOR (REF.)	CONSTANT A_1	CONSTANT A_2	VARIABLE RANGE	TRANSITION ℓ OR ϵ
RAO $u^+=A_1 \ln\{a^+ \ln(1+\frac{y^+}{a^+})\}+ A_2$	RAO (19)	2.5	5.75	a^+ - 93 to 40,200	
	WHITE (21)	2.5	5.5	a^+ - 93 to 1500	
	RAO AND KEVESHAN (20)	$f(R_a)$	$f(R_a)$ $\frac{0.1R_a - a^+}{.01016R_a - 4}$	R_a - 425 to 218,500 x - 0.635 to 223.52 cm	
	CHASE (9, 23)	2.5	5.1	u - 460 and 1240 cm/sec	
DERIVATIVE	CEBECI (28)			R_a - 253 and 40,200	$\epsilon_i=(ky)^2\{1-\exp\frac{-y}{A\nu}(\frac{\tau_w}{\rho})^{\frac{1}{2}}\}^2\frac{du}{dy}$ $\epsilon_o = 0.0168\, u_\delta^* \gamma$ $k = 0.4$

Table 1.3b Various Laws of the Wall

original mixing length theory is given and an extension of this theory to obtain the mean velocity for two-dimensional flow is shown.

1.2.1.a Derivation of Mixing Length

Because of the difficulty in describing turbulent motion exactly due to its random nature, the instantaneous velocity is set equal to the sum of a mean value plus a fluctuating component. Therefore, for the xy coordinate directions,

$$u = \bar{u} + u' \quad \text{and} \quad v = \bar{v} + v' \tag{1.6}$$

where

$$\bar{u} = \frac{1}{T}\int_0^T u\,dt \quad \text{and} \quad \bar{v} = \frac{1}{T}\int_0^T v\,dt \tag{1.7}$$

with T being a long time in comparision to the time scale of the turbulence examined. The mean values for u' and v' which are $\bar{u}'$ and $\bar{v}'$ respectively, are zero by definition, but this is not true for the mean values of the squares and products of u' and v'.

For a two-dimensional boundary layer developing in a pressure gradient, the equations of motion are

Momentum

$$\bar{u}\frac{\partial \bar{u}}{\partial x} + \bar{v}\frac{\partial \bar{u}}{\partial y} = -\frac{1}{\rho}\frac{dp}{dx} + \frac{1}{\rho}\frac{\partial \tau}{\partial y} \tag{1.8}$$

Continuity

$$\frac{\partial \bar{u}}{\partial x} + \frac{\partial \bar{v}}{\partial y} = 0 \tag{1.9}$$

When there is no pressure gradient, the pressure term is equal to zero.

When the Navier-Stokes equations are written in terms of mean velocities and fluctuations from the mean are then averaged with respect to time, re-arrangement of the resulting equation enables the total shear stress τ, to be written as

$$\tau = u\frac{\partial \bar{u}}{\partial y} - \rho\overline{u'v'} \tag{1.10}$$

where $\bar{u}$ is the mean velocity parallel to the wall, u' is the instantaneous fluctuation of velocity in the direction of $\bar{u}$, $\bar{v}$ the cross fluctuation of velocity in the direction normal to the wall, y the length scale normal to the wall and measured positive from the wall, ρ the density of the fluid, and μ the coefficient of viscosity of the fluid. The first term, the apparent molecular stress, on the right-hand side of Eqn. 1.10 represents the effect of viscosity on the mean flow, whereas the second term is the Reynolds stress dependent on the state of turbulent motion. For laminar flow, the Reynolds stress term is zero. For turbulent flow away from a wall, the Reynolds stress is of considerable greater magnitude than the viscous stress so that often the first stress term is neglected. However, as the wall is approached, the portion of the viscous stress increases. At the wall, viscosity predominates.

The second term can be explained on the basis of the momentum interchange between fluid elements as they fluctuate. In Fig.1.1 the fluid in layers a and b moves with different mean velocities with $\bar{u}_a$ having a smaller value than $\bar{u}_b$. If the smaller velocity fluid in layer a were to fluctuate with a v' velocity into layer b, its velocity in the direction of the stream would be less than $\bar{u}_b$ by an amount -u'. The drag of the faster moving surroundings would accelerate the element and therefore increase its momentum. The flux crossing from a to b, $\rho v'$, mass/sec-m^2, when multiplied by -u' results in $-\rho v'u'$ which is the change of momentum per second for this flux. The rate of change of momentum is an effective shearing stress. Over a period of time the average value would be $-\rho\overline{u'v'}$. Now Prandtl also defined

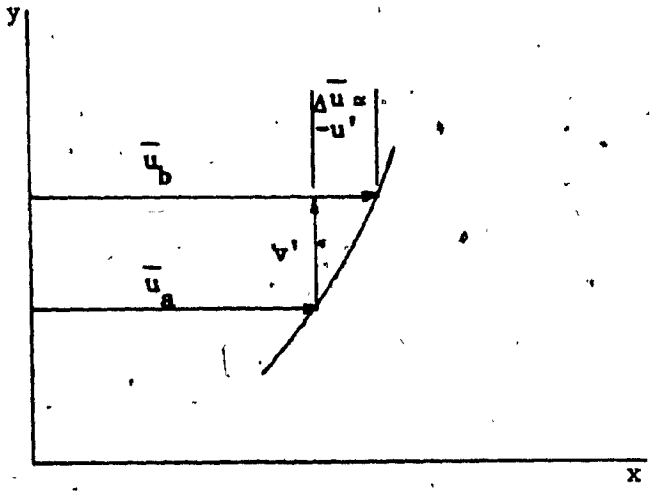

Fig. 1.1 Notation For Mixing Length Theory

$$\overline{u'v'} = -R\sqrt{\overline{u'^2}}\sqrt{\overline{v'^2}} \tag{1.11}$$

where R is the correlation coefficient. Introduction of the mixing lengths ℓ_1 and ℓ_2 defined by

$$\sqrt{\overline{u'^2}} = \ell_1 \frac{\partial \bar{u}}{\partial y} \tag{1.12a}$$

and

$$\sqrt{\overline{v'^2}} = \ell_2 \frac{\partial \bar{u}}{\partial y} \tag{1.12b}$$

respectively, then gives

$$\tau = \mu\left(\frac{\partial \bar{u}}{\partial y}\right) + \rho R \ell_1 \ell_2 \left(\frac{\partial \bar{u}}{\partial y}\right)^2 \tag{1.13}$$

The quantity $R\ell_1\ell_2$ is set equal to ℓ^2 and therefore

$$\tau = \mu\left(\frac{\partial \bar{u}}{\partial y}\right) + \rho \ell^2 \left(\frac{\partial \bar{u}}{\partial y}\right)^2 \tag{1.14}$$

which represents the total shear stress for mean fully developed turbu-

lent flow near a wall.

1.2.1.b Two-Dimensional Law of the Wall

In the laminar sublayer for two-dimensional flow, the velocity $\bar{u} = u$ and the velocity gradient $\frac{\partial u}{\partial y}$ is nearly constant. Therefore, the shear stress may be assumed constant and equal to τ_w as follows

$$\tau \simeq \tau_w = \mu \left.\frac{\partial u}{\partial y}\right|_{y=0} \equiv \mu \frac{u}{y} \tag{1.15}$$

Substituting $u_* = \sqrt{\tau_w/\rho}$ where u_* is the friction velocity and $\nu = \mu/\rho$ which is the kinematic viscosity, the following dimensionless relation is obtained

$$\frac{u}{u_*} = \frac{\bar{u}}{u_*} = \frac{u_* y}{\nu} \tag{1.16}$$

Setting $$u^+ = \frac{\bar{u}}{u_*} \quad \text{and} \quad y^+ = \frac{u_* y}{\nu} \tag{1.17}$$

then $$u^+ = y^+ \tag{1.18}$$

In the turbulent boundary layer zone for two-dimensional flow with the approximation that the mean shear stress remains nearly equal to the wall shear, then in terms of Prandtl's mixing length

$$\tau_w \simeq \tau = \rho \ell^2 \left(\frac{\partial \bar{u}}{\partial y}\right)^2 \tag{1.19}$$

Integrating this formula with the basic assumption that $\ell = ky$ for the fully turbulent region

$$\frac{\bar{u}}{u_*} = \frac{1}{k} \ln y + C_1 \tag{1.20}$$

Extrapolated towards the wall, the logarithm gives a definite value $y = y_1$ at $\bar{u} = 0$. Setting y_1 proportional to ν/u_* which is a characteristic

length at $\bar{u} = 0$, then

$$C_1 = -\frac{1}{k} \ln y_1 = A_2 - \frac{1}{k} \ln \frac{\nu}{u_*} \tag{1.21}$$

Substituting Eqn. 1.21 into Eqn. 1.20 gives the dimensionless equation

$$\frac{\bar{u}}{u_*} = \frac{1}{k} \ln y \frac{u_*}{\nu} + A_2 \tag{1.22}$$

which can also be written with $A_1 = 1/k$ as

$$u^+ = A_1 \ln y^+ + A_2 \tag{1.23}$$

which is the two-dimensional law of the wall for fully turbulent flow over smooth walls.

1.2.1.c Comparision of Sublayer and Transition Region Equations

Three semi-empirical relationships for the two-dimensional sublayer and transition region by Deissler (1), Van Driest (2), and Landweber and Porch which was presented by Patel (3) are shown in Table 1.4. The equations for the dimensionless velocity ratio u^+ as a function of the dimensionless vertical length y^+ by Van Driest and Landweber are valid also for the fully turbulent region while Deissler specifies that his equation holds true until a demarcation point at $y^+ = 26$ and $u^+ = 12.9$, afterwhich he recommends using the classic two-dimensional law of the wall with the constants A_1 and A_2 specified in Table 1.4.

A comparision of the results of the two mixing length expressions of Van Driest and Landweber and Porch obtained from writing a Fortran program were plotted in Fig. 1.2. The latter takes on the linear mixing length relation $\ell^+ = ky^+$ for values of y^+ of approximately 50. The mean velocity distribution using the three relations was plotted in Fig. 1.3. Since no experimental sublayer data is

Deissler (1) $\frac{\varepsilon}{\nu} = nu^+y^+$	$y^+ = \dfrac{\frac{1}{\sqrt{2\pi}} \int_0^{nu^+} e^{-\left(\frac{nu^+}{2}\right)^2} d(nu^+)}{\frac{1}{\sqrt{2\pi}} e^{-\left(\frac{nu^+}{2}\right)^2}}$	$n = 0.109$ $A_1^{-1} = k = 0.36$ $A_2 = 3.8$
Van Driest (2) $\ell^+ = ky^+\{1-\exp(-y^+/A^+)\}$	$u^+ = \int_0^{y^+} \dfrac{2\, dy^+}{1+\sqrt{1+4k^2y^{+2}\{1-\exp(-y^+/A)\}^2}}$	$A^+ = 26$ $A_1^{-1} = k = 0.40$
Landweber and Porch (3) $\ell^+ = ky^+\{\tanh(\lambda^2y^{+2})\}^{\frac{1}{2}}$	$u^+ = \int_0^{y^+} \dfrac{2\, dy^+}{1+\sqrt{1+4k^2y^{+2}\tanh(\lambda^2y^{+2})}}$	$\lambda = 0.02749$ $A_1^{-1} = k = 0.418$

Table 1.4 Composite Correction Terms for Two-Dimensional Sublayer and Transition Region.

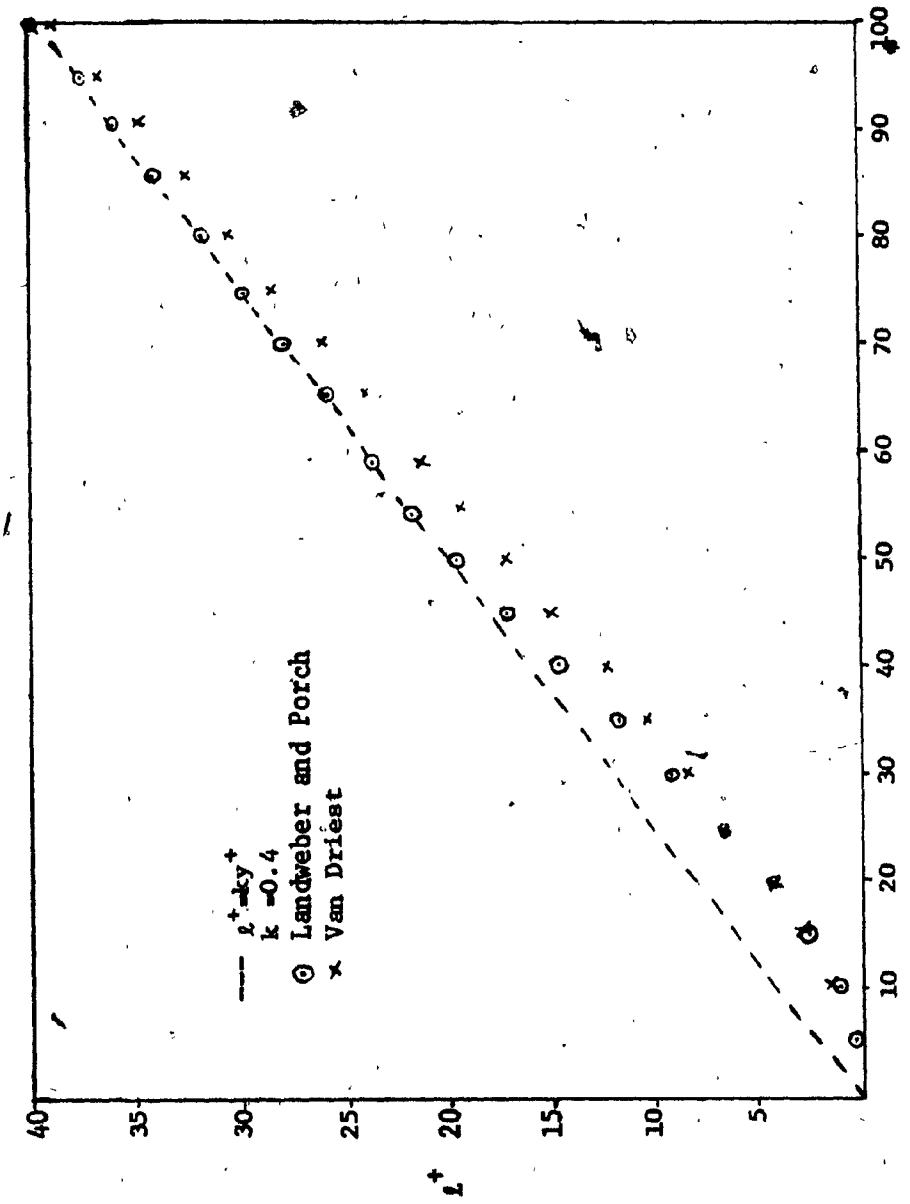

Fig. 1.2 ℓ^+ versus y^+

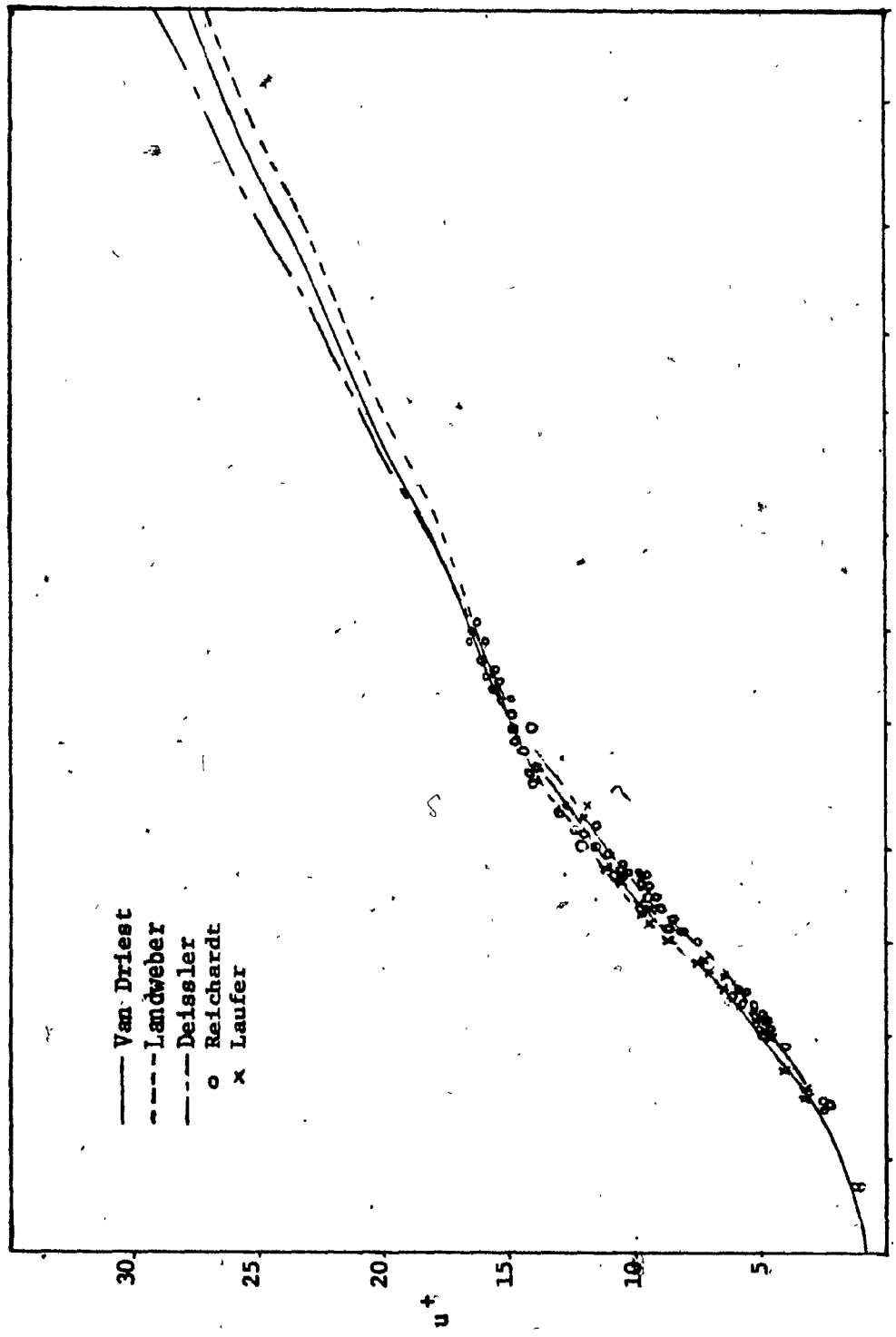

Fig. 1.3 u^+ versus y^+

available for the boundary layer flow along a flat plate, data for flow through a smooth two-dimensional channel and a smooth circular pipe obtained by Reichardt (29) and Laufer (30) are used. No definite conclusion can be drawn concerning a preference for any of the three semi-empirical relations because of the relatively large scatter of experimental data. None of these relations appears to be in strong contradiction with the experimental data. The results of the three relations overlap in several sections and probably could be made to coincide further through slight modification in choice of empirical constants.

1.2.1.d Van Driest's Relation

As a modified version of Van Driest's relation is used in the study of the viscous sublayer and transition region for axisymmetric conditions later on in this chapter, a brief derivation of his two-dimensional work follows.

The Eqn. 1.14 supposedly represents mean fully developed turbulent flow near a wall. However, such fully developed turbulent motion occurs only beyond a distance sufficiently remote from the wall that the eddies themselves are not damped in turn by the nearness of the wall. The viscous effect of the proximity of the wall may be estimated in the following manner. Consider an infinite flat plate undergoing simple harmonic oscillation parallel to the plate in an infinite fluid. As shown by Stokes (31), the ampliude of the motion diminishes from the wall as a consequence of the factor $\exp(-y/A)$ where A is a constant depending upon the frequency of oscillation of the plate and the kinematic viscosity ν of the fluid. Hence, when the plate is fixed and the fluid oscillates relative to the plate, the factor $(1-\exp(-y/A))$ must be applied to the fluid oscillation to obtain the damping effect on the

wall. Hence, Eqn. 1.14 should be modified from

$$\tau = \mu\left(\frac{\partial \bar{u}}{\partial y}\right) + \rho \ell^2 \left(\frac{\partial \bar{u}}{\partial y}\right)^2 \qquad (1.14)$$

to $$\tau = \mu\left(\frac{\partial \bar{u}}{\partial y}\right) + \rho k^2 y^2 \left\{1 - \exp\left(\frac{-y}{A}\right)\right\}^2 \left(\frac{\partial \bar{u}}{\partial y}\right)^2 \qquad (1.24)$$

in order to take into account the mean motion all the way to a smooth wall.

One could argue that the presence of the wall modifies the universal constant in that

$$K = k \{1 - \exp(-y/A)\} \qquad (1.25)$$

or that the mixing length must be changed to

$$\ell = ky \{1 - \exp(-y/A)\} \qquad (1.26)$$

Writing Eqn. 1.25 and 1.26 in a dimensionless form in which A^+ is a constant of turbulence equal to $A\, u_*/\nu$, then

$$K = k \{1 - \exp(-y^+/A^+)\} \qquad (1.27a)$$

and $$\ell^+ = ky^+ \{1 - \exp(-y^+/A^+)\} \qquad (1.27b)$$

where $\ell^+ = u_* \ell/\nu$ and $y^+ = u_* y/\nu$

Thus Eqn. 1.24 would become

$$\frac{\tau}{\tau_w} = \left(\frac{\partial u^+}{\partial y^+}\right) k^2 y^{+2} \{1 - \exp(-y^+/A^+)\} \left(\frac{\partial u^+}{\partial y}\right) \qquad (1.28)$$

For a boundary layer flow with zero pressure gradient, $\partial\tau/\partial y$, equal to zero at the smooth wall and therefore, $\tau = \tau_w$. Through integration of Eqn. 1.28 one then obtains the expression for u^+ which is

$$u^+ = \int_0^{y^+} \frac{2\,dy^+}{1 + \sqrt{1 + 4k^2 y^{+2} \{1 - \exp(-y^+/A^+)\}^2}} \qquad (1.29)$$

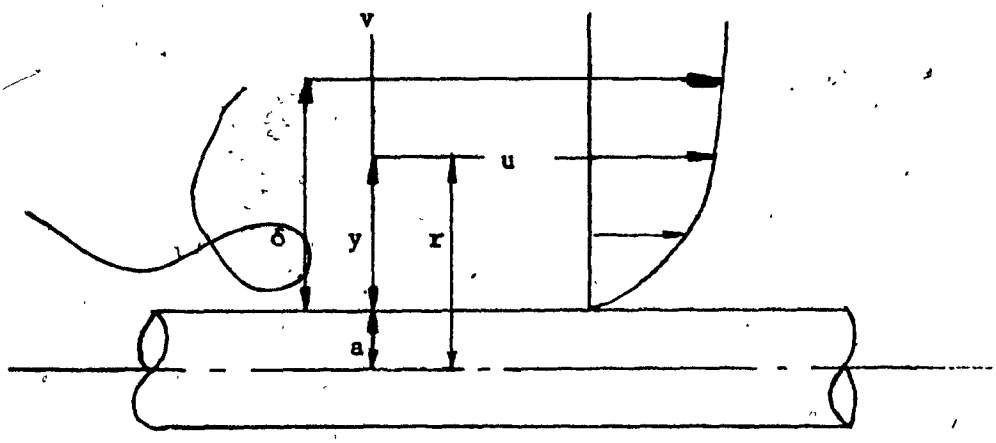

Fig.1.4 Definition Sketch for the Thick Boundary Layer Along a Cylinder

1.2.2 Axisymmetric Equations of Motion

The equations of motion for axisymmetric flow over a cylinder of radius a (See Fig. 1.4) with all the symbols the same as for two-dimensional flow, are given by

Momentum

$$\bar{u}\frac{\partial \bar{u}}{\partial x} + \bar{v}\frac{\partial \bar{u}}{\partial y} = -\frac{1}{\rho}\frac{d\bar{p}}{dx} + \frac{1}{r\rho}\frac{\partial}{\partial y}\{r(\mu\frac{\partial \bar{u}}{\partial y} - \rho\overline{uv})\} \qquad (1.30)$$

Continuity

$$\frac{\partial}{\partial x}(r\bar{u}) + \frac{\partial}{\partial y}(r\bar{v}) = 0 \qquad (1.31)$$

1.2.3 Derivation of Rao's Method

Rao (19) developed a law of the wall for thick axisymmetric turbulent boundary layer in which the sublayer thickness is comparable to the radius of transverse curvature. He states that very close to the wall, the mean velocities as well as turbulent fluctuations will be so

small that the inertia and stress terms in the axisymmetric momentum equation may be neglected. Therefore, in the absence of any pressure gradient, then

$$\tau r = \tau(y + a) = \tau_w a \qquad (1.32)$$

which suggests the absence of a constant stress layer. This expression indicates that the decrease in the viscous stress away from the wall is not fully compensated by the corresponding increase in Reynolds stress in axisymmetric flows, unlike in two-dimensional flows. The net effect is is the existance of a shear gradient, which can be expected to extend the effects of viscosity to regions farther away from the wall than in two-dimensional flows.

Substituting the equation for shear in the viscous sublayer,

$$\tau = \mu \partial u/\partial r \qquad (1.32a)$$

into Eqn.1.32 and integrating one obtains

$$\frac{u}{u_*} = u_* \frac{a}{\nu} \log \frac{r}{a} = u_* \frac{a}{\nu} \log \left(1 + \frac{y}{a}\right) \qquad (1.33)$$

Rao states Eqn. 1.33 is the linear relation of the law of the wall which must hold very close to the wall and suggests it is valid for values of his axisymmetric sublayer equation when y^+ is less than 5.

Rao makes the assumption that the correct law of the wall in the turbulent region for axisymmetric flow is in the same form as in the two-dimensional case. When the right side of Eqn.1.33 is greater than 30, it is substituted for y^+ in the two-dimensional law. Therefore, with this special scaling, the law of the wall in Rao's form with A_1 and A_2 as constants is

$$\frac{u}{u_*} = A_1 \log \left(\frac{u_* a}{r} \log \frac{r}{a}\right) + A_2 \qquad (1.34)$$

which can also be represented by

$$u^+ = A_1 \log\{a^+ \log(1 + \frac{y^+}{a^+})\} + A_2 \qquad (1.35)$$

1.2.4 Derivation of Richmond's Streamline Method

Richmond (15) assumed that there was a region near the wall where the mean flow was dominated by the wall. He obtained a law of the wall for the axisymmetric boundary layer using Coles' (32) streamline hypothesis in that region. In the region near the wall of a two-dimensional turbulent boundary layer, Coles has pointed out that the mean streamlines of the flow are given by lines of constant u^+. Therefore, Richmond's procedure for the wall region of the axisymmetric boundary layer should be valid in the region near the wall where the turbulent flow is essentially two-dimensional as in the case when the ratio y/a is small. Otherwise the similarity law derived from the streamline hypothesis may be incorrect.

His procedure assumes that u^+ is constant on the mean streamlines. Therefore, using the stream function ψ

$$u^+ = \frac{u}{u_*} = \phi\ (C\ \psi) \qquad (1.36)$$

inverting this expression

$$\psi = \frac{1}{C} H\ (\frac{u}{u_*}) \qquad (1.37)$$

The continuity equation defines the stream function

$$ur = \frac{\partial \psi}{\partial r} \quad \text{and} \quad vr = -\frac{\partial \psi}{\partial x} \qquad (1.38)$$

If the Eqn. 1.37 and 1.38 are combined then

$$u_* = \frac{1}{urC} H' \left(\frac{u}{u_*}\right) \frac{\partial u}{\partial r} \tag{1.39}$$

At any given position, if the stream function is interpreted as a measure of the fluid flow between the wall and the line at a distance y from the wall, the same stream function must vary in axisymmetrical flow as $\{(a + y)^2 - a^2\}$, where a is the radius of the circular cylinder used. Therefore, integrating u_* in Eqn.1.39 over the area between the wall and radius term (a + y), yeilds

$$\frac{1}{2}Cu_*\{(a + y)^2 - a^2\} = G\left(\frac{u}{u_*}\right) \tag{1.40}$$

or

$$\frac{u}{u_*} = F\{\frac{1}{2}Cu_*\{(a + y)^2 - a^2\}\} \tag{1.41}$$

The constant C is evaluated at the wall (assume F'(0) = 1) and $C = 1/\nu a$. Introducing the factor 1/2a to let the result tend to the two-dimensional value as $a \to \infty$ with y fixed then Eqn.1.41 becomes

$$\frac{u}{u_*} = F\{\frac{yu_*}{\nu}(1 + \frac{y}{2a})\} \tag{1.42}$$

Using the new coordinate $(u_*y/\nu)(1 + y/2a)$, one can write the law of the wall in Richmond's form as

$$u^+ = A_1 \ln\{y^+(1 + \frac{y^+}{2a^+})\} + A_2 \tag{1.43}$$

1.2.5 Derivation of Local Similarity Method

Bradshaw and Patel (25) base this method on the similarity arguments discussed by Townsend (33) of which the basic assumptions are that the eddy length scales are proportional to $(\tau/\rho)^{\frac{1}{2}}$ when τ is the shear stress at height y. These assumptions are found to be valid for

$y/\delta < 0.2$ in a plane boundary layer where δ is the displacement thickness. From these assumptions

$$\frac{\partial u}{\partial y} = \left(\frac{\tau}{\rho}\right)^{\frac{1}{2}}/ky \tag{1.44}$$

Substituting Eqn. 1.32 into Eqn.1.44 and integrating with $A_1 = 1/k$,

$$\frac{u}{u_*} = A_1 \ln\left[\frac{u_* y}{\nu} \frac{4}{(1 + (1 + y/a)^{\frac{1}{2}})}\right] + A_2 \tag{1.45a}$$

which can also be represented as

$$u^+ = A_1 \ln\left[y^+ \frac{4}{(1 + (1 + y^+/a^+)^{\frac{1}{2}})}\right] + A_2 \tag{1.45b}$$

or equivalently

$$u^+ = A_1 \ln\left[4a^+ \frac{(1 + y/a)^{\frac{1}{2}} - 1}{(1 + y/a)^{\frac{1}{2}} \quad 1}\right] + A_2 \tag{1.45c}$$

1.3.0 DISCUSSION OF COMPETING HYPOTHESES

1.3.1 Two-Dimensional Hypothesis

The basic assumption of all the authors using the two-dimensional wall law for axisymmetric flow was that the total shear stress, τ, was equal to the shear stress at the wall, τ_w, thereby ignoring the effect of the transverse curvature on the shear stress. The effects of the transverse curvature increase with decreasing cylinder radius, a. The two-dimensional hypothesis is of sufficient accuracy only for relatively large cylinder radii. The transverse curvature effects were partly taken into account through variation the values given the constants A_1 and A_2 in the two-dimensional wall law.

As with other authors, Afzal and Narasimha (12) reverted back to the two-dimensional laws because of their simplicity but they used

asympotic expansion terms. They limited their work though, for $a^+ >> 1$ and δ/a of the order unity. They justified their use of the two-dimensional laws by saying that if a^+ is large in the equation for the total shear stress τ in an axisymmetric wall layer, $\tau = \tau_w/(1 + y^+/a^+)$, then τ can be taken as constant equal to τ_w. Consequently, the sublayer profile is linear so that the effects of transverse curvature on the inner layer must be capable of being regarded as higher order perturbations to a basically two-dimensional flow. For moderately large values of a^+, they suggest that the additive term in the wall law is a linear function of $1/a^+$ but because of the scattering of the existing experimental data, they could not conclusively verify this hypothesis.

1.3.2 Richmond's Streamline Hypothesis

From Richmond's derivation (15), he assumed that Coles' (32) hypothesis, (that in the region near the wall of a two-dimensional turbulent boundary layer the mean streamlines of the flow are given by lines of constant u^+,) should be valid for axisymmetric flows if the flow is essentially two-dimensional as in the case of small values of y/a. Otherwise its usage may be incorrect and the accuracy of the results questionable.

Willmarth and Yang (17) suggested that if the amount of transverse curvature is not too large, $\delta/a << 1$, then the most logical approach would be to assume the two-dimensional law of the wall. Since their work dealt with $\delta/a \approx 2$, they chose Richmond's method to take the curvature into account but questioned its validity for large y/a for the same reasons as mentioned above.

Huffman and Bradshaw (18) also utilized Richmond's method for

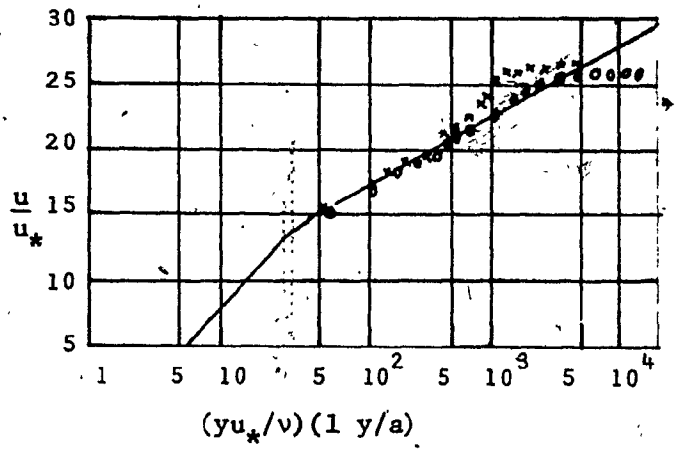

Fig. 1.5 Comparision of Streamline, o, and Rao+s, x, Hypotheses With the Two-Dimensional, —, for the same C_f equal to 0.0029. (Ref. 19)

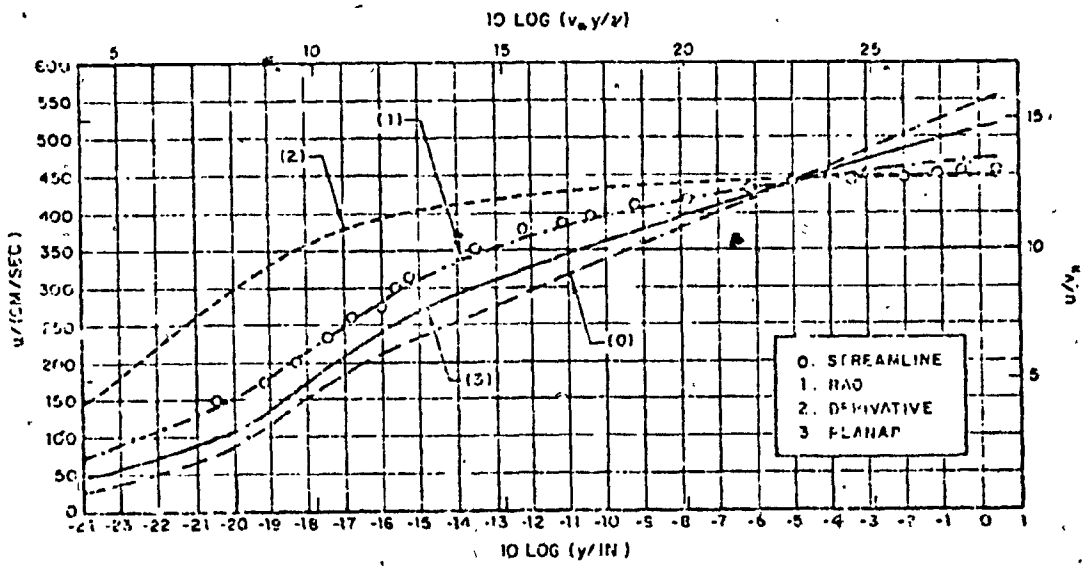

Fig. 1.6 Measured Mean Velocity Profile for Cylinder and Those Computed from Various Hypotheses with Wall Friction Velocity Chosen in Each Case to Yeield Measured Velocity at y=0.8001 cm. Dimensionless Scales Refer to u_*=35.2 cm/sec of Rao Curve. (Ref. 23)

y/δ or $y/a < 0.2$ with the reasoning that though it is not uncontroversial, it should suffice for calculation of the mean velocity profiles within the limits imposed.

1.3.3 Rao's Hypothesis

Rao's hypothesis (19) was derived on the basis that for a slender cylinder, the sublayer thickness is comparable to the radius of transverse curvature. He states that for small y/a, the Eqn.1.33 ($u^+ = au_*/\nu \log r/a$) reduces to $u^+ = u/u_* = (yu_*/\nu)(1-y/2a)$. Therefore, the use of the streamline hypothesis or the two-dimensional law of the wall near the surface to estimate skin friction assuming a linear relation is incorrect unless $y/2a \ll 1$. The error increases as y/a becomes comparable to unity. Physically this means that, as the thickness of the sublayer becomes comparable to the radius of transverse curvature, it is more correct to use Rao's equation for the region very close to the wall than either the two-dimensional wall law or the streamline hypothesis as a linear relation. A graph of a comparision between the streamline hypothesis and Rao's is shown in Fig.1.5. and Fig. 1.6..

Willmarth and Yang.(17) agree with Rao that Eqn.1.33 is correct in the region very near the wall, but doubt that it can be valid in a region extending from the wall as far as the radius of curvature of the cylinder when $\delta/a \gg 1$. Their conception of the sublayer is a region dominated by wall effects and that no matter how large the ratio δ/a becomes, the sublayer thickness is always small compared to the radius of curvature of the surface, a. If this were not true, they state that the turbulent eddying flow would wash the fluid in the sublayer completely off the cylinder. They also question Rao's velocity profile law used throughout the boundary region, because it takes the

logarithm of r/a which reduces the scatter of data points for large r and requires extremely accurate measurements to determine the validity of the formalation.

1.3.3.a Validity of Rao's Hypothesis for Transpiration Flow

Bradshaw and Patel (25) state that the argument on which Rao's formula is based is unreliable and cite the example of the turbulent boundary layer flow with transpiration as a case of the failure of Rao's hypothesis that the same scaling laws that apply to the sublayer should persist into the region of the law of the wall. The sublayer equation for transpiration (for two-dimensional boundary layers with suction or injection at velocity V_w) is

$$\frac{u}{u_*} = \frac{u_*}{V_w} \left(\exp\left(\frac{V_w y}{2} - 1\right)\right) \tag{1.46}$$

When the above sublayer value of u/u_* was substituted for u_*y/ν in Eqn. 1.22 (the usual two-dimensional logarithmic law of the wall for the turbulent region) then

$$\frac{u}{u_*} = A_1 \ln\left[\frac{u_*}{V_w}\left\{\exp\left(\frac{V_w y}{2}\right) - 1\right\}\right] + A_2 \tag{1.47}$$

Patel and Bradshaw showed this equation resulted in vastly different values of u/u_* compared to the ones obtained from the bilogarithmic law

$$\frac{2u_*}{V_w}\{(1 + V_w^+ u^+)^{\frac{1}{2}} - 1\} = A_1 \ln y^+ + A_2 \tag{1.48}$$

which is generally accepted as a good fit to experimental data outside the viscous sublayer.

Rao (34) contends that if the transpiration equation was recast in the following form

$$\left(\frac{u_*}{V_w}\right) \ln\left(1 + \frac{V_w u}{u_* 2}\right) = \frac{y u_*}{\nu} \qquad (1.49)$$

then the law of the wall would be

$$\left(\frac{u_*}{V_w}\right) \ln\left(1 + \frac{V_w u}{u_* 2}\right) = K \ln\left(\frac{y u_*}{\nu}\right) + C \qquad (1.50)$$

With the known variation of the constants, C and K, with suction and injection, Rao therefore set K=half its normal value and C=6. This resulted in a difference of only 4% when the above equation was solved for u/u_* and compared with the u/u_* value obtained from the bilogarithmic law. Unlike Eqn. 1.48, the Eqn. 1.50 tends to the ordinary logarithm for small values of $(V_w u/u_*)$.

1.3.4 Local Similarity Hypothesis

The similarity arguments discussed by Townsend (33), based on the basic assumptions that the eddy length scales are proportional to $(\tau/\rho)^{\frac{1}{2}}$, are valid for $y/\delta < 0.2$ in a plane boundary layer. In a slender axisymmetric boundary layer, Bradshaw and Ratel (25), who used the local similarity hypothesis, predicted an upper limit on y/a as well as y/δ. Their reasoning was that if y/a is larger, the lateral length scale of the eddies will be much larger than a, so that the eddies will not be constrained as they would by an effective infinite wall. Then any wall law analysis including Rao's will be invalid with y/a=3 given as an optimistic figure for the upper limit. Chase (23) states that Rao's hypothesis yeilds excellent agreement with the measured profile even out to y/a≈50, (see Fig. 1.6), even though one has no right to expectany wall law analysis to retain validity at such a large y/a.

Rao (34) believes the eddy structure, at least in the region

of the wall, cannot be considered in isolation from the effects of the wall and that the wall effects appear to be stronger than hitherto assumed. Rao also questions the assumption that the eddy length scale is proportional to the distance from the wall in axisymmetric flows. He doubts that the eddy structure on cylinders of 5mm and 50mm diameters should be the same at 2mm from the wall even if the thickness of the turbulent boundary layer is the same in both cases. For example, the velocity induced by one ring vortex on another in the two cases will be different even if the strengths of the two vortices are the same in both cases. For this reason, Rao justifies the use of his alternate formulation for the mixing length and law of the wall for axisymmetrical flows.

Two of the reports, published before Rao, attempted to improve results over the two-dimensional and Richmond's method. Ginevski and Solodkin (27) adapted Prandtl's mixing length theory to the thick cylindrical boundary layer and included consideration of concave and convex surfaces, pressure gradients and flow separation. They divided the flow field into a purely laminar one and a fully turbulent one. After examining this approach, Sparrow, Eckert and Minkowyez (26) suggested that the use of local turbulent transport coeffients would improve results and used the two-layer eddy viscosity formulation of Diessler(1) to take the transition region into account.

Patel(3) and (25) explained his choice of the local similarity method over Rao's method in that he desired to avoid Rao's special scaling assumption that the laws applying to the sublayer should persist when substituted in the equation for the region of the law of the wall. He used a recently introduced mixing length formulation by Land-

weber (5) to reflect the transition region.

1.3.5 Derivative Hypothesis

Only two authors used the derivative hypothesis, Cebeci (28) and Chase (9), with the latter only to show that it was less accurate than Rao's method. Cebeci (28) used an implicit finite difference method for solving the equations of continuity and momentum after a combination of Probstein-Elliot and Levy Lees co-ordinate system transformations while also incorporating Van Driest's mixing length. The derivative hypothesis corresponds to an eddy viscosity at a given y and u_* that is independent of the cylinder radius. The use of this planar formulation when solving axisymmetric problems is critized by Coles(32) and White (21), who suggest that a cylindrical body has less ability to influence turbulence than a flat plate. Therefore, the mixing length used by Cebeci should be proportional, not to y, but to Rao's variable, $(a \ln(1 + y/a)$, which is less than y for thick boundary layers. Cebeci(35), the only proponent of the derivative hypothesis, followed these suggestions and abandoned the derivative hypothesis to use Rao's variable, correcting Van Driest's eddy viscosity for axisymmetric flow.

1.3.6 Comparision of Competing Hypotheses With Experimental Results

Chase(9) and (23) examined competing hypotheses for the mean velocity profile of a turbulent boundary layer on a cylinder in axial flow. Rao's, Richmond's, the planar, and the derivative hypotheses were discussed and their results explicity compared with experiment. Chase plotted the various alternate hypotheses in Fig.1.6,1.7, and 1.8 after computing the profiles using Squire's transitional profile for the planar limit given by

$$F(y^+,0) = y \qquad \text{for } 0 < y^+ < C_1 \qquad (1.51a)$$

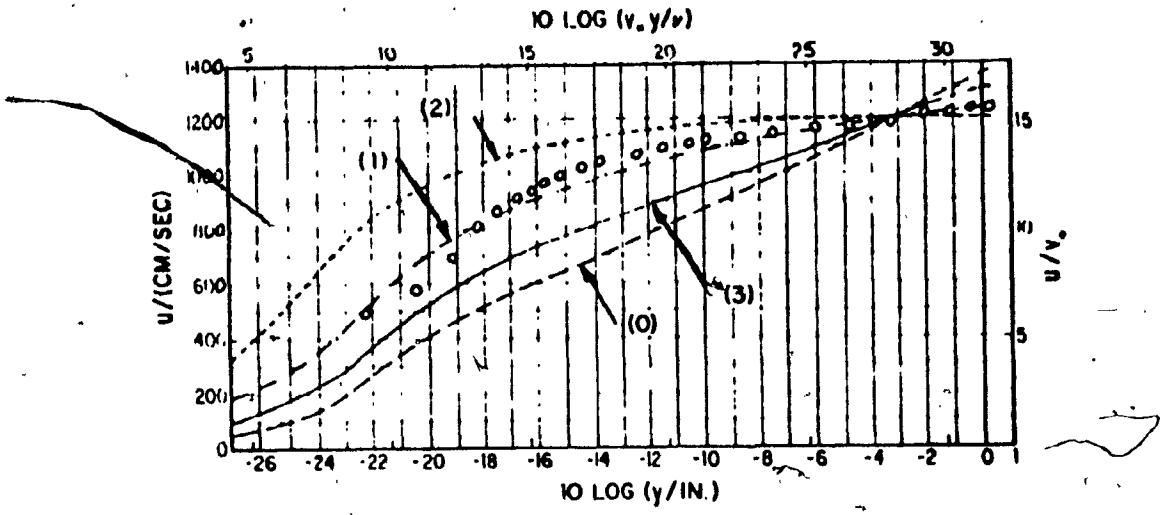

Fig. 1.7 Measured Mean Velocity Profile for Cylinder and Those Computed from Various Hypotheses with Friction Velocities Chosen to Yield Measured Velocity at y=1.21158 cm. Dimensionless Scales Refer to u_*=78.9 cm/sec of Rao curve. (Ref. 9)

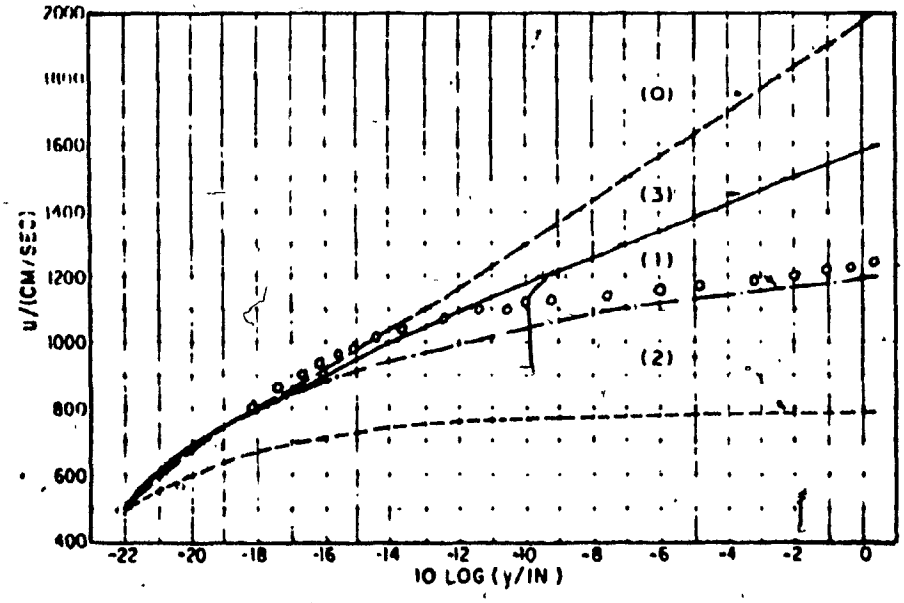

Fig. 1.8 Mean Velocity Profiles as in Fig. 1.7 But With Friction Velocities Chosen to Yield Measured Velocities at y=0.01524 cm. (Ref. 9)

$$F(y^+,0) = A_1 \ln(y - J_1) + A_2 \qquad \text{for } C_1 < y^+ \qquad (1.51b)$$

with $A_1 = 2.5$ and $A_2 = 5.1$

and $C_1 = A_1 \ln A_1 + A_2 = 7.4$

and $J_1 = C_1 - A_1 = 4.9$

The results were compared with Richmond's (15) experiments with a = 0.3048 cm and u = 1240 cm/sec with natural transition and u = 460 cm /sec with clay-centerbody and enveloping stovepipe. Since the friction velocity, u_*, was not measured and not reliably derivable from the slope of the measured profile at small wall distances, this parameter was regarded adjustable for each of the hypothesis and was adjusted in two different ways for each set. In the first instance (see Fig.1.6 and 1.7), the values of u_* were chosen to yeild a comman value of u(y) in agreement with the measured result at a chosen y well out in the boundary layer (but at a minor fraction of boundary layer thickness). In the second method (see Fig.1.8), the values were chosen instead to yeild a common value in agreement with the measured u(y) at the measured point nearest the wall.

As illustrated in Fig. 1.6, 1.7, and 1.8, the Rao hypothesis suceeds best in describing the experimental profile over most of the thickness, even at very large y/a. The advantage is not substantially weakened if the result is compared with that of Cebeci (36). Cebeci assumed an eddy viscosity independent of y/a, as in the derivative hypothesis, but integrated the mean momentum and continuity equations instead of assuming shear force per unit streamwise distance of y.

A recent comparision by Cebeci(35), after he rejected his deriv-

ative hypothesis, between the calculated and experimental values for velocity and Mach number profiles, can be seen in Fig.1.9. Here the two-dimensional hypothesis using Van Driest's planar equation is compared with Cebeci's present use of Rao's variable modifying Van Driest's equation. As can be seen, the two-dimensional hypothesis inadequately predicts the condition of thick axisymmetric turbulent boundary layers where δ/a is large which emphasizes the limitations of its application.

Chase(23) states that even if the local similarity hypothesis for the logarithmic range with parameters u_* and A_2 both adjustable, was plotted along with the four other methods, no profile conforms to the measured one in Fig.1.6,1.7, and 1.8 over such a large range of y/a (outside the sublayer) as does the Rao curve. Patel (24) compared the values obtained from the two terms from the local similarity and Rao's equations (see Table 1.3)

$$4\,\frac{(1 + y^+/a^+)^{\frac{1}{2}} - 1}{(1 + y^+/a^+)^{\frac{1}{2}} + 1} \quad \text{with} \quad \ln(1 + y^+/a^+)$$

and discovered that the disagreement is of the order of 1% for $y^+ = a^+$ and less than 8% for $y^+ = 6a^+$. For larger y^+/a^+ the difference between these two terms increased.

1.4.0 EFFECTS OF TRANSVERSE CURVATURE

1.4.1 Influence on Wall Law

In respect to the wall regions of a thick axisymmetric boundary layer, small values of a^+ bring significant variations in stress throughout the region as a consequence of the flow geometry. The stress continues to fall monotonically from its value at the wall. This can be compared to the situation in a two-dimensional boundary layer developing in a favourable pressure gradient, where the stress falls from its

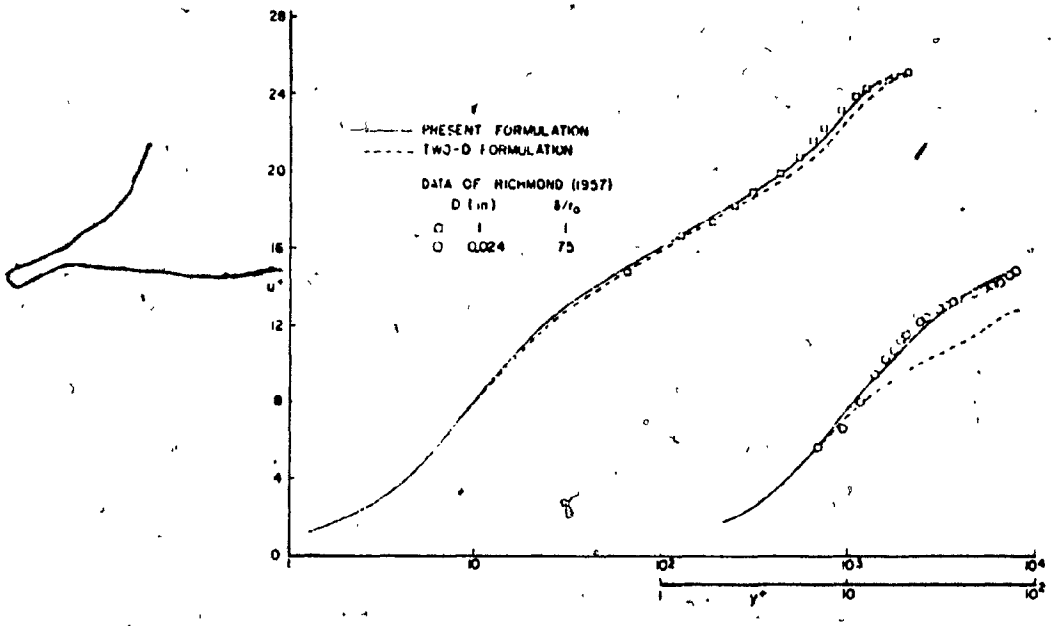

Fig. 1.9 Comparision of Calculated and Experimental Dimensionless Velocity Profiles for Two Cylinders. The Experimental u^+ Values were Obtained by Normalizing the Measured u Values by the Calculated Velocity u_τ. The Lower y^+ Scale Refers to the 0.06096 cm Cylinder. (Ref. 35)

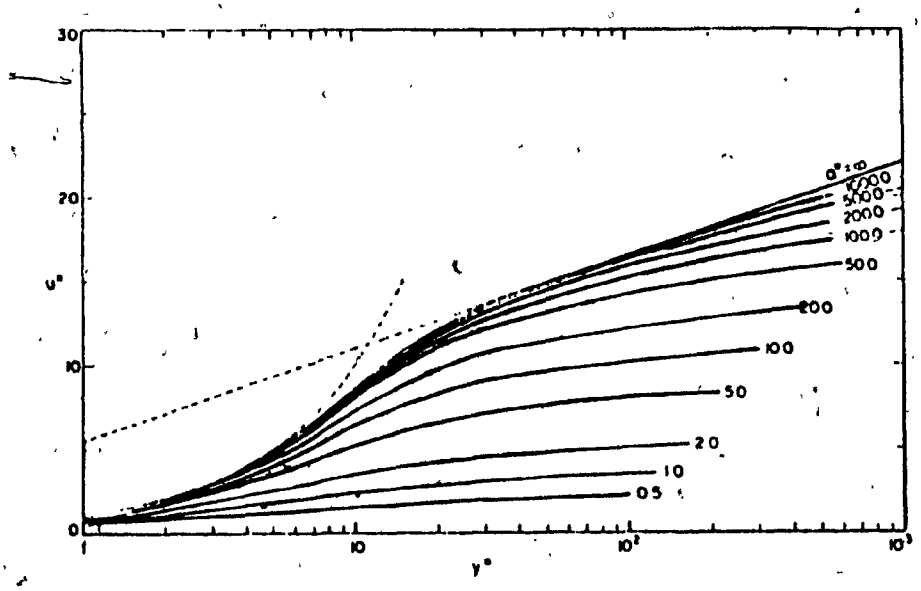

Fig. 1.10 The Influence of Transverse Curvature on the Law of the Wall. (Ref. 24)

value at the wall as a result of the pressure gradient and the accompanying flow accelerations. The influence of transverse curvature on the law of the wall can be seen in Fig. 1.10 which uses the local similarity hypothesis with a^+ equal to infinity being the flat plate case.

1.4.2 Relaminarisation

All the presented methods have been found somewhat inaccurate in predicting the stress and velocity distribution in comparision with experimental results for low values of a^+. Patel (24) proposed an explanation for the discrepency based on the similarity between the influence of transverse curvature and a favourable pressure gradient on the stress and velocity distributions in the wall region. Patel and Head (37) had reported that there is a definite limit to the favourable pressure gradient that can be imposed on a turbulent boundary layer without destroying the essential equilibrium that exists between the production and dissipation of the turbulent kinetic energy in the wall region, and thereby provoking relaminarisation. They had suggested a limiting value of -0.009 for the stress gradient parameter, τ^+, as the criterion for the onset of this reverse transition process. Patel (24) proposes that a similiar limiting value exists for the curvature parameter, a^+. Computing the stress gradient, $\tau^+ = \tau / \tau_w$, for the axisymmetrical boundary layer on a slender cylinder from the equation $\tau^+ = 1/(1 + y^+/a^+)$ and setting it equal to -0.009, he found the corresponding limiting value of a^+ was about 28. Below this value, the flow would therefore be considered as transitional and not fully turbulent as assumed by the various methods. Therefore, τ_w and $u_* = (\tau_w/\rho)^{\frac{1}{2}}$ would be less, while $u^+ = u/u_*$ would have a greater value than if the flow was fully turbulent. Since the shear would be less, the shear coefficient would

also have a smaller value.

Rao and Keshaven (20) propose a limiting value for the onset of relaminarisation in terms of R_a less than 15,000. This value is close to the value of 11,000 calculated by Rao(38) below which all small disturbances to laminar axisymmetric boundary layers will damp out.

In a recent experiment by Willmarth et al (14) no tendency towards relaminarisation was found at the lowest value of a^+ tested which was 33.4. Their measured shear stress at that value on a 0.0508 cm diameter cylinder was slightly more than a factor of 6 larger than the laminar value predicted from the laminar theory of Glauret and Lighthill (39). Their velocity profile measurements showed consistent behaviour as the cylinder radius was reduced. It was verified that the boundary layer profile on a cylinder is very full. However,this was postulated as a result of the cylindrical geometry of the flow. In the boundary layer on a cylinder there is no acceleration of the free stream, which in two-dimensional flow is directly responsible for the favourable pressure gradient which produces a full velocity profile.

Willmarth (40) has proposed a mechanism for the cyclic occurrence of bursts in a plane boundary layer which may be useful in understanding the difference between the turbulent production mechanisms in a plane boundary layer with a favourable pressure gradient and a boundary layer on a cylinder with zero pressure gradient. The pressure field from the large eddies in the outer flow is thought to produce a massaging action on the sublayer flow and prepare it for the occurence of a burst. The massaging action of the large eddies passing over the sublayer is presumed to create, during random periods of time, an unstable inflexional profile in localized regions near the wall. Bursts

which generate new turbulence occur in these regions of locally unstable inflexional profiles. When there is a very favourable pressure gradient, the outer flow containing the large eddies is strongly accelerated so that the large eddies pass more quickly over the sublayer flow field , so that their massaging action at a given point near the wall has a greatly reduced time scale. Then, the flow near the wall is locally more stable since the degree of instability and therefore the number of locally unstable regions in the sublayer are reduced. The result is that the number and intensity of bursts are reduced. Ultimately, a reversion to laminar flow occurs.

1.4.3 Variation in the Viscous Damping Constant A^+

The viscous damping constant, A^+, represents the effect of the viscous sublayer , ($y^+ \geq 40$), as it determines the additive constant A_2 in the logarithmic law of the wall. Huffman and Bradshaw (18) made a comparision study on the change in A^+ and k with respect to the dimensionless shear stress gradient, $\partial\tau^+/\partial y^+$, in the inner layer where $y/\delta \leq 0.2$ for two-dimensional and axisymmetrical flows. As the data for the boundary layer itself has been shown insufficient in accuracy to reach a conclusion to whether k and A^+ have variable values as suggested by Simpson(41) and Cebeci and Mosinski (36) or constant values as suggested by Coles (32) and Herring and Mellor (42), their comparison analysis was based on flows in which low Reynolds number effects are expected to be larger than in a boundary layer. They state that if the value of k were varied but assumed constant in the profile fitting process, one would expect the optimum A^+ to vary to compensate. If this optimum A^+ were found to be constant even in the presence of rather stronger Reynolds number effects than those found in low Reynolds num-

ber boundary layers, then the assumption of constant A^+ and constant k would be confirmed with fairly probability.

Their plotted velocity profiles for axisymmetrical flows, although found less in agreement with experimental values than the two-dimensional plots, were of sufficient accuracy to ascertain that the general trend of A^+ to $\partial\tau^+/\partial y^+$ for axisymmetrical flows was to vary in the opposite sense to the two-dimensional case (see Fig. 1.11). The best-fit value of A^+ maintained the basic value of about 26 in a wide range of low Reynolds number flow if the shear gradient, $\partial\tau^+/\partial y^+$, is numerically less than 10^{-3}. At larger values of the dimensionless shear stress gradient, the damping constant departs from this basic value but the best-fit value of Von Karman's constant, k, appears to remain at 0.41. The value of $\partial\tau^+/\partial y^+$ at which the values of A^+ diverge correspond to $\delta_{sub}/a = 0.1$ wheras the ratio of the inner layer thickness to a is about 0.2.

The "local-equilibrium" analysis for the inner layer described by Townsend(33) suggests that the first effect of external influences will be felt by $\partial\tau^+/\partial y^+$ and the consistency of results from different flows for $\partial\tau^+/\partial y^+$ less than 10^{-3} shown by Huffman and Bradshaw (18) support this. These results contradict Simpson's (41) suggestion that k and A_2 (or A^+) vary, compensating each other to maintain the same velocity profile, in a constant pressure boundary for $1000 < R_a < 6000$, because $\partial\tau^+/\partial y^+$ is numerically less than 10^{-3} throughout this range.

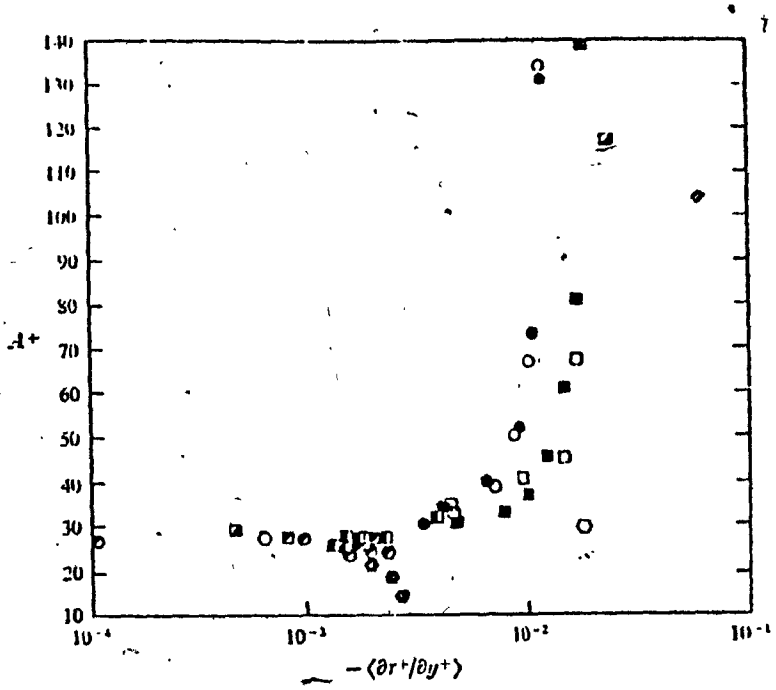

Fig. 1.11 The Viscous Length Scale A^+ for Two-dimensional and Axisymmetric Flows. Axisymmetric Flows on Concave Surfaces, Fully Developed Pipe Flow: ○, ●, Patel & Head; ◐, Laufer. Two-dimensional flows: ◧, Bradshaw & Gee, Two-dimensional wall jet; ■, Patel & Head, Fully Developed Channel Flow; ◪, Laufer, Fully Developed Channel Flow; □, Julien et al, Two-dimensional Boundary Layers; ▣, Badri Narayanan & Ramjee, Two-dimensional Boundary Layers. Axisymmetric Flows on Convex Surfaces: ⬤, Starr & Sparrow, axisymmetric wall jet; ◍, Lawn, Fully Developed Annular Flow; ⬡, Cebeci, Axisymmetric Boundary Layer. (Ref. 18)

Since A^+ varies for large $\partial\tau^+/\partial y^+$ and the apparent constancy of k, it is implied that the viscous sublayer is more sensitive to external influences than the fully turbulent part of the inner layer. From the consistent differences in the values of A^+ between two-dimen-

sional and axisymmetric flow for large $\partial\tau^+ / \partial y^+$ it can be concluded that the transverse curvature may affect the viscous sublayer. It is generally accepted, however, that the transverse curvature does not effect the rest of the inner layer since the ratio of the inner layer thickness to the radius of curvature is independent of Reynolds number.

The reasons for the sensitivity of the sublayer to transverse curvature remain conjectures. A possible clue comes from the observation by Kline et al (43) and Gupta et al (44) of a tendency to transverse periodicity in the sublayer with a wavelength λ given by $u_*\lambda/\nu = \tau^+ = 100$. Moreover, $\lambda/a \simeq 3\delta_{sub}/a \simeq 100(\partial\tau^+ /\partial y^+)$; consequently, λ/a is about 0.3, i.e. one transverse wavelength subtends about 20°, when significant curvature effects begin. This transverse scale is quite large when compared with the eddy length scales just outside the viscous sublayer, i.e. $\ell_{sub} \simeq 16$ when $y \simeq 40$, so that it is plausible that the sublayer is affected while the remainder of the inner layer is not.

1.4.4 Reduction in Turbulent Eddies Size

Willmarth and Yang (17) suggest that there are two primary effects in a boundary layer with transverse curvature that reduce the size of turbulent eddies. The first effect causing this reduction is the increased fullness of the velocity profile when compared with a flat plate (see Fig. 1.12), where $\delta/a = 0$ is the flat plate case. In a boundary layer with a fuller velocity profile, the turbulent eddies near the wall moving at any given convection speed must be smaller because the mean velocity corresponding to that convection speed is reached at a point nearer the wall. The second more direct effect where the large eddies suffer a greater reduction in transverse scale than small eddies

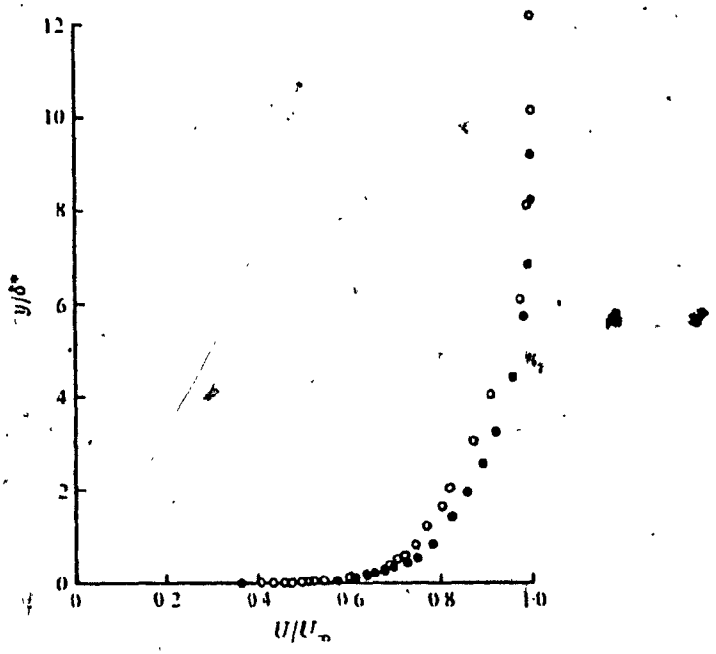

Fig. 1.12 Comparision of the Mean Velocity Profiles, • , δ/a = 2, R_θ = 26,000; ○ , δ/a = 0, R_θ =38,000. (Ref. 17)

is because the wall is curved transversely. Thus if one visualizes a large eddy adjacent to the curved wall, it is apparent that in the transverse direction at either side of the periphery of a large eddy, the mean velocity is higher than it would be at the sides of the same eddy in a plane bondary layer. This shearing motion also acts to reduce the transverse scale of large eddies.

1.4.5 Intensity of Turbulence

Afzal and Singh (13) made measurements of mean velocity profiles and turbulence characteristics such as longitudinal velocity fluctuations, Reynolds shear stress, transverse correlation and spectrum. They reported that for a fixed x/a, as y/δ decreases from outside the boundary layer, the intensity of the longitudinal velocity fluctuations increases to a maximum value very near the wall after which it decreases to zero at the wall. Also for a fixed y/δ, it was found as

x/a increases, which also means δ/a incresing, the turbulence intensity decreases. Compared with the flat plate case, the effect of the transverse curvature decreased the intensity of turbulence.

1.5.0 Conclusions

This chapter examined the law of the wall for axial turbulent flow along a cylinder without a pressure gradient. Previous studies were classified according to six major approaches. As no previous agreement existed regarding the appropriate similarity laws for the mean flow, these competing hypotheses were compared with respect to accuracy of prediction, the range of application and the constraints existing on their respective utilization.

This chapter considered the sublayer and transition regions as well as the fully turbulent flow region of the inner layer. A comparision of the three semi-empirical composite correction terms for eddy viscosity and mixing length used in previous studies was examined. None of the three relations were found to be in strong contradiction with experimental data. Their results overlapped in several instances and could possibly coincide further through slight modification in choice of empirical constants.

Modifying Van Driest's equation through substitution of Rao's variable improved correlation with experimental results. It should be noted that the viscous damping constant, A^+, varies for large values of $\partial\tau^+/\partial y^+$ and that the transverse curvature may affect the viscous sublayer but it generally is accepted that the rest of the inner layer is not affected.

The first attempt at axisymmetric flow theories, based on the assumption of a power law velocity profile, has long been abandoned due

to limited Reynolds number range application and its inaccuracy. Therefore it was not examined closely.

Of the remaining five modern hypotheses, the one often chosen because of its simplicity is the two-dimensional hypothesis. The effect of the transverse curvature was partly taken into account through variation in the values of the constants A_1 and A_2 for different radii in the two-dimensional wall law. The total shear stress though, was assumed equal to the shear stress at the wall as in the planar case. Therefore, this hypothesis becomes increasingly more inaccurate for smaller radii as the transverse curvature effect increases and thereby places a limit on its application. Comparison with experimental results revealed that this hypothesis was sufficiently accurate for use with large cylinder radii.

Richmond's streamline hypothesis was based on the assumption that in the region near the wall of a two-dimensional turbulent boundary layer, the mean streamlines of the flow are given by lines of constant u^+. This pattern should also be valid for axisymmetric flows if the flow is essentially two-dimensional, as in the case of small values of y/a. Otherwise, its usage may be incorrect and the validity of it's results questionable. In comparison with experimental results, it proved sufficiently accurate for use with small y/a values but because of this restriction on its use, this hypothesis is not often utilized. Variation in its values of A_1 and A_2 improve its accuracy somewhat.

Rao's hypothesis was derived on the basis that for a slender cylinder, the sublayer thickness is comparable to the radius of transverse curvature. Unlike the previous two hypotheses, Rao's appears not limited by the size of the radius and was found valid for large values

of y/a. This hypothesis was also proven valid for transpiration flow. He also assumed a special scaling that the laws applying to the sublayer should persist when substituted into the equation for the region of the law of the wall. In comparison with the other hypotheses, Chase (9) found that Rao's results most closely agreed with experimental results over a large range of values for y/a.

The local similarity hypothesis is based on the similarity arguments that the eddy length scales are proportional to $(\tau/\rho)^{\frac{1}{2}}$ which have been found valid for $y/\delta < 0.2$ in a planar layer. The axisymmetric shear is the same as used by Rao. The results were found to be relatively close to those of Rao's without Rao's special scaling.

The derivative hypothesis corresponds to a two layer eddy viscosity model where at a given y, the value of u_* is independent of the cylinder radius as in the planar case, but with certain other parameters changed for cylinderical theory. As a result, there would be greater inaccuracy for smaller values of radii expected. This method shows no advantage over Rao's or the streamline hypothesis. The only author who suggested its use, Cebeci (28) , recently abandoned it in favour of an eddy viscosity which places Rao's variable into an axisymmetrical modification of Van Driest's equation.

Of the five modern hypotheses investigated, three (the two-dimensional, the streamline, and the derivative) have been found adequate when used within their specified limits of use only for large values of a and consequently smaller values of y/a. When studies are required over a larger range of values of radius, a, and consequently y/a, the Rao and the local similarity hypotheses have been found to be superior.

All the presented methods have been found somewhat inaccurate in predicting the velocity distribution in comparison with experimental results for low values of a^+. Patel (24) proposed that there was a definite limit that can be imposed on a turbulent boundary layer by transverse curvature effects without destroying the essential equilibrium that exists between the production and dissipation of turbulent kinetic energy in the wall region and thereby provoking relaminarisation. Patel proposed that this limiting value of a was about 28. Rao and Keshaven (20) also proposed a relaminarisation in terms of R_a less than 15,000.

CHAPTER 2

THE VELOCITY DEFECT LAW AND THE WALL OF THE WAKE

2.1.0 INTRODUCTION

Presently no agreement exists regarding the appropriate similarity laws, the law of the wall and the velocity defect law, for the mean flow in a axisymmetrical boundary layer with no pressure gradient. In contrast with the axisymmetric wall law, very little attention has been given to the axisymmetrical velocity defect law. This chapter presents the various proposals for modification of the two-dimensional velocity defect law to take into account the transverse curvature effect.

As can be seen in Table 2.1, previous studies on the velocity defect law can be classified according to four major approaches. Three of these methods are based on modification of the classical two-dimensional velocity defect law

$$\frac{U - u}{u_*} = B_1 \log \left(\frac{y}{\delta}\right) + B_2 \qquad (2.1)$$

with respect to variation in the empirical constants B_1 and B_2. Chin et al (11) suggested using modifications of the constants to values which were obtained by curve-fitting his experimental data. Yu (10) stated that B_2 was a function of R_a, the Reynolds number based on the cylinder radius a. Willmarth and Yang (17) & Willmarth et al (14), Afzal and Narasimha (12), and Afzal and Singh (13) stated that B_2 was a function of δ/a where δ was the displacement thickness. For these three methods the authors plotted the experimental velocity defect in the two-dimensional form of $U - u/u_*$ versus y/δ. However, only three reports (Ref. 10, 11, and 12) actually suggested values for the constants (see Table

Hypothesis	Author (Ref.)	$(U-u)/u_*$
1. Two-Dimensional	Chin et al (11)	$f(\frac{y}{\delta})$
2. Yu's	Yu (10)	$f(\frac{y}{\delta}, R_a)$
3. Willmarth and Yang's	Willmarth and Yang (17) Willmarth et al (14) Afzal and Narasimha (12) Afzal and Singh (13)	$f(\frac{y}{\delta}, \frac{\delta}{a})$
4. Rao and Keshaven's	Rao and Keshaven (19)	$f(\frac{ru_*}{\nu}, R_a)$

Table 2.1 Various Hypotheses for Velocity Defect Laws in Functional Form

2.2). In the fourth method Rao and Keshaven (20) found that there was not any similarity when the velocity defect curves were plotted against y/δ but similarity was obtained for each R_a value when plotted against a local Reynolds number, r_*. No velocity defect law was suggested in Ref. (20).

In the following sections the various methods will be examined in comparision with experimental results to find any restrictions that may exist on their respective utilization. Discussions will include the justification of the various authors and their criticisms of the competing approaches. As the various methods are based on the two-dimensional defect law, a brief discussion of that law will first be given for comparative purposes.

This chapter also deals with the existance of a specific outer layer eddy viscosity, enabling calculation of velocity profiles as was examined by Cebeci (28 and 35) and Sparrow et al (26). Their observations are compared with White (21 and 22) who stated, without substantiation, that no law of the wake or velocity defect law was necessary for thick axisymmetrical boundary layers as no portion of a truly thick axisymmetrical velocity profile existed that was not wall-related. The validity of this statement will be examined.

2.2.0 DISCUSSION OF COMPETING HYPOTHESES

2.2.1 The Two-dimensional Velocity Defect Law

For flow along a flat plate it is necessary to treat the two-dimensional turbulent boundary layer as a composite layer consisting of inner and outer regions. For turbulent boundary layers there is no single dimensionless y co-ordinate that collapses all the velocity profiles into a single curve because the viscous-dependent part of the

Proposed Law	Hypotheses	Constants B_1	Constants B_2	Variable Range
$\frac{U-u}{u_*} = B_1 \log(\frac{y}{\delta}) + B_2$	1. Two-Dimensional	$-\frac{2.3}{k}$	2.5	$k=.41$; $\frac{y}{\delta}<.15$
		$-\frac{2.3}{k}$		$k=.267$; $\frac{y}{\delta}>.15$
	Chin et al (11)	- 4.485	$.925(2-w)$	$w=1 - \cos(\frac{y}{\delta})\pi$
	2. Yu (10)	- 5.75	$f(R_a)$	length scale L was used instead of δ R_a-15,250 to 45,060 B_2- -5.82 to -5.37
	3. Afzal and Singh (13)	- 5.5	$f(\frac{\delta}{a})$	$\frac{x}{a}$ - 54 to 150 $B_2=2.5 - 72\frac{\delta}{a}$; $\frac{\delta}{a}<2$

Table 2.2 Velocity Defect Laws

profile and the Reynolds-stress-depedent part of the profile require different length scaling parameters.

The inner region which contains 10 to 20 % of the entire boundary layer thickness can be divided into three sections as indicated in Fig. 2.1 : 1) the viscous sublayer, 2) the transition region, and 3) the fully turbulent region. The outer region contains the remaining 80 to 90 % of the boundary layer thickness. In the outer portion of the turbulent boundary layer the Reynolds stresses dominate the viscous stresses to produce the velocity profile. According to experiments it was observed that the mean velocity distribution in the outer region can be described by the velocity defect law (see Fig.2.2)

$$\frac{U - u}{u_*} = f(\frac{y}{\delta}) \qquad (2.2)$$

This equation is invalid close to the wall, where the viscosity becomes important. Therefore, the flow must depend on a Reynolds number ($\delta u_*/\nu$) as well as the ratio (y/δ). The velocity defect law does overlap into the fully turbulent region where the logarithmic law of the wall

$$\frac{U}{u_*} = \frac{2.3}{k} \log (\frac{u_* y}{\nu}) + A_2 \qquad (2.3)$$

applies. A logarithmic relation for the right side of Eqn. 2.2 can be obtained by assuming that the Eqn. 2.3 will give u=U if $y = \delta$ and A_2 is modified. Then by subtraction one obtains

$$\frac{U - u}{u_*} = \frac{-2.3}{k} \log (\frac{y}{\delta}) + B_2$$

where k and B_2 are empirical constants.

A semilogarithmic plot of velocity defect data for zero

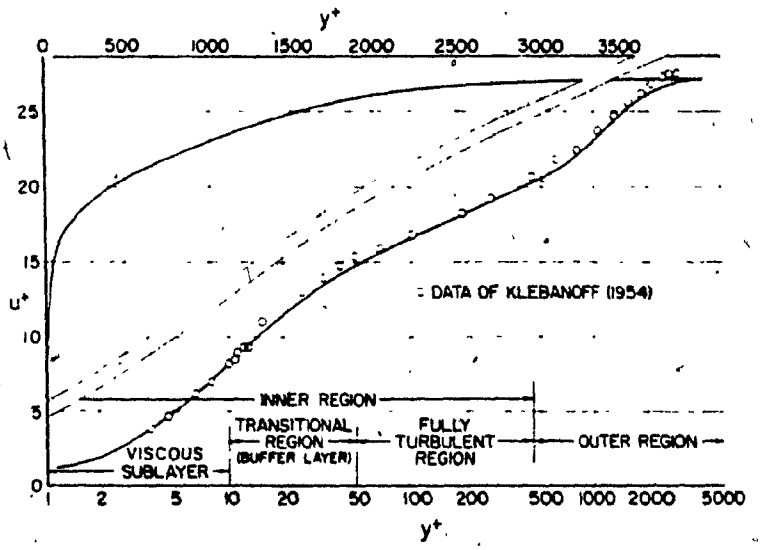

Fig. 2.1 Semilogarithmic and Linear Plots of Mean Velocity Distribution Across a Turbulent Boundary Layer with Zero Pressure Gradient. The Linear Plot is Included to Show a True Picture of Various Portions. (Ref. 46)

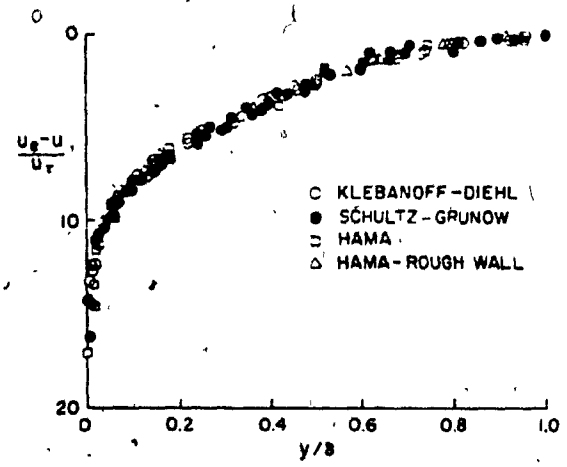

Fig. 2.2 Universal Plot of Turbulent Boundary Layer Profiles in Zero Pressure Gradient. (Ref. 46)

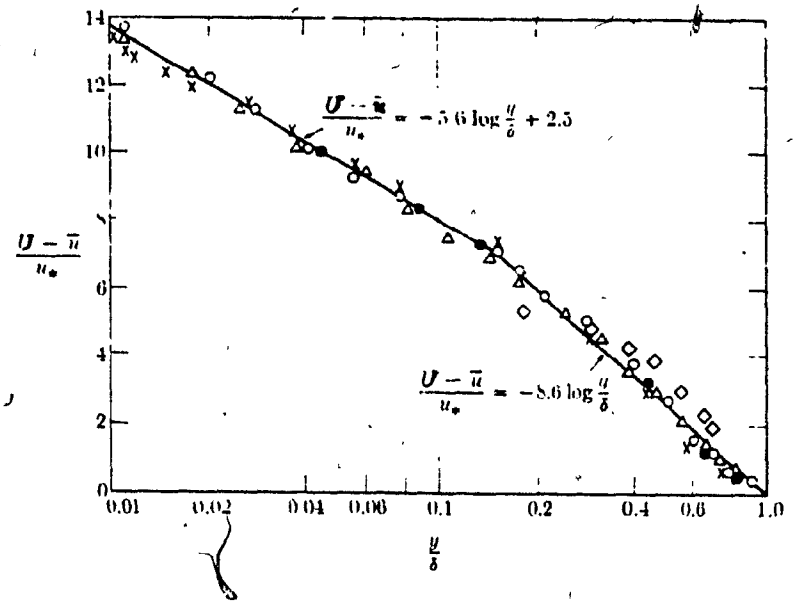

Fig. 2.3 Velocity Defect Plot With Experimental Data From Various Sources (Ref.47)

pressure gradient flow along flat plates can be seen in Fig. 2.3. Although the experiments closely correlate on the velocity defect basis, a single logarithmic equation does not fit the data over the entire bounday layer. One equation is necessary for the inner region overlapping with the law of the wall equation, while a second approximates the outer region. Therefore, if k=0.41 and B_2=2.5 then

$$\frac{U - u}{u_*} = -5.6 \log \left(\frac{y}{\delta}\right) + 2.5 \quad ; \quad \frac{y}{\delta} < 0.15 \qquad (2.4)$$

and when k=0.267 and B_2=0

$$\frac{U - u}{u_*} = -8.6 \log \left(\frac{y}{\delta}\right) \quad ; \quad \frac{y}{\delta} < 0.15 \qquad (2.5)$$

2.2.1a Chin's Variation

In the study of the axisymmetric turbulent boundary layer, Chin et al (11) started with Coles (45) two-dimensional law which is

$$\frac{U - u}{u_*} = -2.5 \ln \left(\frac{y}{\delta}\right) + 1.38(2-w) \tag{2.6}$$

where $w=1-\cos(y/\delta)$ and did a curve fitting (Fig. 2.4) to better reflect the effect of wall curvature on the profile shape for their experimental data. They therefore suggested the following velocity defect law for the single cylinder that was tested

$$\frac{U - u}{u_*} = -1.95 \ln \left(\frac{y}{\delta}\right) + 0.925(2-w) \tag{2.7}$$

where w has the same definition as above. They did not check if this equation would change for other cylinder radii.

2.2.2 Yu's Hypothesis

Among the first to study axisymmetrical flow was Yu (10), who assumed that the similarity laws for a circular cylinder with radius a were dependent upon the radius Reynolds number, R_a. Therefore, the velocity defect law proposed in functional form was

$$\frac{U - u}{u_*} = f\left(\frac{y}{L}, \frac{Ua}{\nu}\right) \tag{2.8}$$

where L was the length scale. The resulting equation was

$$\frac{U - u}{u_*} = -B_1 \ln\left(\frac{y}{L}\right) + B_2 \tag{2.9}$$

in which B_1 is independent of R_a and where

$$L = \frac{e^{\sigma/k}\nu}{u_*} \tag{2.10}$$

and

$$\sigma = \frac{U}{u_*} \tag{2.11}$$

From his experimental mean velocity distributions, Yu found

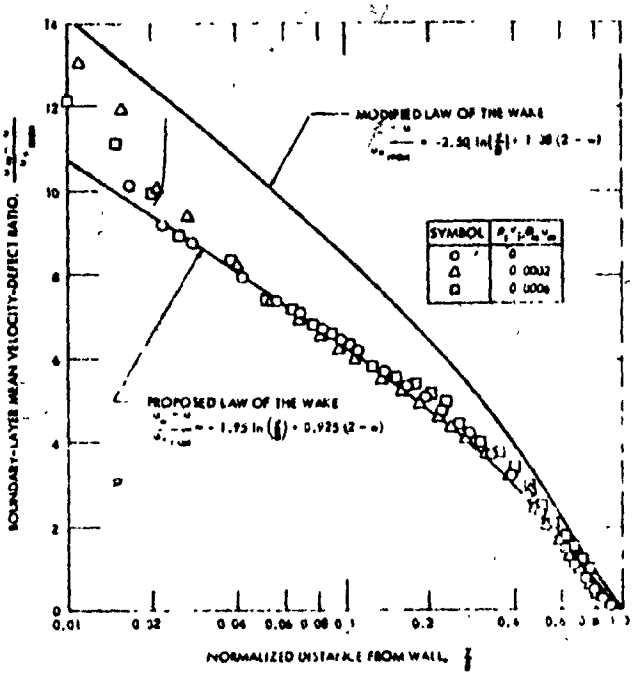

Fig. 2.4 Velocity Defect Law (Ref. 11)

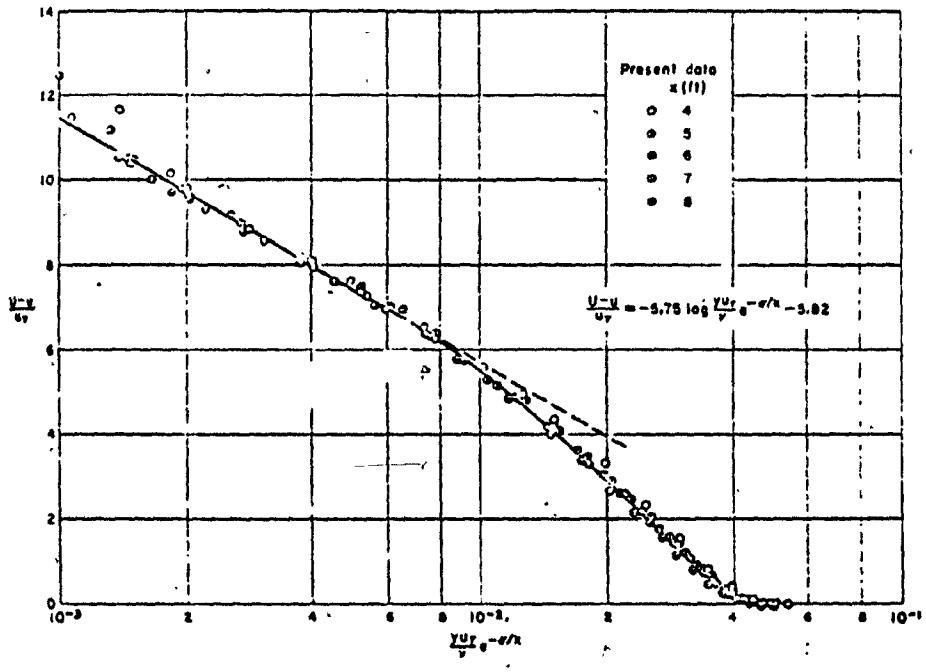

Fig.2.5 Velocity Defect Law With R_a=15,250 (Ref. 10)

that similarity did not seem to exist until a section 1.2192 meters from the nose of the cylinder. Mean velocity data for the outer region at sections 1.2192 to 2.4384 meters were plotted on semi-logarithmic paper according to Eqn. 2.9 as shown in Figs. 2.5 to 2.7. The linear region on the semi-log graph was well defined in the outer law plots with a slight scattering of their data , otherwise they would collapse on one profile for their respective R_a values.

2.2.3 Willmarth and Yang's Hypothesis

Willmarth and Yang (17) state that if the amount of transverse curvature is not large, the most logical approach might be to assume that the usual two-dimensional law of the wall and the velocity defect law are still valid but with consideration given to an additional dimsional length parameter, a, the cylinder radius. Therefore, with the addition of parameter a, the velocity defect law in functional form would be

$$\frac{U - u}{u_*} = f(\frac{y}{\delta}, \frac{\delta}{a}) \qquad (2.12)$$

They state that possibility the traditional division of mean flow properties into wall and wake regions might not be valid when the transverse curvature is large, $\delta/a \gg 1$. Visualizing a very small radius of wall curvature, the region occupied by fluid motions obeying the law of the wall is always a very small fraction of the region occupied by the turbulent boundary layer flow. In other words they propose that the boundary layer on a slender rod ($a/\delta \to 0$) be considered all wake-like flow. The region near the wall (which, if it is called the wall region, must be independent of free stream conditions) would be a very small

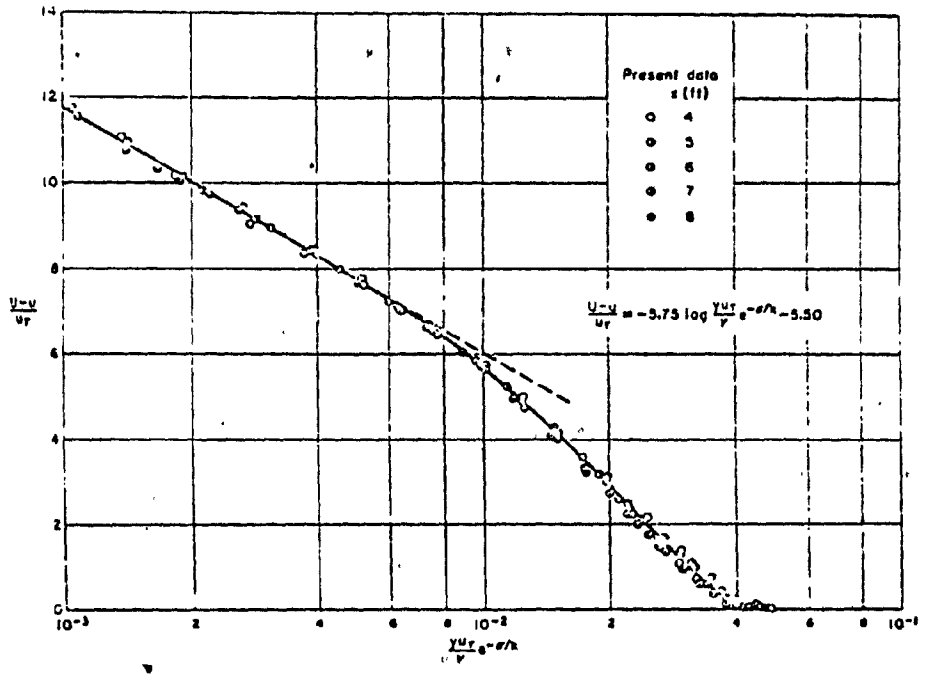

Fig. 2.6 Velocity Defect Law With R_a=30,740. (Ref. 10)

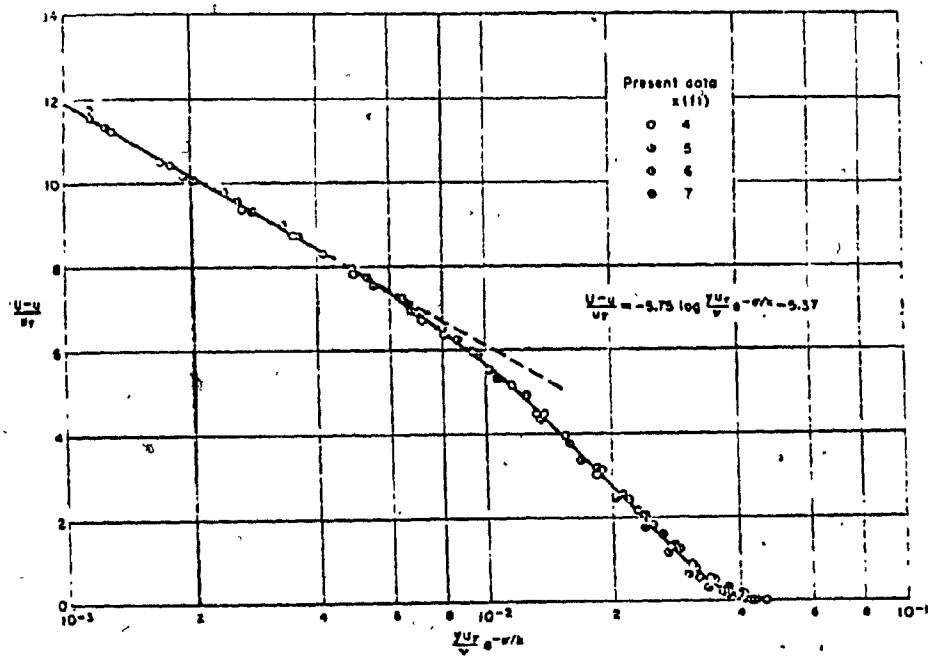

Fig. 2.7 Velocity Defect Law With R_a=45,060. (Ref. 10)

region containing the viscous sublayer. They state that it is possible that in the limit (at $a/\delta=0$) the wall region contains only the viscous sublayer. As their work was restricted to boundary layers in which $\delta/a=2$, they felt that their modified wake region equation relationship was valid.

2.2.3.a Willmarth et al's Application

In a later study, Willmarth et al (14) state that from the geometry of the boundary layer flow along a cylinder it is apparent that as the cylinder radius, a, decreases, the perimeter of the boundary layer adjacent to the wall becomes small in comparision to the perimeter at $y=\delta$, adjacent to the free stream. Therefore, when δ/a is large the wakelike outer portion of the mean velocity profile should have a structure quite independent of the wall region. They found that almost the entire profile apparently obeyed the two-dimensional wall law for values of $\delta/a < 9.4$ in Fig. 2.8. It was also observed in Fig. 2.8 that for the cylinders of smaller diameter the profiles depart from the log portion by falling below it. Yet, in analogy with two-dimensional flow with zero pressure gradient, the wakelike outer flow should obey a defect law and suggest the same functional form as Willmarth and Yang (17). The velocity defect is plotted in Fig. 2.9 as a function of y/δ as in the two-dimensional case for a representative set of eight profiles with values of δ/a ranging from 1.8 to 42.5. For large δ/a the profiles are very full with a small velocity defect. For small values of δ/a the defect profiles approach the flat plate universal data shown by the solid line.

2.2.3.b Afzal and Narasimha's Application

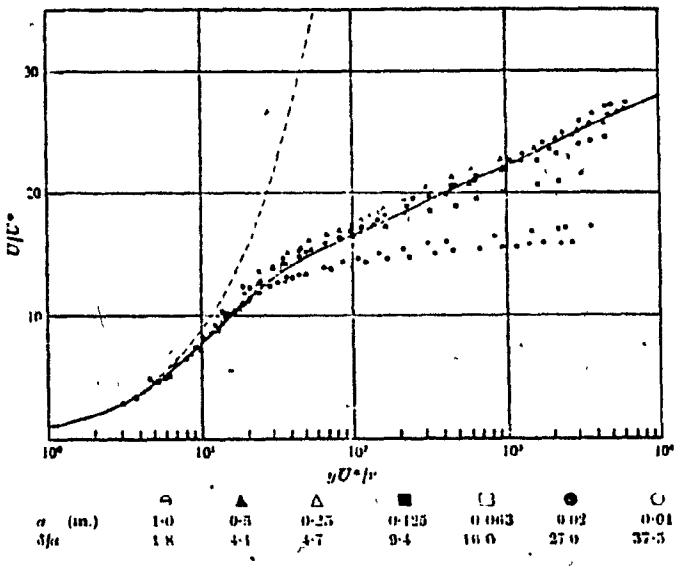

Fig. 2.8 Seven Velocity Profiles in Wall Co-ordinates Showing the Influence of Increasing Transverse Curvature. —— , Flat Plate, ----, Eqn.1.35 , $a^+ = 33.4$ (Ref. 14)

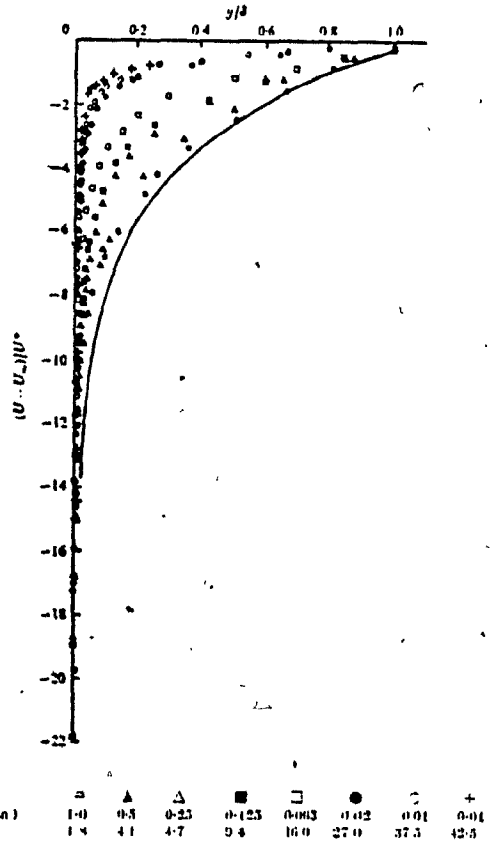

Fig. 2.9 Eight Velocity Defect Profiles Showing the Influence of Increasing Transverse Curvature. —— Flat plate. (Ref. 14)

Afzal and Narasimha (12) examination of available experimental data from various sources (Richmond (15), Willmarth and Yang (17), and Rao and Keshaven(20) when plotted in the two-dimensional defect law co-ordinates, as can be seen in Fig. 2.10 to 2.12 respectively, reveal the clear existence of a substantial logarithmic region. Previously a logarithmic outer law region had been reported by Yu (10) and Chin et al (11). Therefore, Afzal and Narasimha (12) state that all available measurements overwhemingly appear in favour of a logarithmic law in classical defect co-ordinates. Unlike the two-dimensional case the value of their intercept D (D is equivalent to B_2) was not a universal constant. They suggest that to the lowest order D could be a function of δ/a. To verify this hypothesis the values of the intercept from the various sources previously mentioned and that of Afzal and Singh (13) were plotted against δ/a in Fig. 2.13. As δ/a approaches zero the values of D approaches the flat plate value. From the above results it follows that the classical defect law can therefore describe axisymmetric turbulent boundary layers provided that $1/a^+$ and δ/a are small. For moderately small values of $1/a^+$, and δ/a of order unity the intercept in the defect law seems to depend on δ/a.

Rao and Keshaven (20), on the basis of their own measurements, however have concluded that the two-dimensional defect law co-ordinates do not show any promise. Afzal and Narasimha (12) dispute this. They attribute the scatter of the formers data points for the same R_a and δ/a as shown in Fig. 2.12 to the artifically tripped boundary layer (20). In view of the known slow recovery of boundary layers from the effects of tripping devices, they claim it is likely that at least the

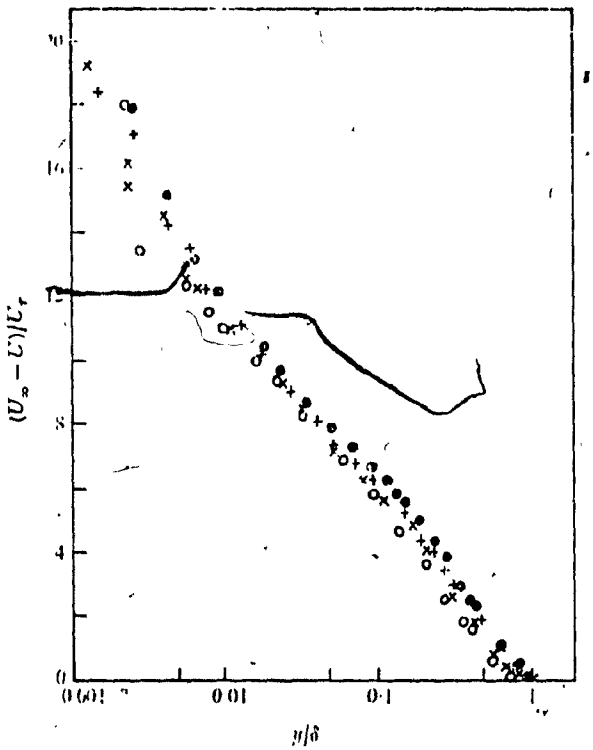

Fig. 2.10 Velocity Defect Law: Willmarth & Yang's Measurements
R_a=70,200 : o ,x 7.135m, x,x 9.7536m ;
R_a=134,000 : • ,x 7.135m, + ,x 9.7536. (Ref.12)

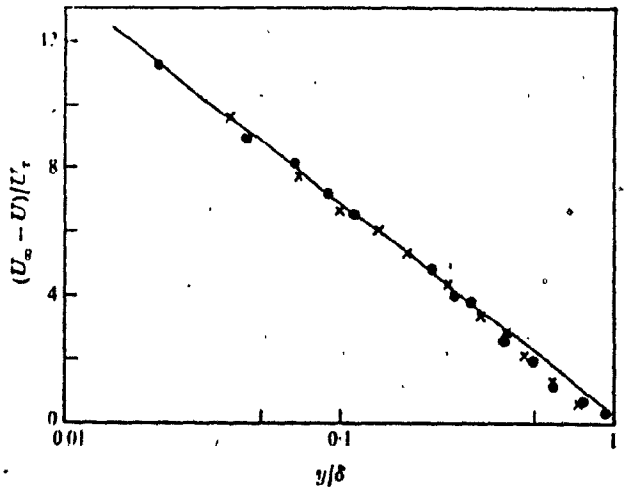

Fig. 2.11 Velocity Defect Law: Richmonds Measurements.
R_a=40,200 : × ,x 2.4384m, • ,x 3.048m. (Ref.12)

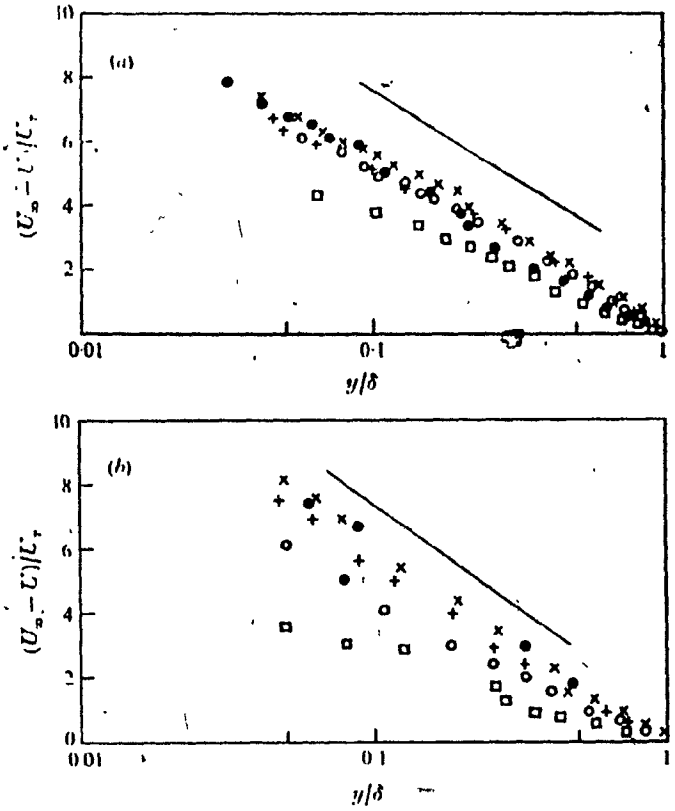

Fig. 2.12 Velocity Defect Law: Rao & Keshaven Measurements. (a) R_a = 3940. (b) R_a =825.•,x 50.8cm,×,x 39.37cm,+,x 29.21cm,o, x 21.59cm,□,x 7.62cm. (Ref. 12)

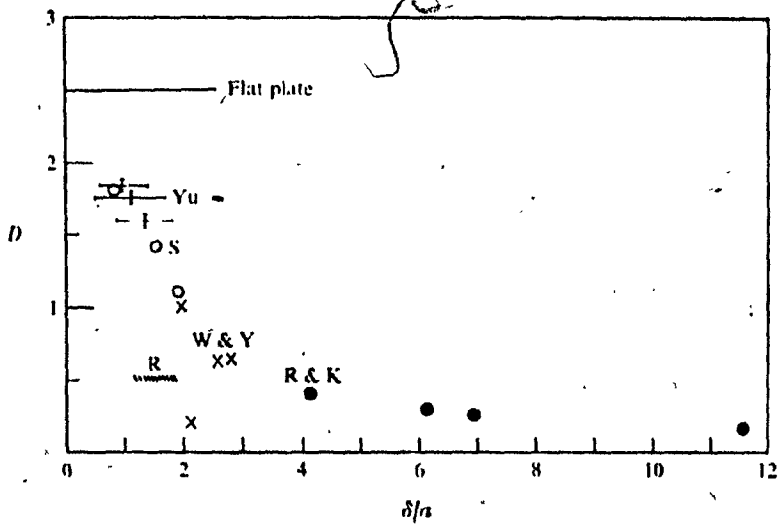

Fig. 2.13 Variation of Additive Term in Velocity Defect Law with Respect to δ/a. (Ref. 12)

initial stations the boundary layers may have not acheived a natural state. This would also explain negative wake components on Rao and Keshaven's wall law plots at the initial stations. Afzal and Narasimha (12) also commented that even though Rao and Keshaven (20) had found that for a given R_a, the velocity defect $(U-u/u_*)$ yeilds similarity in terms of the variable r_*, based on the radius r=a+y, their wall and defect laws cannot be matched as can be seen in Fig. 2.12. Therefore, a skin friction law does not follow and Rao's law is not complete.

Afzal and Narasimha (12) concluded that except in those extreme situations where a^+ is small (in which case the boundary layer may not be in a fully developed turbulent state anyway), the simplist analysis of axisymmetrical flow would utilize the two-dimensional laws but with parameters that are dependent on a^+ and δ/a for the inner and outer laws respectively. Using the equations of asymptotic expansions they formulated a velocity defect law valid for conditions when $a^+ >> 1$ which was given by

$$\frac{U-u}{u_*} = -\frac{1}{k}\ln\left(\frac{y}{\delta}\right) + D\left(\frac{\delta}{a}\right) + O(1) \qquad (2.13)$$

where k and D are constants and O(1) is the order of error.

2.2.3.c Afzal and Singh's Application

Afzal and Singh (13) utilized the velocity defect equation previously derived by Afzal and Narasimha (12). When the former plotted $(U-u/u_*)$ versus y/δ as seen in Fig. 2.14 no universal line was obtained. The parallel shift was explained as a function of δ/a. The variable in the additive constant D in the velocity law is shown in Fig. 2.15 with the flat plate value of D being equal to 2.5 obtained from Hinze

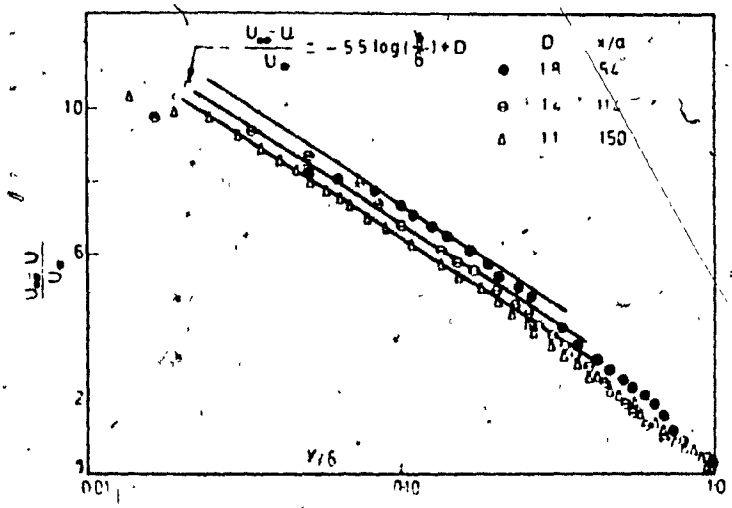

Fig. 2.14 Semi-log Plot For Velocity Defect Region, R_a=14,200. (Ref. 13)

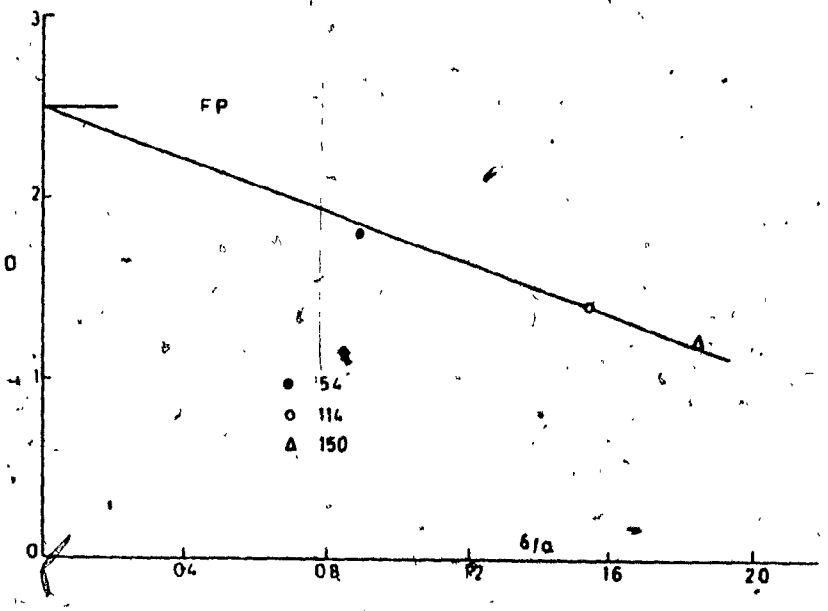

Fig. 2.15 Variation of Additive Constant in Velocity Defect Law With δ/a, R_a=14,200. FP (Flat Plate). Solid Line Represents the Proposed Correlation D=2.5 - 0.72δ/a. (Ref. 13)

(48). Therefore, for their experimental data for $\delta/a < 2$, they present the correlation expression

$$D = 2.5 - 0.72 \frac{\delta}{a} \tag{2.14}$$

which they state is also consistent with all previous work. Therefore, if Eqn. 2.14 is substituted into Eqn. 2.13 the velocity defect is

$$\frac{U - u}{u_*} = -5.5 \log \left(\frac{y}{\delta}\right) + 2.5 - 0.72 \frac{\delta}{a} \tag{2.15}$$

2.2.4 Rao and Keshaven's Hypothesis

Rao and Keshaven (20) investigated the velocity profiles measured farther downstream of the marginal profile (explained in section 2.3.2) for the existance of similarity. A check on the two-dimensional form, $(U - u)/u_*$ versus y/δ did not seem promising. They state that since the turbulent boundary layer is already under the influence of R_a, similarity can be sought using two techniques. First, with R_a fixed, similarity may exist in terms of some suitably formed Reynolds number which includes the outer flow variables. The second possibility is that similarity might exist for all values of R_a at a given value of the local Reynolds number, r_*. The first technique with r_* plotted versus $(U - u)/u_*$ in Fig. 2.16 and 2.17 reveals that similarity exists only for the various individual R_a values. No similarity was obtained in terms of the generally used geometric parameters y/δ, r/r_δ, δ/a, and r_δ/a when the velocity defect at various values of R_a was plotted.

They reason that the difference between axisymmetrical and two-dimensional flow is the penetration of the wall shear to regions farther from the wall in the former case. For axisymmetrical flows near the wall $\tau = \tau_w a/r$ and for two-dimensional flows near the wall $\tau = \tau_w$. These

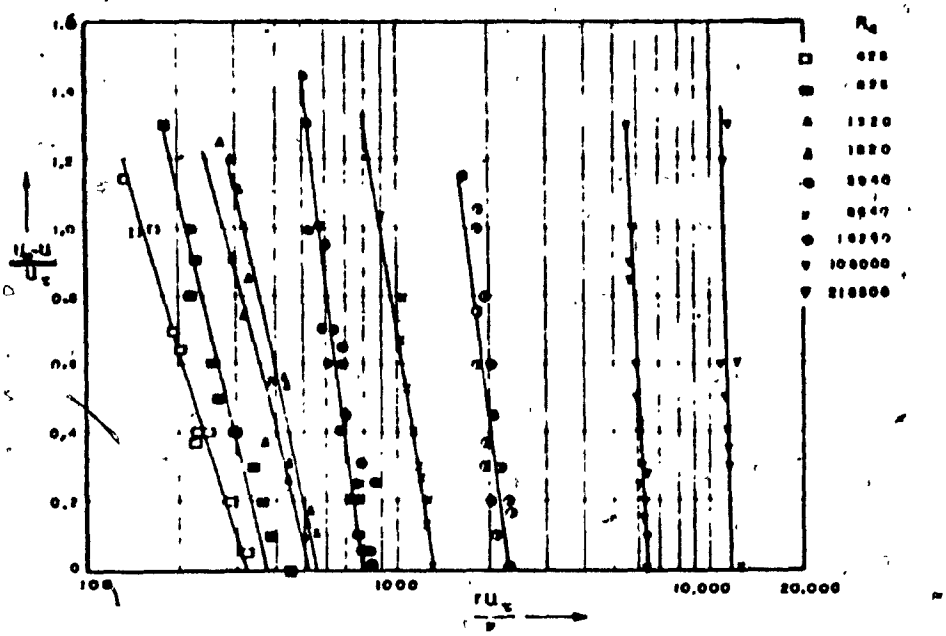

Fig. 2.16 Correlation in Outer Portion. (Ref. 20)

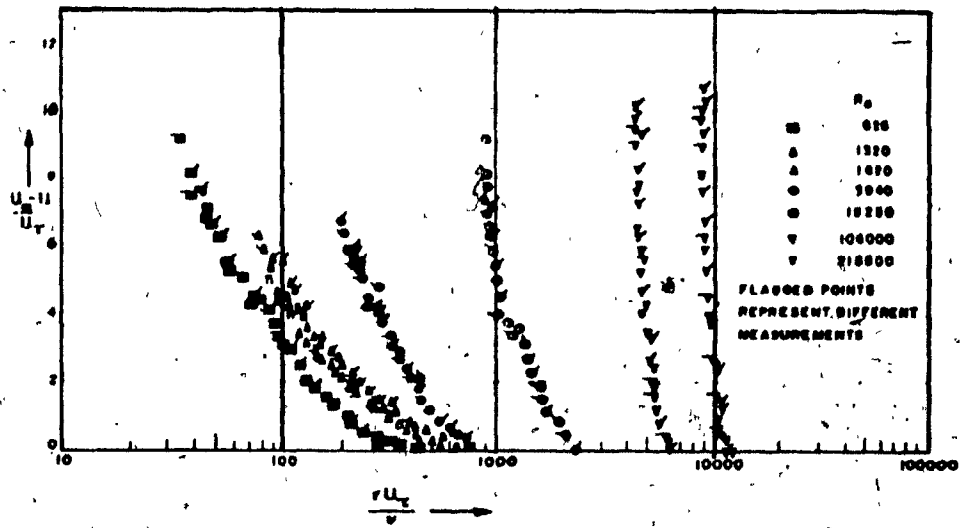

Fig. 2.17 Correlation of Defect versus ru_τ/ν Across Boundary Layer. (Ref. 20)

expressions indicate that the reduction in the viscous stress away from the wall is not fully compensated by the corresponding increase in Reynolds stress in axisymmetrical flows as is the case in two-dimensional flows.The net effect is the existance of a shear gradient, which can be expected to accentuate viscosity to regions farther away from the wall than in two-dimensional flow. This viscosity effect becomes progressively marked as the thickness of the boundary layer increases in comparision with the radius. When the entire axisymmetrical turbulent boundary layer is affected by the viscosity throughout, it is not a pure turbulent boundary layer.

2.3.0 AXISYMMETRCAL WAKE

2.3.1 Existance of the Axisymmetrical Wake

Cebeci (35) states that it has been well established that at sufficiently high Reynolds numbers a turbulent boundary layer has a wake component. For two-dimensional flows the lower limit for this Reynolds number, R_θ, is approximately 5000. According to Coles (32) the wake component varies with R_θ in the range 425 to 5000 becoming zero at R_θ=425 (see Fig. 2.18). Recent studies (Ref. 18, 49, 50, and 51) confirm this result. Cebeci (35) assumes that for axisymmetrical flows that the trend is the same and that a wake component exists. For two-dimensional flows the wake region in Fig. 2.19 can be seen rising above the solid line, representing the law of the wall, for large values of y^+. In two reports, Cebeci (28 and 35) assumed the two-dimensional eddy viscosity for the outer region

$$\varepsilon_0=\alpha u_e \delta_{k^*} \gamma \qquad (2.16)$$

which is assumed to be constant except for the intermittency factor γ,

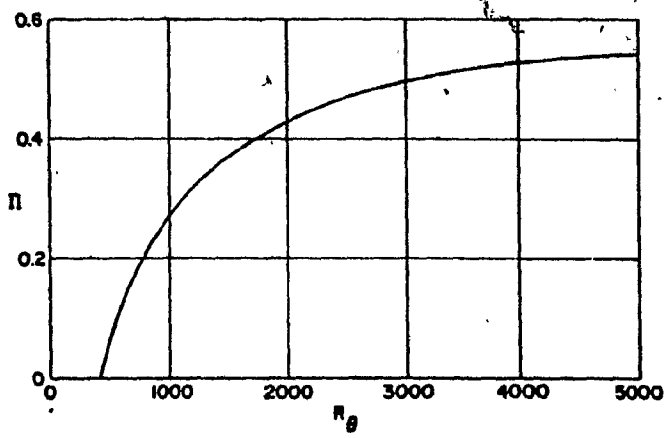

Fig. 2.18 Variation of Cole's profile parameter Π with Momentum Thickness Reynolds number R_θ for Zero Pressure Gradient (Ref. 46)

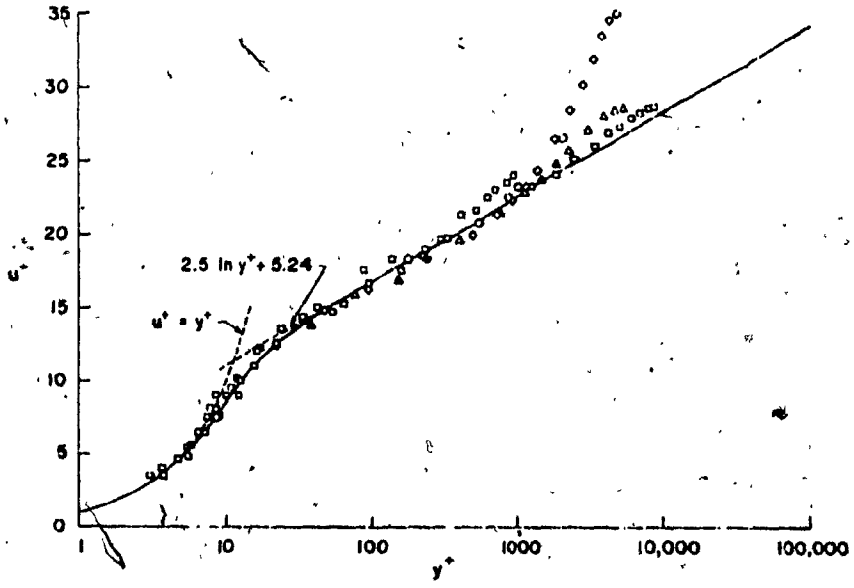

Fig. 2.19 Mean Velocity Distribution (Ref. 46)

$$\gamma = 1 + 5.5 \left(\frac{y}{\delta}\right)^{6^{-1}} \tag{2.17}$$

In Eqn. 2.16 the kinematic displacement thickness is

$$\delta_k^* = \int_0^\infty 1 - \left(\frac{u}{u_e}\right) \, dy \tag{2.18}$$

The parameter Ω in Eqn. 2.16 is an universal constant at high Reynolds numbers; at low Reynolds numbers (R_{θ_k} <5000), it varies in accordance with Eqn. 2.19

$$\Omega = 0.0168(1.55/(1 + \Pi)) \tag{2.19}$$

where

$$\Pi = 0.55(1 - \exp(-0.243\beta^{\frac{1}{2}} - 0.298\beta)) \tag{2.20}$$

$$\beta = (R_{\theta_k}/425) - 1 \tag{2.21}$$

For two-dimensional incompressible flows, a complete velocity distribution excluding the sublayer and the transition region across the boundary layer can be described by Coles (32) law of the wall and wake expression which is

$$U^+ = \frac{1}{k} \ln y^+ + c + \frac{\Pi}{k} w \left(\frac{y}{\delta}\right) \tag{2.22}$$

where k and c are constants. For a flat plate flow, the profile parameter Π is a constant equal to 0.55, provided that R_θ>5000. At Reynolds numbers less than this value, it varies according to Eqn. 2.20. The addition of $\frac{\Pi w}{k} y$ to the law of wall is a correction for the velocity distribution given by the law of the wake.

For axisymmetrical boundary layers, Cebeci (35) considered the experimental data of Richmond (15), for incompressible flows past slender cylinders of various diameters, in the co-ordinates proposed by Rao

(19) which is (u, Y^+) where $Y^+ = a^+ \ln(r^+/a^+)$. The velocity profiles in Fig. 2.20 for a 0.06096 cm. (0.024 inches) diameter cylinder at R_θ = 2100 and for a 2.54 cm. (1 inch) diameter cylinder at R_θ = 8750, reveal that the former has no wake componet while the latter does have one. Calculations for the former show that its entire boundary layer was represented with only the inner layer eddy viscosity expression so that the entire velocity profile was represented by the law of the wall . Calculations for the latter revealed the necessity of the use of both inner and outer layer eddy viscosities so that the velocity distribution was given with both the law of the wall and the law of the wake.

For axisymmetrical flows Cebeci (35) felt that Ω should be expressed as a function of the two-dimensional definition of the momentum thickness Reynolds number, R_θ, because Π decreases with decreasing R_θ, and Ω in Eqn. 2.19 increases, making the wake component smaller. As a result Cebeci (35) uses the two-dimensional definition for the outer eddy viscosity formula for thick axisymmetrical boundary layers.

For thick axisymmetrical turbulent boundary layers excluding the sublayer region White (21 and 22) utilize Rao's law of the wall

$$U^+ = 2.5 \ln (Y) + 5.5 \qquad (2.23)$$

where

$$Y = a^+ \ln \left(\frac{r}{a} \right) \qquad (2.24)$$

Cebeci (21) pointed out that neglecting the wake contribution leads to appreciable errors that may be especially noted for large cylinders and suggested that White take the wake into account and change Rao's equation to

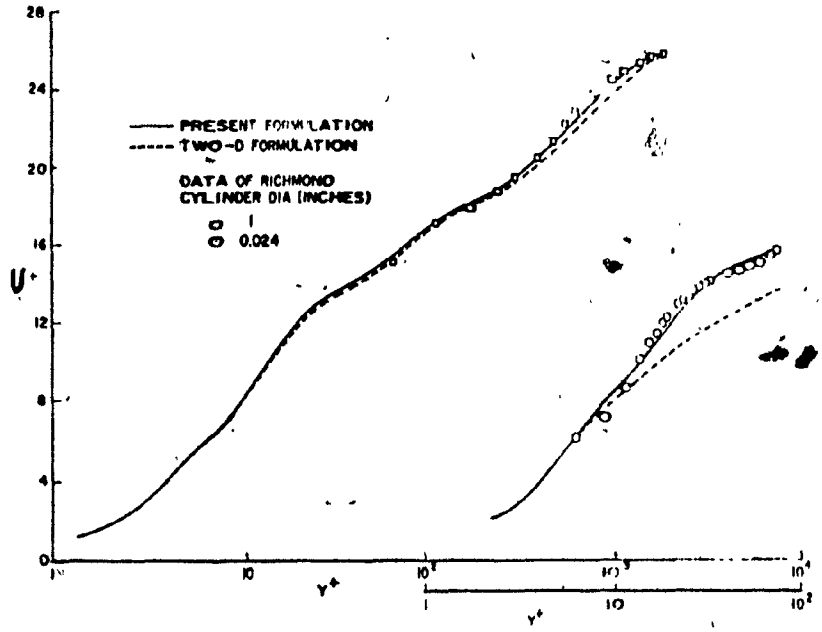

Fig. 2.20 Velocity Profile Comparision (Ref.35)

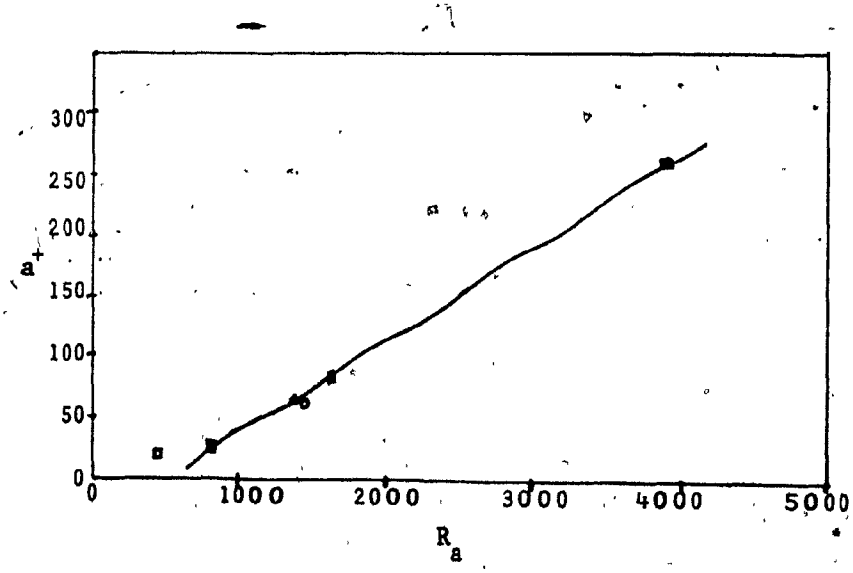

Fig. 2.21 Marginal value a^+ versus R_θ (Ref. 20)

$$U^+ = 2.5 \ln Y + 5.5 + \frac{G\,Y}{k\,Y_{max}} w \qquad (2.25)$$

where k and G are constants and $w=2\sin^2(\pi y/2)$ according to Coles (32). White's rebuttal, which he admits suffers from a large credibility gap, was that there is no law of the wake in a thick axisymmetrical boundary layer for turbulent flow. He suggested that the parameter G in Eqn. 2.25 uniformly vanishes as the cylinder boundary layer becomes thicker and that there is no portion of a truly thick cylinderical velocity profile which is not wall related. By a thick layer he means when $a^+ \ll 1000$, while flows with $a^+ > 1000$ are effectively two-dimensional and do show a wake.

2.3.2 Negative Wake and Marginal Profiles

Rao and Keshaven (20) reported that at low values of R_a their velocity profiles obtained through their wall law

$$U^+ = 2.5 \ln (a^+ \ln (\tfrac{r}{a})) + 5.5 \qquad (2.26)$$

revealed a negative wake component initially as the flow developed in the downstream direction. At a certain position in the axial direction, all the negative wake portion apparently disappeared. They termed the velocity profile corresponding to this condition as the " marginal profile ". Farther downstream, positive wake components similar to the two-dimensional wake components appeared developing with the flow in the downstream direction. The value of the friction Reynolds number, a^+, at which the marginal profile appeared was plotted against R_a in Fig. 2.21. The variationappears to be linear except at very low values of R_a. All their experimental velocity profiles confirmed that when the local value of a^+ is less than the marginal value a positive wake compon-

ent appears.

The axial extent of the flow which exhibited the negative wake was confined only to the first two or three stations in the test section at the lower R_a values. The disappearance of the negative wake at higher R_a values was extremely rapid and therefore they assume that the axisymmetrical turbulent boundary layer starts with the marginal profile, if R_a is more than 5000. The appearance of such marginal profiles at low R_θ values in the two-dimensional flows has been discussed by Coles (32). A plot of the measured R_θ of the marginal profiles versus R_a in Fig. 2.22 reveal that their measurements tend to the two-dimensional R_θ value of about 500 given by Coles as $R_a \to \infty$.

Afzal and Narasimha (12) state that the negative wake components on Rao and Keshaven's wall law plots at the intial stations were a result of the experimental data being obtained by artifically tripping the boundary layer. The initial stations may not have reached a natural state because of the known slow recovery of boundary layers from tripping devices.

The point of departure of the wake portion from the logarithmic portion is also of interest in predicting the wake portion. It was observed that while B (which is equivalent to constant A_2) increased in the downstream direction, the point of departure in terms of Y^+ decreased and the product BY^+ tended to be constant at a particular R_a. A few trials indicated that better correlation is obtained if KBY^+ was plotted against R_a which is shown in Fig. 2.23.

2.4.0 ALTERNATE OUTER LAYER VELOCITY EQUATION

Sparrow et al (26) did not suggest any velocity defect law nor

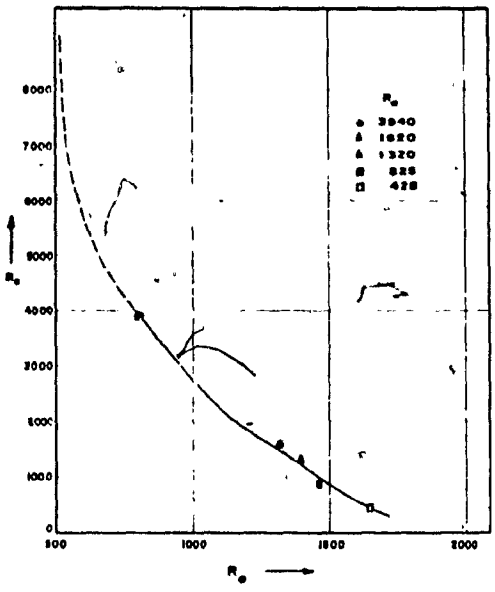

Fig. 2.22 Critical Value of Momentum Thickness Reynolds Number for No Wake Rortion in the Law of the Wall. (Ref. 20)

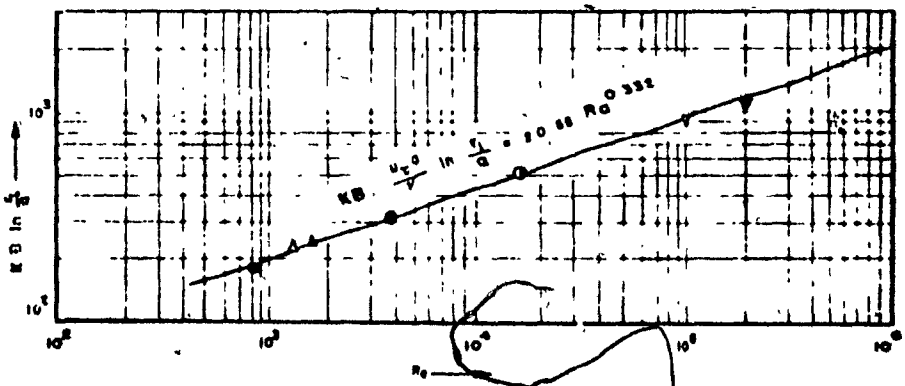

Fig. 2.23 Radial Distance at Which Outer Region Departs from Log. Line. (Ref. 20)

did they draw specific plots for the outer region but they did obtain the velocity profiles in the outer region away from the wall through utilization of Diessler's(1) two-dimensional turbulent eddy viscosity relationship

$$\varepsilon = K^2 \frac{(du/dy)^3}{(d^2u/dy^2)^2} \tag{2.27}$$

where K^2 was a constant of proportionality determined experimentally. This equation indicates that ε, the mechanisms for the turbulent transfer of momentum at a point away from the wall, can be considered to be dependent only on the derivatives of the velocity with respect to distance from the wall. In other words, on the velocities in the vicinity of the point relative to the velocity at the point, and to be unaffected by the velocity relative to the wall or the distance from the wall. In dimensionless form the equation 2.27 becomes

$$\frac{\varepsilon}{\nu} = \frac{\varepsilon}{\mu\ \rho} = K^2 \frac{(du/dy)^3}{(d^2u/dy^2)^2} \tag{2.28}$$

where K is an empirical constant equal to 0.36. Within a turbulent boundary layer the expression relating the time averaged shear stress, , and the velocity gradient is

$$\tau = (\mu + \rho\varepsilon)\frac{du}{dy} \tag{2.29}$$

The first term within the parentheses in Eqn. 2.29 represents the laminar contribution to the shear, while the second term represents the turbulent contribution. Eqn. 2.29 can also be written as

$$\frac{\tau}{\tau_w} = (1 + \frac{\varepsilon}{\nu})\ \frac{du^+}{dy^+} \tag{2.30}$$

Using the shear stress distribution for a circular cylinder given by

$$\frac{\tau}{\tau_w} = \frac{a}{a + y} \tag{2.31}$$

and integrating Eqn. 2.30 once Sparrow et al (26) obtained the following differential equation for the velocity distribution away from the wall

$$dy^+ = \frac{2}{3} ka^+ \left(\left(1 + \frac{y^+}{a^+}\right) - 1 \right) du^+ \tag{2.32}$$

where

$$a^+ = \frac{a}{\nu} \left(\frac{\tau_w}{\rho} \right)^{\frac{1}{2}} \tag{2.33}$$

The demarcation between the regions near the wall and away from the wall as determined by Deissler (1) from pipe flow data with $y^+ = y_1^+ = 26$ and $u^+ = u_1^+ = 12.9$. Sparrow et al (26) used $u_1^+ = 12.9$ as their demarcation point. The velocity profiles in the form of y^+ as a function of u^+ were obtained by numerical integration of Eqn. 2.32 for parametric values of a^+. Numerical values of a^+ were selected according to the identity

$$a^+ = \frac{u_\infty a}{\nu} \frac{(\tau_w/\rho)^{\frac{1}{2}}}{u_\infty} = \frac{R_a}{u_\infty^+} \tag{2.34}$$

in which u_∞ is the free stream velocity. For a given R_a, a sequence of equally spaced values of u_∞^+ was assigned and to each of these corresponded an a^+. For each of the assigned u_∞^+ values, Eqn. 2.32 was integrated from $u^+ = 0$ to $u^+ = u_\infty^+$.

They also suggested the following closed form solution for the

outer layer velocity diffential equation ,although they did not use it themselves

$$u^+ - u_1^+ = 3^{\frac{1}{2}} \left(\tan^{-1}\left(\frac{2b+1}{3^{\frac{1}{2}}}\right) - \tan^{-1}\left(\frac{b_1+1}{3^{\frac{1}{2}}}\right)\right)$$

$$+ \frac{1}{k} \ln\left(\frac{b-1}{b_1-1}\right) - \frac{2}{k} \ln\left(\frac{b^2+b+1}{b_1^2+b_1+1}\right) \quad (2.35)$$

where

$$b = \left(1 + \frac{y^+}{a^+}\right)^{\frac{1}{2}} \quad (2.36)$$

$$b_1 = \left(1 + \frac{y_1^+}{a^+}\right)^{\frac{1}{2}} \quad (2.37)$$

2.5.0 CONCLUSIONS

The objective of this chapter was to examine the velocity defect law for axial turbulent flow along a cylinder without a pressure gradient. As no consensus presently exists regarding the appropriate axisymmetrical similarity laws for the mean flow in the outer turbulent boundary layer region, the various competing hypotheses were compared and classified according to four major approaches.

Three approaches are based on modification of the classical two-dimensional velocity defect law with respect to variation in the empirical constants B_1 and B_2. In the first method Chin et al (11) obtained new empirical constants simply by curve fitting from their experimental data for the single cylinder radius tested, while not verifying if the new constant would be applicable for other radii. The second method, Yu's (10), stated that constant B_2 was a function of R_a, the Reynolds number based on the cylinder radius,a . The third method

which was suggested by Willmarth and Yang (17), states that B_2 was a function of δ/a where δ was the displacement thickness. All three of these modified two-dimensional velocity defect laws are therefore apparently dependent on the cylinder radius, taking into account that the first method modified the equation for one particular radius.

For each of these three methods, (the respective reports where B_2 was presented not only in functional form but given specific values) the velocity defect plots in two-dimensional co-ordinates of $(U-u)/u_*$ versus y/δ closely coincided with experimental results. The only exception was Rao and Keshaven's (20) data, which did not collapse into a single curve for the same R_a and δ/a values. Afzal and Narasimha (12) explained that the discrepency was due to the fact that the data was obtained through artifically tripping the boundary layer and in view of the known slow recovery of boundary layers from tripping devices, the initial stations may not have acheived a natural state therefore invalidating those initial results. As the functional relationships of each of the three methods are apparently equally valid, the only difference appears to be in terms of the presentation of $(U-u)/u_*$ versus y/δ with variables a, R_a, and δ/a. For increasing values of cylinder radius, a, which also means increasing values of R_a and decreasing values of δ/a, the velocity defect plots approached the two-dimensional values.

In the fourth approach, Rao and Keshaven (20) found that the two-dimensional velocity defect co-ordinates did not reveal any similarity for their experimental data. When the velocity defect was plotted against a local Reynolds number, r_*, similarity did exist for each individual value of cylinder radius Reynolds number, R_a.

Questions remain on whether the traditional divisions of mean flow properties into a wall and wake region is valid when the transverse curvature effect is large; i.e. small values of a and large values of δ/a. Willmarth and Yang(17) proposed that the boundary layer on a slender rod $(a/\delta \to 0)$ is almost all wake-like flow and the region near the wall, which must be independent of the free stream conditions, would be a very small region of the turbulent boundary layer flow containing the viscous sublayer. They state that possibly for the limit $a \to 0$ the wall region contains only the viscous sublayer.

Willmarth et al (14) state that from the geometry of the boundary flow along a cylinder it is apparent that as the radius decreases, the perimeter of the boundary layer adjacent to the wall becomes small in comparision to the perimeter at $y=\delta$, adjacent to the free stream. Therefore, when δ/a is large, the wakelike outer portion should have a structure quite independent of the wall region. For larger δ/a values their resulting respective velocity profiles departed increasingly below the two-dimensional logarithmic wall position.

Afzal and Narasimha (12) comment that in those extreme situations where a^+ is small, the boundary layer may be in a fully developed turbulent state and therefore for those conditions their modified two-dimensional velocity defect laws may be invalid.

Rao and Keshaven (20) state that since for axisymmetrical flows near the wall the shear $\tau=\tau_w a/r$ and for two-dimensional flow near the wall $\tau=\tau_w$, the reduction in the viscous stress away from the wall is not fully compensated by the corresponding increase in Reynolds stress in axisymmetrical flow as it is in two-dimensional flows. The net ef-

fect is the existance of a shear gradient which accentuates viscosity effects in regions farther away from the wall than in two-dimensional flow. They suggest that since the entire axisymmetrical turbulent boundary layer is apparently affected by the viscosity throughout, it is not a pure turbulent boundary layer. The viscosity effect becomes progressively noticable as δ/a increases.

Cebeci (35) tested for the existance of a wake region in the velocity profiles for a 0.06096 cm. diameter cylinder at R_θ=2100 and on a 2.54 cm. diameter cylinder at R_θ=8750. The velocity plot for the former had no wake component and therefore could be described just using the law of the wall, while the latter did have a wake component necessitating the use of both the law of the wall and the law of the wake.

White (21) and (22) states that there is no law of the wake in thick axisymmetrical turbulent boundary layer as the wake component in Coles law of the wall and the wake uniformly vanishes as the cylinder boundary layer becomes thicker. Also he states that there is no portion of a truly thick axisymmetrical velocity profile which is not wall related. He specifies a thick boundary layer occurs when $a^+ << 1000$, while flows with $a^+ > 1000$ are effectively two-dimensional and do show a wake.

Therefore, agreement apparently exists between the various reports that the traditional division of mean flow properties into wall and wake regions may be invalid when there is a large transverse curvature effect as when a is very small or δ/a is very large or for thick boundary layer. Unfortunately, not enough data presently exists to specify a precise value at which the traditional division of the law of

the wall and the law of the wake hold true.

CHAPTER 3

COMPARISON OF EXPERIMENTAL AND THEORETICAL TURBULENT SHEAR COEFFICIENTS AND AVERAGE CONICAL ANNULUS EXIT VELOCITY

3.1.0 INTRODUCTION.

This chapter deals with the experimental and theoretical analysis of shear coefficients of a thread subjected to a steady jet of water discharging from a conical annular nozzle design utilized in industry in shuttleless fluid jet looms for weaving fabric. The various parameters affecting nozzle performance are examined, thereby enaling possible optimization of nozzle design for specific operation conditions. Two theoretical approaches are used in comparison with the average shear coefficients based on experimental data. The first uses the standard two-dimensional equation for the average shear coefficient while the second is White's (21) axisymmetrical approximation average shear coefficient.

The predictive capacity of two theoretical methods by Kwok and Lee (52) for calculating values for the average jet velocity and flow at the end of a conical annulus for an incompressible fluid were also examined in comparison with experimental data. The first method consisted of obtaining the integral momentum equations for the inner and outer boundary layers of the conical annulus so that the displacement thickness and the jet velocity could be determined. In the simpler second solution consideration was given to a macroscopic energy balance between the annulus entrance and exit, while incorporating a head loss to account for the friction loss for flow in the nozzle passage. A brief summary of each theoretical method is presented in this report.

Having obtained theoretical values of the jet velocity and knowing the annular area of the nozzle, the values for flow through a conical annulus was derived and compared with experimental results.

3.1.1 Fundamentals of Shuttleless Jet Loom Operation With Conical Annular Nozzles

While the majority of modern industries have leapt forward with technological advances and newly perfected techniques of design and production, the textile industry's production techniques still remain firmly in the early 19th century. The machinery designed at that period has been somewhat refined, but is still in use at the present time. This experiment is part of a series to modernize and greatly increase the potential production capacity of the looms utilized in making fabric. In particular, it deal with replacing the mechanical shuttle which brings the tread horizontally from one side of the loom to the opposite side. The speed of the mechanical shuttle has been limited by the force required, friction factors, mechanical wear and the actual design of the device. Maximum speeds using this part are unlikely to be increased by a very large factor indicating the necessity for a new approach of moving the from one point to another. The mechanical shuttle was abandoned in this experiment and replaced with a system that shot the thread through a nozzle and across the loom with a jet of water, potentially increasing the production by a factor of two. (Ref. 53)

A basic description of the operation of a fluid jet loom follows (Ref. 54). Figure 3.1 is a perspective view showing the position of a nozzle (part 20) as a part of a shuttleless fluid jet loom. It shows the weft yarn (10) drawn out from the bobin (11), then going through thread tensioner (12) with thread guides (13 and 14) to measuring drum

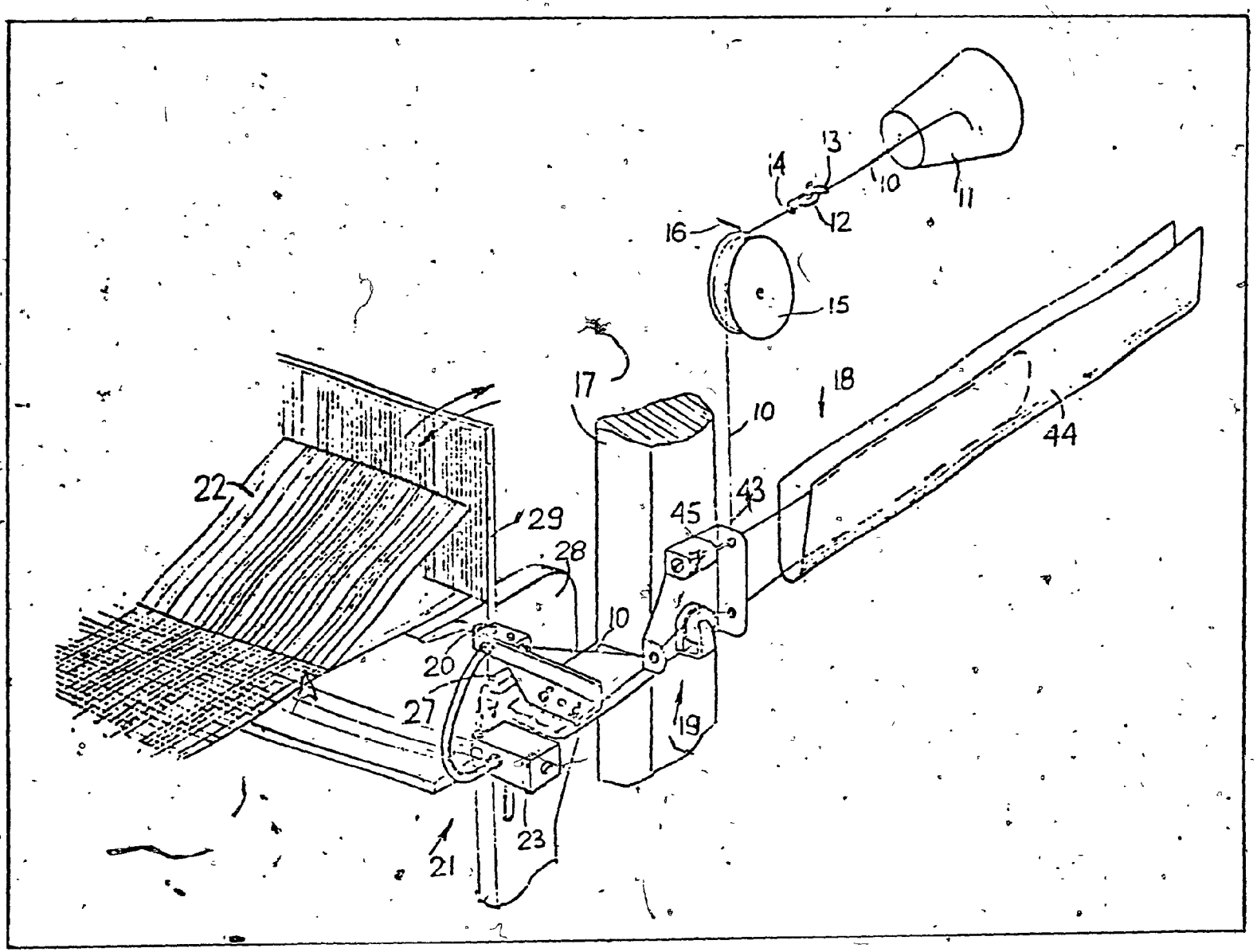

Fig. 3.1 Perpective View of Shuttleless Fluid Jet Loom

(15) driven in a continuous manner by the loom at a predetermined rate. Finger (16) mounted on the frame (17) separates the yarn (10) on the circomferencial surface of the drum (15). The yarn (10) is then temporarily detained in the storage device (18) between each weft inserting cycle. The weft yarn (10) leaving the storage device (18) runs through gripping device (19) into nozzle (20). Each time the fluid under pressure is admitted from the inserting device, generally indicated by reference (21) to the nozzle (20), a jet of fluid with the weft yarn (10) is thrown into the shed of the warp yarns (22). In practice, the thread would be subjected to a pulsating flow of water shooting one thread with each pulse. In the experiment presented here the study of the nozzle was conducted using steady flow rather than pulsating flow.

3.1.2 Literature Search For Previous Work

3.1.2.a Review on Flow From a Conical Annulus

Literature on the flow from a conical annulus was found to be scarce, although flow for a concentric annulus has been investigated by Brighton and Jones (55), Fredrickson and Bird (56), Okiishi and Servoy (57), Rothfus (58 and 59), and Sparrow and Lin (60). A report on the water jet exit velocity from a thread shooting conical annulus nozzle, having minor differences in dimensions and the conical angle in comparison to the one utilized in the present experiment, was published by Kwok and Lee (52). Their report investigated two theoretical methods previously described in Section 3.1.0 for calculating the average jet velocity at the exit of a conical annulus for an incompressible fluid. Both predictions were practically identical (having a variation of less than 1%) and both differing from their experimental values by

less than 3% over the pressure range of 310.3 to 379.2 kPa which they examined. As the predictive capacity of the methods (Ref. 52) produced apparently excellent results, the methods were chosen for comparison with the present experimental work. As a greater range of flow and pressure conditions are presently invovled, the two methods are examined to find if the same predictive accuracy is maintained.

3.1.2.b Review on Flow Along a Circular Cylinder in Experiments

The majority of experimental work for flow along a cylinder has been under turbulent conditions beginning with that performed by Kempf (61). Subsequent data was reported by Telfer (62), Hughes (63), Richmond (15), Yu (10), Yasuhara (16), Selwood (64), Willmarth and Yang (17), Willmarth et al (14), Rao and Keshaven (20), and Afzal and Singh (13). (See Table 3.1)

Only three of the above reports obtained the skin friction from direct measurements. Local friction factors were measured by Kempf (61) for water flowing along a cylinder of radius 1.7526 cm. and lengths of up to 9.144 m.. The cylinder was rigidly attached to an outside towing device which moved it horizontally through the water. The range of length Reynolds number, R_x, extended from 3.5×10^6 to 2.4×10^7, while the cylinder Reynolds number, R_a, ranged from 2.3×10^4 and 5×10^4. Hughes (63) measured average friction factors for water flowing along a cylinder with a radius of 1.27 cm. and lengths up to 25.6032 m.. The cylinder was towed by a line attached to its nose, but was completely free of constraining support. During the towing, a slight yaw was noted (-1°); which is small in view of the lack of constraints. No observations of sidewise motions were mentioned and there was not any statements as

AUTHOR (REF.)	R_a	Range of x/a
Richmond (15)	93.8	1600
	253	1600
	40,200	16 to 20
Yu (10)	15,250	12 to 96
	30,740	12 to 96
	45.060	12 to 84
Yasuhara (16)	218,000	100
Willmarth and Yang (17)	68,800	128
	136,000	128
	70,200	192
	115,000	192
	134,000	192
Rao and Keshaven (20)	425	96 to 640
	825	96 to 640
	1,320	48 to 320
	1,420	24 to 160
	1,620	48 to 320
	3,940	24 to 160
	106,000	5.3 to 16.4
	218,500	5.3 to 16.4
Willmarth et al (14)	482	21,960
	736	21,960
	899	21,960
	1,439	10,980
	4,330	3,513.6
	6,203	1,756.8
	9,494	1,756.8
	11,693	1,756.8
	12,790	878.4
	19,230	878.4
	23,100	878.4
	36,680	439.2
	74,260	219.6
	92,310	219.6
Afzal and Singh (13)	14,200	30 to 162
Present Work	2,189	272.72 to 2181.82
	2,306	
	2,571	
	2,693	
	2,922	
	3,085	
	2,862	
	3,260	
	3,428	
	3,198	
	3,822	
	3,942	
	4,040	
	4,046	
	4,285	

Table 3.1 Experimental Work on Flow Along a Circular Cylinder

to whether the cylinder remained horizontal. The measurements were uncorrected for possible effects of the wake, yaw or sidewise motion which result in higher readings than for pure skin friction measurements. The range of R_x was from 7×10^6 to 10^8, and R_a from 3.5×10^3 to 10^4. The only other direct skin friction measured was by Selwood (64) on moving nylon fibres through air between 5m/sec and 20m/sec. Therefore at present there exists the necessity of more experimental data, including that data within this chapter, to verify previous experimental work.

The other authors obtained the skin friction and shear co-efficients by different indirect methods. Yu (10) and Willmarth and Yang (17) determinined the wall shear from a preston tube, using the calibrations of Landweber and Siao (65) and Patel (66). Richmond (15) obtained the wall friction by fitting data to his wall law. However, Rao and Keshaven (20) found that in some of Richmond's flows the momentum thickness increased downstream, suggesting that the flow may not have been axisymmetric. Extensions of Head's (67) two-dimensional integral methods were done by Patel (68) and Shanebrook and Summer (69) for thick and thin axisymmetrical turbulent boundary layers respectively. Chin et al (11), Rao and Keshaven (20), Sparrow (26), and White (21, 22) obtained the skin friction from other momentum integral methods. Patel (24) and Afzal and Narasimha (12) deduced the wall friction from Clauser's plot method (70). A differential computer method was presented by Cebeci (28, 35, 36, 46, and 51).

3.2.0 EQUATION FORMULATION

3.2.1 Average Exit Velocity From an Annulus and Average Shear

Coefficient Along a Circular Cylinder Using Experimental Data

For the experimental thread shear coefficients with various nozzle conditions, the following assumptions for the flow of the water jet from a nozzle into a stationary atmosphere were made:

a) The pressure along the jet boundary and across section of the jet is atmospheric.

b) The jet has no external forces acting on it.

c) The jet flow is uniform at the nozzle exit.

d) The velocity of the jet remains constant.

e) There is no mixing of the jet with the surrounding atmosphere

f) The friction between the jet and the air can be neglected.

The Reynolds number R is the ratio of the inertial forces to the viscous forces and is applicable in situations where these forces are the dominant ones. At low Reynolds number, the viscous forces are dominant, and the interial forces negligible, and at high Reynolds number the inertial forces are dominant and the viscous forces negligible. The formula for R_D, the Reynolds number based on D_H, the hydraulic diameter

$$R_D = \frac{D_H U_{jet}}{\nu} \qquad (3.1)$$

and U_{jet} is taken as the average velocity in the direction of flow, and and ν is the kinematic viscosity of the fluid. The hydraulic diameter is four times the ratio of cross section to wetted perimeter. Therefore for the nozzle annulus area in this experiment,

$$D_H = 2c \qquad (3.2)$$

where c is the nozzle clearance. With D_o as the outer diameter and D_{in} as the inner diameter of the nozzle through which the flow passes. The

annular area A_n is given by

$$A_n = \frac{\pi}{4} (D_o - D_{in}) \qquad (3.3)$$

The average velocity was obtained from the rate of flow, Q and A_n with

$$U_{jet} = \frac{Q}{A_n} \qquad (3.4)$$

The experimental stress τ on the thread is a function of the measured force and the thread surface area A_{TS}

$$\tau = \frac{F}{A_{TS}} = \frac{F}{2\pi ax} \qquad (3.5)$$

where a is the radius of the thread and x is the length of the thread from the end of the nozzle protrusion. The experimental shear stress can be expressed in terms of an average shear coefficient, C_f, times the dynamic pressure $\rho_w U_{jet}^2/2$, where ρ_w is the density of the water

$$\tau = C_f \frac{\rho_w U_{jet}^2}{2} \qquad (3.6)$$

$$C_f = \frac{2\tau}{\rho_w U_{jet}^2} \qquad (3.7)$$

The two-dimensional theorectical average shear coefficient formula is

$$C_f = \frac{.074}{R_x^{0.2}} \qquad (3.8)$$

where R_x is the Reynolds number based on thread length, x.

3.2.2 White's Axisymmetric Shear Coefficients

In comparision with the other methods discussed in 3.1.2.b on theoretical shear coefficients, White's approximation average shear coefficient compared very favourably with experimental results yet did

not involve complex calculations. There, as his method is apparently as accurate in prediction and is more efficient, it was chosen over the other methods for the initial comparision with experimental data obtained for turbulent flow along a circular thread.

White (21) suggested an approximate formula for engineering use based on modifying Tefler's (62) proposed formula based on drag data for floating cylinders which is

$$C_f = 0.0012 + \{0.34 + 0.07(\frac{x}{a})^{\frac{1}{3}}\} R_x^{-\frac{1}{3}} \qquad (3.9)$$

where C_f is the average shear coefficient, x is the length of the cylinder, and a is the cylinder radius. Altering the constants to better fit with more extensive data studies White recommends

$$C_f = 0.0015 + \{0.30 + 0.015(\frac{x}{a})^{\frac{1}{3}}\} R_x^{-\frac{1}{3}} \qquad (3.10a)$$

for $10^6 < R_x < 10^9$ and for $x/a \leq 10^6$. For the range indicated, this formula is within ± 5% of his empirical results. For long cylinders and low R_a, the asymoptotic series of Glauret and Lighthill (39) is added

$$C_f = \frac{4}{R_a} \left(\frac{1}{G} + \frac{1.5772}{G^2} + \ldots\ldots\ldots\ldots \right) \qquad (3.10b)$$

where

$$G = \ln \left(\frac{4R_x}{2R_a}\right) \qquad (3.10c)$$

for $G > 6$ and $R_a < 20$. For larger R_a, the formula drops too low. These two expressions cover the range of interest for turbulent flow calculations, and also Eqn. 3.10b is valid for laminar flow.

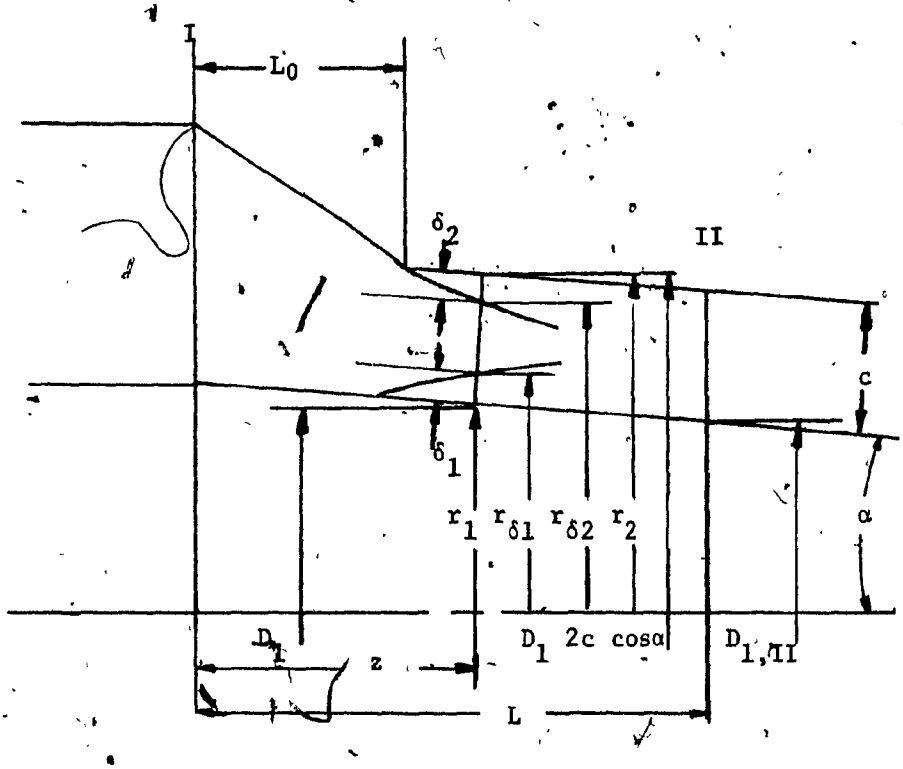

Fig 3.2 Definition Sketch For Conical Annulus (Ref. 52)

3.2.3 Two Theoretical Methods for Calculation of Average Exit Velocity at the End of a Conical Annulus

The equation utilized in the the following two methods are for a developing turbulent boundary layer. Such conditions are shown to exist for $r_1/r_2 = 0.531$ where the boundary was still developing at the point of 35 D_H (Ref. 57). The latter length further increases with larger r_1/r_2 ratios. For the nozzle utilized in this experiment r_1/r_2 = 0.10287 cm./0.1295 cm. = 0.7942. Even when the length is assumed to be 35 D_H = 1.8669 cm., this value is greater than the length (L) of the channel (see Fig. 3.2) which is equal to 1.3208 cm.. Therefore the methods are valid for the present experimental conditions.

3.2.3.a Method 1 - Integral Momentum Equations

For the inner boundary layer, the force and momentum-flux

relation in the flow direction is given by

$$-\tau_{01}(2\pi r_1 dz \sec\alpha) - dp\{\int_{r_1}^{r\delta_1} 2\pi r\, dr \sec\alpha\}$$

$$= d\int_{r_1}^{r_{\delta_1}} \{\rho u (2\pi r\, dr \sec\alpha)\}u - Ud\int_{r_1}^{r_{\delta_1}} u(2\pi r\, dr \sec\alpha) \quad (3.11)$$

the continuity equation is,

$$\frac{d}{dz}\{U(r_2^2 - r_1^2) - 2r_1\delta_1^* U - 2r_2\delta_2^* U\} = 0 \quad (3.12)$$

The clearance, c, is much smaller in magnitude compared with the inner radius r_1. Therefore, the flow can be considered as that between parallel plates in the presence of a pressure gradient. With the shape factor H defined as the ratio of displacement to momentum thickness i.e. $H = \delta^*/\theta$ then the shearing stress at the wall is

$$\frac{\tau_0}{\rho U^2} = 0.0128\left(\frac{\nu}{U\theta}\right)^{\frac{1}{4}} = 0.0128\, H^{\frac{1}{4}}\left(\frac{\nu}{U\delta^*}\right)^{\frac{1}{4}} \quad (3.13)$$

Choosing $H = 1.4$; the resulting integral momentum equation are:

$$\frac{d\delta_1^*}{dz} + 3.4\frac{\delta_1^*}{U}\frac{dU}{dz} = 0.0195\left(\frac{\nu}{U\delta_1^*}\right)^{\frac{1}{4}} \quad (3.14)$$

$$\frac{d\delta_2^*}{dz} + 3.4\frac{\delta_2^*}{U}\frac{dU}{dz} = 0.0195\left(\frac{\nu}{U\delta_2^*}\right)^{\frac{1}{4}} \quad (3.15)$$

The solution to the above are:

$$\delta_1^* = \delta_2^* = 0.0512\,\nu^{\frac{1}{5}}\,U^{-\frac{17}{5}}\left(\int_{L_0}^{L} U^4\, dz\right)^{\frac{4}{5}} \quad (3.16)$$

Previous investigations have shown that the pressure gradient is

practically constant (Ref. 57). Therefore, assuming that

$$P = -\frac{P_I}{L} z + P_I \tag{3.17}$$

and

$$P_I = P + \frac{\rho U^2}{2} \tag{3.18}$$

then Eqn. 3.16 becomes

$$\delta_1^* = \delta_2^* = 0.0644\, \nu^{\frac{1}{5}} \left[\frac{L^3 - L_0^3}{\{\rho L^2\}^2}\right]^{\frac{4}{5}} \frac{P_I^{\frac{8}{5}}}{U^{\frac{17}{5}}} \tag{3.19}$$

also

$$U_{II} = \left(\frac{2P_I}{\rho}\right)^{\frac{1}{2}} \tag{3.20}$$

Therefore, from the continuity equation the mean jet velocity at the exit is given by

$$U_{eII} = \left(\frac{2P_I}{\rho}\right)^{\frac{1}{2}} \left(1 - \frac{2\delta_1^*}{c}\right) \tag{3.21}$$

3.2.3.b Method 2 - Head Loss Equations

The macroscopic mechanical energy balance between section I (entrance) and section II (exit) in Fig. 3.2 is given by:

$$\frac{P_I}{\gamma} + \frac{V_I^2}{2g} = \frac{P_{II}}{\gamma} + \frac{V_{II}^2}{2g} + h_L \tag{3.22}$$

To evaluate the head loss, h_L, the friction factor, f, has to be determined. Where R_D, the Reynolds number based on hydraulic diameter, ranges from 0.4 to 1.7×10^4, f can be approximated (Ref. 55) by

$$f = 0.087\, R_D^{-\frac{1}{4}} \tag{3.23}$$

With V equal to the mean flow velocity at any position z, it can be shown that

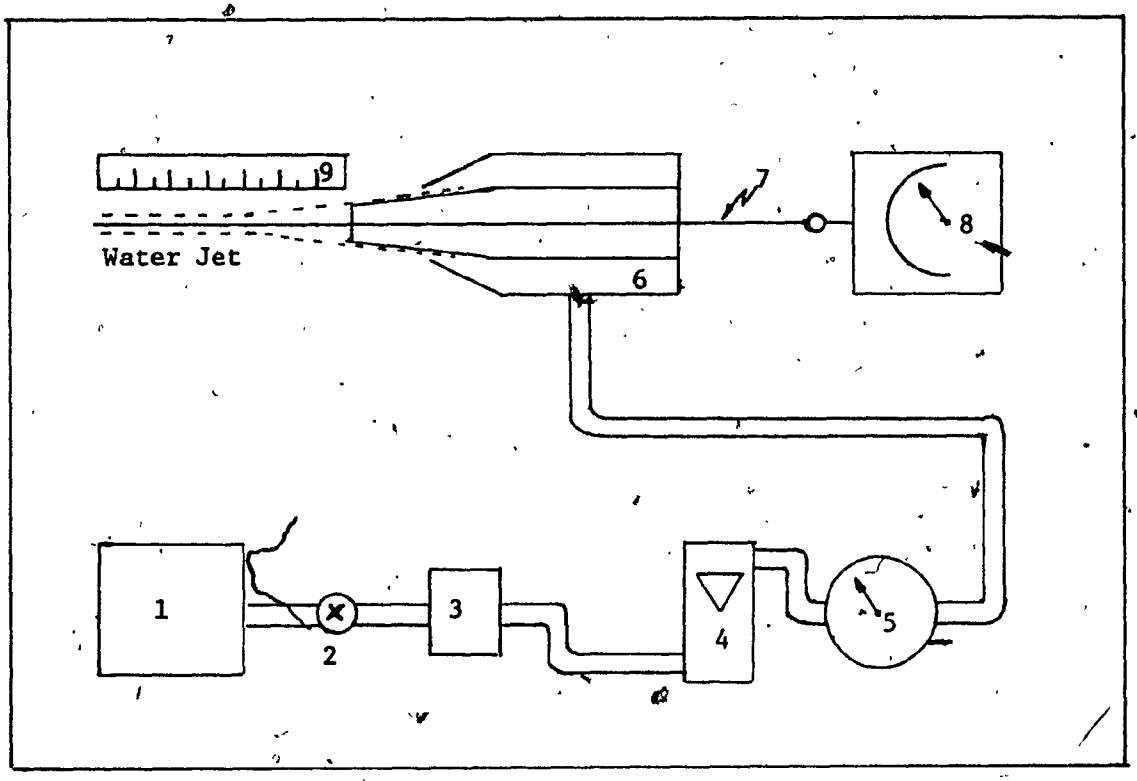

Fig. 3.3 Schematic of Test Setup

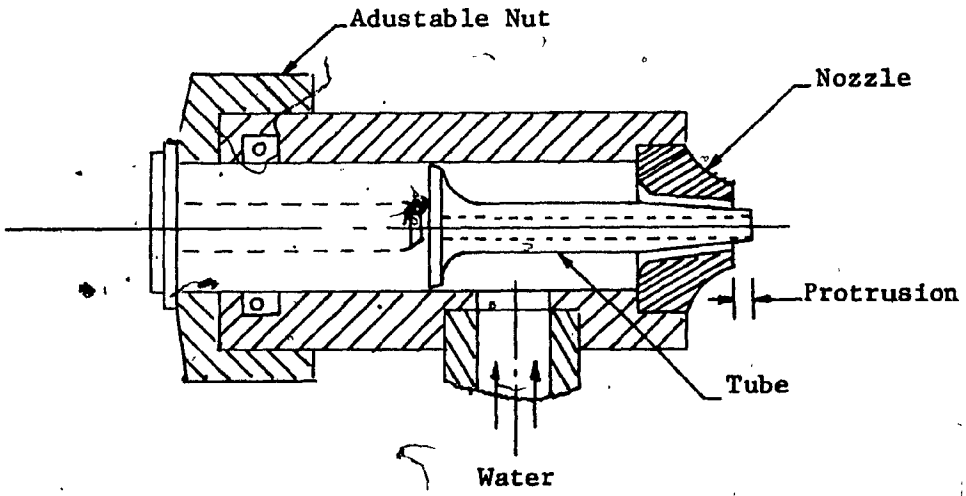

Fig. 3.4 Water Jet Nozzle (Ref. 52)

$$V = (\{2(\tan\alpha)\frac{L - z}{D_{1,II}}\} + 1)^{-1} V_{II} \qquad (3.24)$$

Consider a length of passage $dx = dz \sec\alpha$. The associated head loss is

$$dh_L = -\frac{dP}{\rho} = f \frac{dx}{D_H} 2V^2 \qquad (3.25a)$$

$$dh_L = 0.087 R_D^{-\frac{1}{4}} \frac{dx}{D_H} 2V^2 \qquad (3.25b)$$

Therefore, with $D_H = 2c$ as stated previously then

$$h_L = \int_{L_0}^{L} dh_L = \frac{4BV_{II}^{1.75}}{3A} \{1 - \{A(L - L_0)+1\}^{.75}\} \qquad (3.26)$$

where

$$A = \frac{2 \tan\alpha}{D_{1,II}} \qquad (3.27)$$

and

$$B = \frac{0.087 \sec\alpha}{cg} \left(\frac{\mu}{2c\rho}\right)^{\frac{1}{4}} \qquad (3.28)$$

Therefore,

$$\frac{V_{II}^2}{2} + \frac{4B}{5A} \{1 - \{A(L - L_0) + 1\}^{-.75}\} V_{II}^{1.75} - \frac{P_I}{\rho} = 0 \qquad (3.29)$$

The jet velocity V_{II} and the head loss h_L are solved in the computer program by iteration with all the other pertinent parameters known.

3.3.0 EXPERIMENTAL INVESTIGATION

3.3.1 Experimental Apparatus

A schematic diagram of the experimental apparatus used is shown in Fig. 3.3. The water flow was obtained from the standard municipal water supply system (1). The water was controlled through the use of a shut-off valve ((2), Jenkins ½" NPT), and a pressure regulator ((3),

Watts - U-5 AB ½" NPT). The flow was measured with a rotameter ((7), Fisher and Porter Co., Precision Base Flowmeter Tube No. FP-½- 50-G-9183) with an accuracy of 2% of maximum flow and a range from 0.281 to 3.52 gpm (1.064 to 13.32 lpm). The pressure after the rotometer was obtained through the use of a pressure gauge ((5), Solfrunt U.S. Gauge Cat. No. 33504) with an accuracy of 0.05% of full scale and a range of 0 to 100 psi (0 to 689.5 kPa). The rest of the flow system consists of an elbow (½" NPT), a reducer bushing (½" NPT x ¼" NPT), a Polyflow fitting (¼" NPT x ⅜" Polyflow Tube), plastic tubing (30 in. (0.762 m) of " Polyflow Tubing 66-P-⅜) and the nozzle (6) itself also shown in greater detail in Fig. 3.4. The force on the thread ((7), 0.011 inch (0.2794 cm) diameter Berkley Viking monofilament) placed within the nozzle was measured by a force meter ((8), Ametek Trim Series Model T-506-TC) with an accuracy of 2% of full scale and a range of 0-50 grams . The length of thread and the nozzle protrusions were obtained using a vernier (Kar Stainless Hardened Vernier Caliper).

3.3.2 Experimental Procedure

After the experimental apparatus was set up as in Fig. 3.3, the nozzle protrusion was set at its intial value of 0 cm through measurement by the vernier caliper. The three nozzle protrusion values that would be tested were 0 cm, 0.127 cm., and 0.254 cm. respectively. With the initial value of nozzle protrusion set, one end of the thread was attached to a force meter and the other end inserted through the center of the nozzle so that there was a thread length of 30.48 cm.. All thread lengths were measured from the end of the nozzle protrusion. A steady flow of water was passed through the nozzle at a constant supply

pressure of 206.85 kPa with only very minor fluctuations on the pressure gauge due to the municipal water supply system used. The force on that length of thread due to water jet was then measured with the force meter. After this measurement was taken the flow was shut off. Then the thread length was shortened by 1.27 cm., and the flow was returned to the same constant pressure. This procedure was repeated until the final thread length was 1.27 cm.. Then, a new 30.48 cm. length of thread was inserted and another set of readings for the same supply pressure conditions was taken. Three sets of force readings for three different threads with the same 0.2794 cm. diameter were taken, maintaining the same supply pressure and protrusion. The average value of these three sets was noted in Tables 3.2 and 3.3 which can be found in Section 3.4. The entire procedure was then repeated using protrusions of 0.127 cm. and 0.254 cm. while maintaining the same supply pressure. The supply pressure was increased in steps of 68.95 kPa and force readings at 275.8 kPa, 344.75 kPa, 413.7 kPa, and 482.65 kPa were recorded for the three nozzle protrusions of 0. cm., 0.127 cm., and 0.254 cm..

3.4.0 EXPERIMENTAL RESULTS

3.4.1 Comparison of Experimental and Theoretical Results

In this experiment the shear force on a circular thread, centered within a specific nozzle configuration and maintained in a certain position while subjected to various flow conditions, was measured and tabulated in Tables 3.2 and 3.3. The pressure and flow were also measured for each set of readings enabling the computation of the two series of Reynolds numbers; R_x, which is based on the length of the thread and R_a, which is based on the radius of the thread. The shear stress and the shear coefficient for the various lengths of thread was then obtained

from a computer program which used the equations found in sections 3.3.1 and 3.3.2. Graphs were plotted (see Figs. 3.5 to 3.19) for flow versus pressure and shear coefficient versus R_x for various R_a values and pressures.

Two theoretical methods for the calculation of the average exit velocity at the end of a conical annulus reported by Kwok and Lee (52) were used for comparison with the presently obtained experimental results (see Fig. 3.20). It should be noted that in their report the variation in theoretical results for their nozzle between the two methods was less than 1%, while their experimental results varied less than 3% from the theoretical. In the present study the two theoretical methods were found to vary up to 10%, a significant difference from their findings. Although the curves obtained by the two methods have the same trend, the curve using the head lost (h_L) equations had higher values than h_Δ, that calculated using the displacement thickness. Except for one point, the experimental results varied from the theoretical ones by less than 10%.A set of curves exists for each protrusion. It can be seen that the flow increases with pressure while increasing the protrusion shifts the curves downward. As the flow has been seen to be extremely sensitive to protrusion variation, a possible source of error explaining the scattering of values for each curve was the difficulty in obtaining exact protrusion lengths during the experiment.

Two performance parameters affecting the annular water-jet are; 1) the supply pressure and 2) the length of the nozzle protrusion which affects the annulus area and changes the R_a value. While maintaining the same supply pressure, the shear coefficient varied with various

PRESSURE	PROTRUSION	FLOW	$AREA_N$	U_{JET}	THREAD LENGTH - cm										
					1.27	2.54	3.81	5.08	6.35	7.62	8.89	10.16	11.43	12.70	13.97
kPa	cm	lpm	$10^{-6} m^2$	m/sec	AVERAGE FORCE - grams										
206.85	0.000	1.999	1.948	17.097	1.25	2.42	3.17	4.25	5.25	6.33	7.50	8.17	9.00	10.00	10.75
	0.127	1.366	1.485	15.322	0.75	1.92	2.83	3.83	4.83	5.50	7.08	8.08	8.67	9.58	10.25
	0.254	0.867	0.9916	14.555	0.75	1.58	2.67	3.50	4.75	5.58	6.42	6.92	7.50	8.00	8.42
275.80	0.000	2.399	1.948	20.516	2.08	3.67	4.92	6.08	7.25	8.75	9.83	10.92	12.33	13.33	14.17
	0.127	1.734	1.485	19.434	1.75	3.42	4.58	5.92	7.00	8.17	8.92	10.17	11.33	12.42	13.58
	0.254	1.067	0.9916	17.911	1.50	2.67	3.75	5.00	6.00	7.08	7.83	8.42	9.42	10.33	11.17
344.75	0.000	2.665	1.948	22.796	1.33	3.33	4.83	6.58	8.33	9.83	11.42	12.92	14.25	15.33	16.67
	0.127	1.931	1.485	21.677	0.90	3.25	5.00	6.50	8.00	9.00	11.17	12.58	13.75	15.00	16.17
	0.254	1.132	0.9916	19.031	0.75	2.17	3.50	4.83	5.67	6.67	7.92	9.08	10.17	10.66	11.67
413.70	0.000	3.066	1.948	26.215	2.00	4.08	5.92	7.67	9.08	10.92	12.50	13.75	15.17	16.58	17.92
	0.127	2.264	1.485	25.416	1.58	3.83	6.08	8.00	9.25	10.50	12.25	13.83	15.08	16.58	17.92
	0.254	1.264	0.9916	21.270	1.42	3.08	4.58	6.00	7.50	8.42	9.67	10.83	11.90	13.33	14.00
482.65	0.000	3.331	1.948	28.495	2.25	4.67	6.75	8.92	10.92	12.83	14.92	16.67	18.25	19.50	21.25
	0.127	2.399	1.485	26.909	2.17	4.42	6.50	8.42	10.25	12.00	13.25	14.50	15.92	17.58	18.75
	0.254	1.597	0.9916	26.869	2.00	4.00	6.08	7.67	9.00	10.67	12.08	13.50	14.92	16.33	17.83

Table 3.2 Force-Pressure Relationships

PRESSURE kPa	X_N cm	FLOW lpm	$AREA_N$ $10^{-6} m^2$	U_{JET} m/sec	THREAD LENGTH - cm												
					15.24	16.51	17.78	19.05	20.32	21.59	22.86	24.13	25.40	26.67	27.94	29.21	30.48
					AVERAGE FORCE - grams												
206.85	0.000	1.999	1.948	17.097	11.92	12.92	13.58	14.17	14.92	15.67	16.42	17.42	17.75	18.25	18.92	19.42	20.17
	0.127	1.366	1.485	15.322	11.08	11.83	12.75	13.25	13.67	14.33	14.92	15.25	16.08	16.67	17.00	17.58	18.25
	0.254	0.867	0.9916	14.555	9.00	9.50	10.00	10.33	10.87	11.33	11.67	12.00	12.33	12.67	12.92	13.33	13.68
275.80	0.000	2.399	1.948	20.516	15.75	16.58	17.75	18.33	19.25	20.25	21.17	22.15	23.00	23.67	24.42	25.17	25.75
	0.127	1.734	1.485	19.434	14.25	15.08	16.00	17.00	17.75	18.58	19.25	20.00	20.83	21.58	22.08	22.92	23.83
	0.254	1.067	0.9916	17.911	12.08	13.00	13.67	14.17	14.58	15.00	15.67	16.42	16.92	17.33	17.75	18.25	18.58
344.75	0.000	2.665	1.948	22.796	18.08	19.00	20.17	21.50	22.67	23.75	24.33	25.50	26.58	27.58	28.25	29.25	30.33
	0.127	1.931	1.485	21.677	17.33	18.25	19.33	20.17	21.17	22.00	23.00	24.17	24.50	25.25	26.25	27.33	28.17
	0.254	1.132	0.9916	19.031	12.92	13.58	14.06	14.75	15.50	16.67	17.25	17.75	18.33	19.08	19.92	20.67	21.33
413.70	0.000	3.066	1.948	26.215	18.92	20.42	21.83	23.33	24.25	25.42	26.75	27.92	28.50	29.75	31.08	32.42	33.33
	0.127	2.264	1.485	25.416	18.83	20.00	20.67	22.33	23.67	24.92	26.17	27.17	28.17	29.08	30.25	31.67	32.67
	0.254	1.264	0.9916	21.270	14.83	15.75	16.83	17.50	18.08	18.92	19.58	20.33	21.25	22.17	22.92	23.33	23.92
482.65	0.000	3.331	1.948	28.495	22.92	24.08	25.25	26.58	27.92	29.25	30.25	31.75	33.25	34.17	35.17	36.33	37.16
	0.127	2.399	1.485	26.909	20.00	21.83	23.42	24.17	25.58	27.08	28.42	29.42	30.50	31.67	32.25	33.25	33.83
	0.254	1.597	0.9916	26.869	18.67	19.83	20.83	22.00	23.00	23.83	24.58	25.58	26.67	27.67	28.25	28.92	29.58

Table 3.3 Force-Pressure Relationships

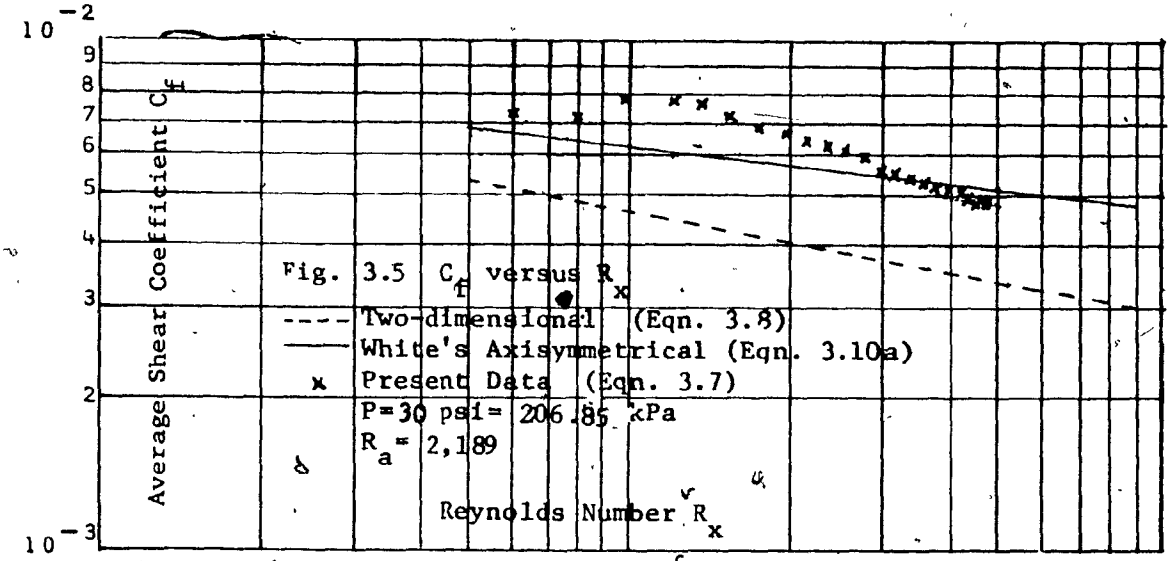

Fig. 3.5 C_f versus R_x
---- Two-dimensional (Eqn. 3.8)
—— White's Axisymmetrical (Eqn. 3.10a)
x Present Data (Eqn. 3.7)
P=30 psi= 206.85 kPa
R_a= 2,189

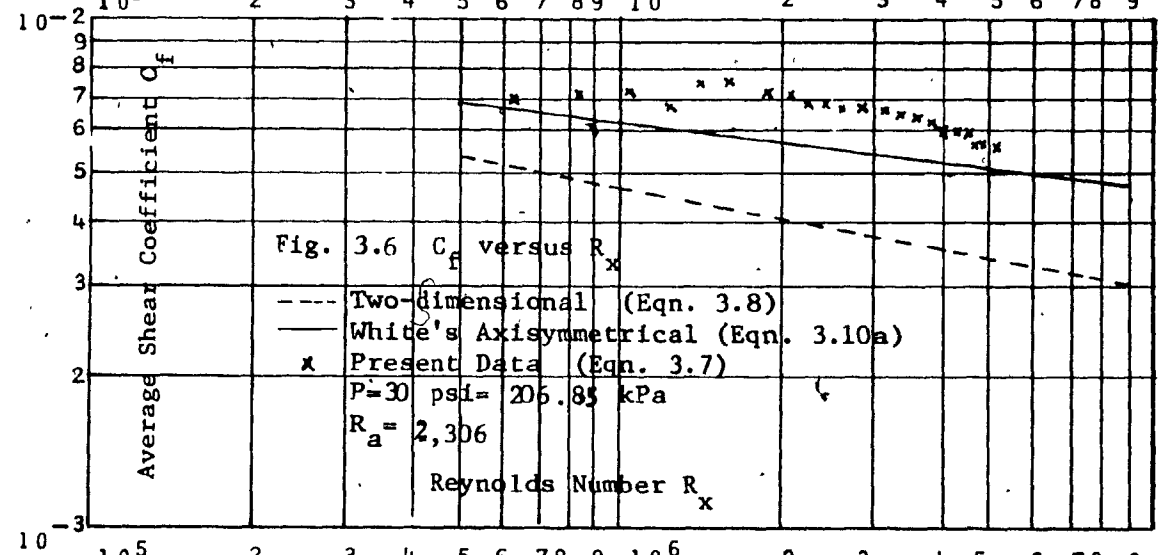

Fig. 3.6 C_f versus R_x
---- Two-dimensional (Eqn. 3.8)
—— White's Axisymmetrical (Eqn. 3.10a)
x Present Data (Eqn. 3.7)
P=30 psi= 206.85 kPa
R_a= 2,306

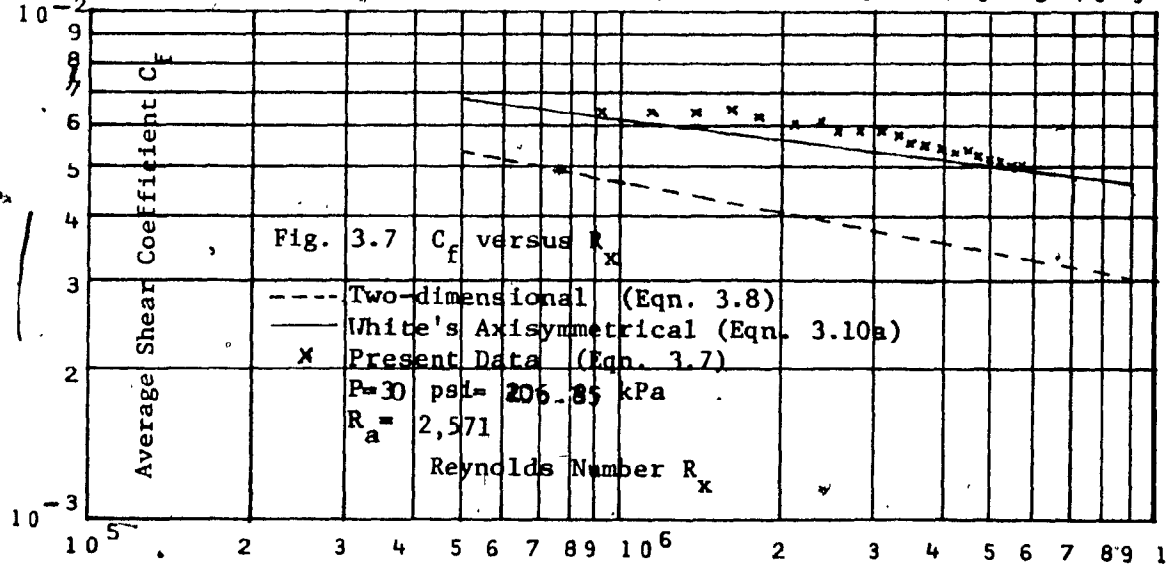

Fig. 3.7 C_f versus R_x
---- Two-dimensional (Eqn. 3.8)
—— White's Axisymmetrical (Eqn. 3.10a)
x Present Data (Eqn. 3.7)
P=30 psi= 206.85 kPa
R_a= 2,571

Figures 3.5 to 3.7 C_f versus R_x with P equal to 206.85 kPa

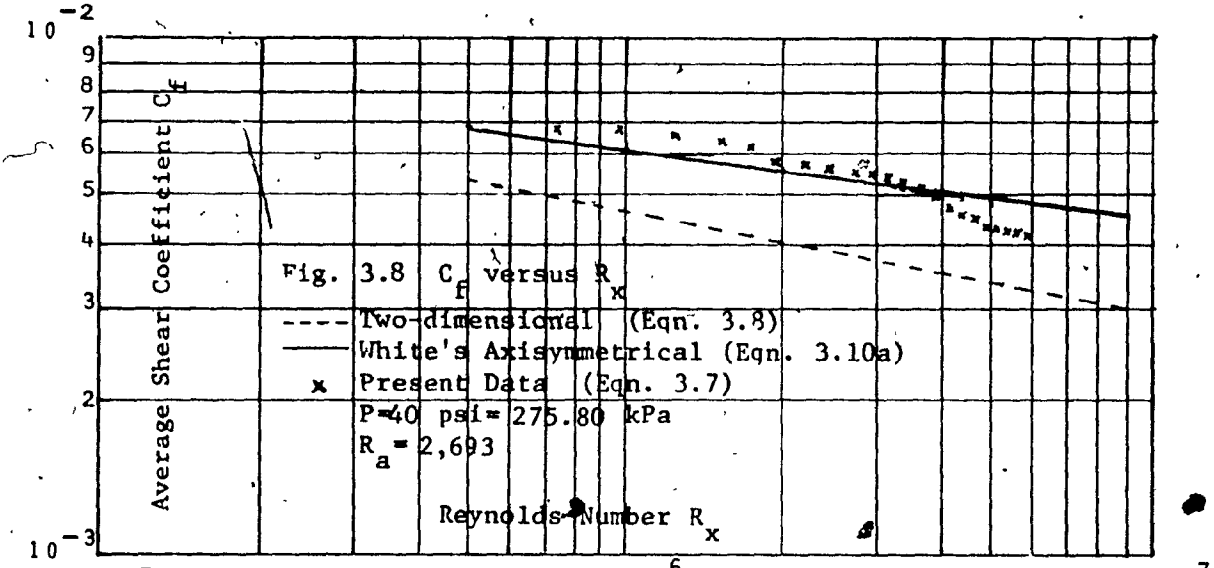

Fig. 3.8 C_f versus R_x
---- Two-dimensional (Eqn. 3.8)
—— White's Axisymmetrical (Eqn. 3.10a)
x Present Data (Eqn. 3.7)
P=40 psi= 275.80 kPa
R_a= 2,693

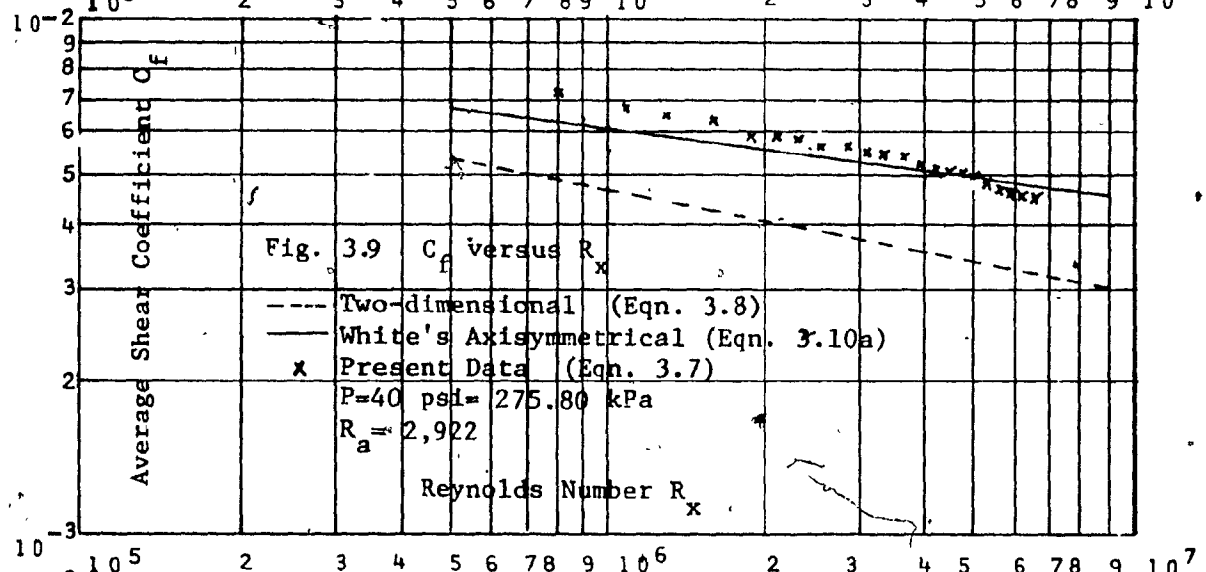

Fig. 3.9 C_f versus R_x
---- Two-dimensional (Eqn. 3.8)
—— White's Axisymmetrical (Eqn. 3.10a)
x Present Data (Eqn. 3.7)
P=40 psi= 275.80 kPa
R_a= 2,922

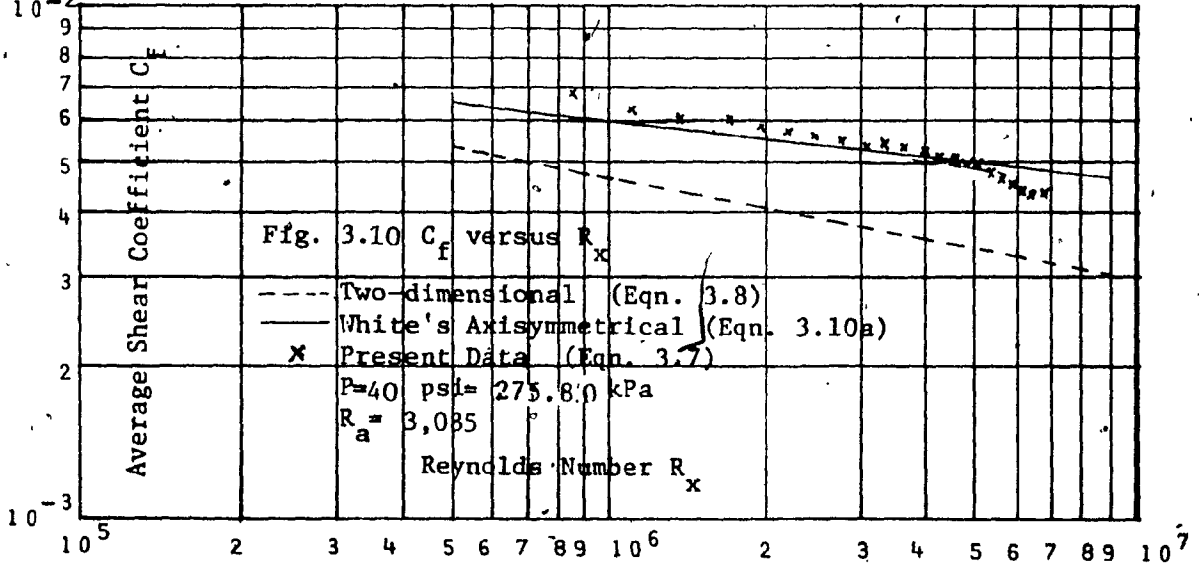

Fig. 3.10 C_f versus R_x
---- Two-dimensional (Eqn. 3.8)
—— White's Axisymmetrical (Eqn. 3.10a)
x Present Data (Eqn. 3.7)
P=40 psi= 275.80 kPa
R_a= 3,085

Figures 3.8 to 3.10 C_f versus R_x with P equal to 275.80 kPa

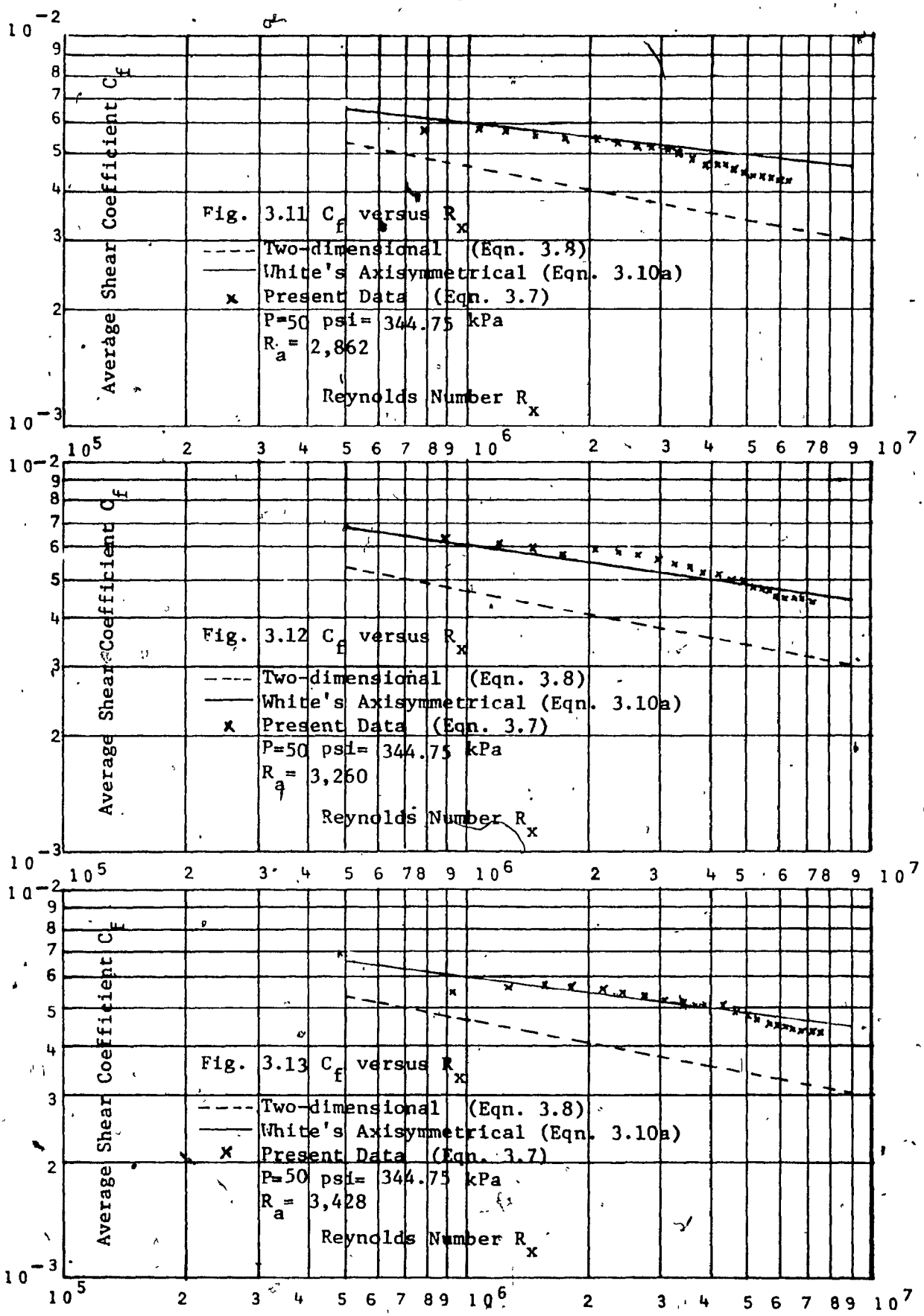

Figures 3.11 to 3.13 C_f versus R_x with P equal to 344.75 kPa

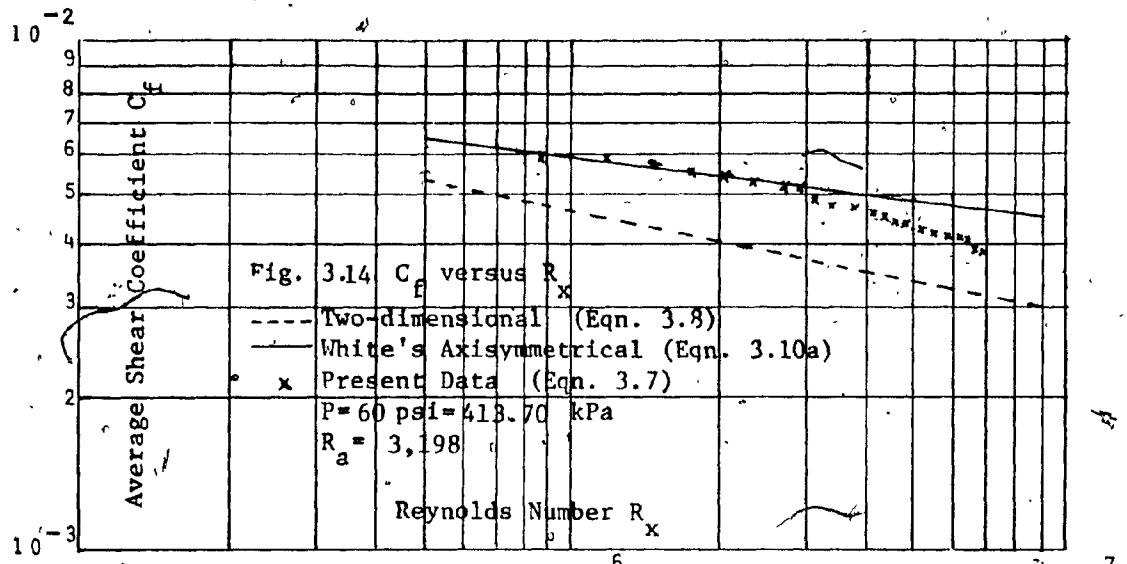

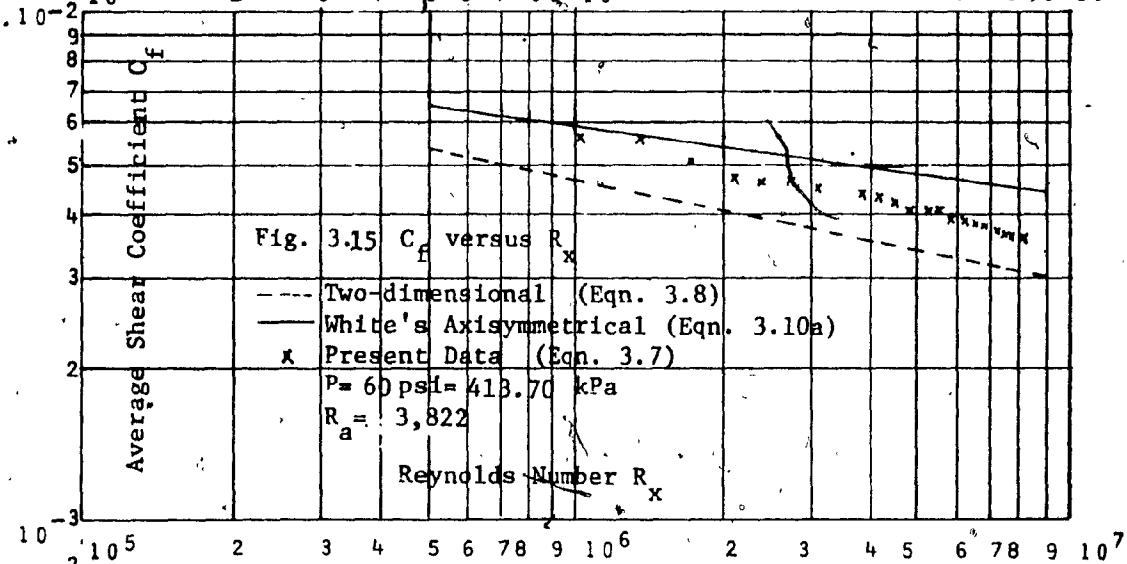

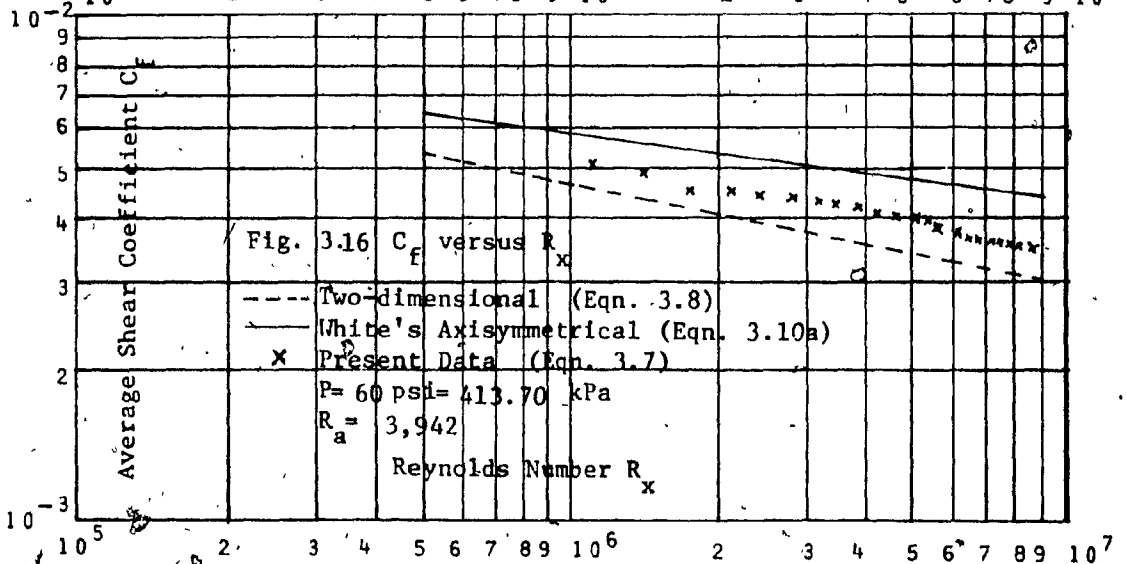

Figures 3.14 to 3.16 C_f versus R_x with P equal to 413.70 kPa

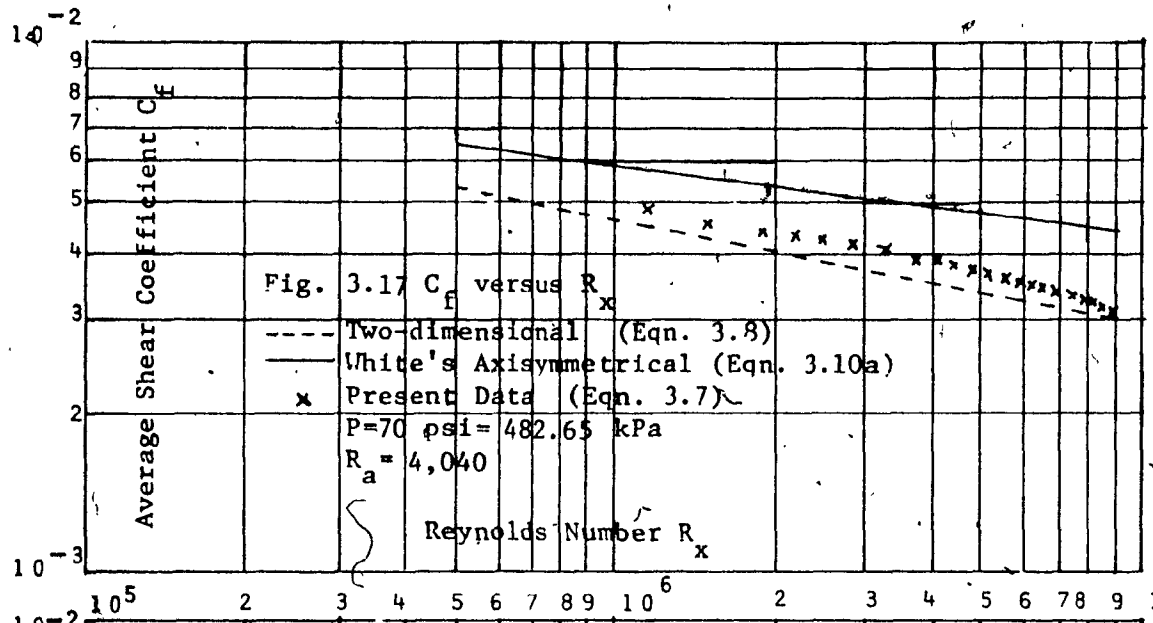

Fig. 3.17 C_f versus R_x

---- Two-dimensional (Eqn. 3.8)
——— White's Axisymmetrical (Eqn. 3.10a)
x Present Data (Eqn. 3.7)
P=70 psi= 482.65 kPa
R_a= 4,040

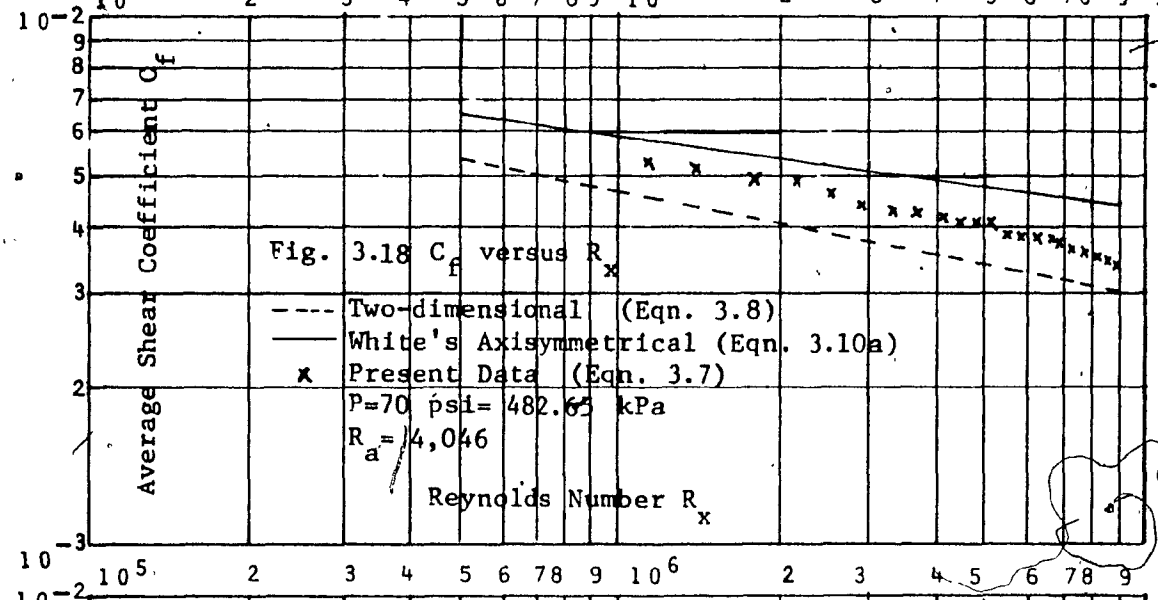

Fig. 3.18 C_f versus R_x

---- Two-dimensional (Eqn. 3.8)
——— White's Axisymmetrical (Eqn. 3.10a)
x Present Data (Eqn. 3.7)
P=70 psi= 482.65 kPa
R_a= 4,046

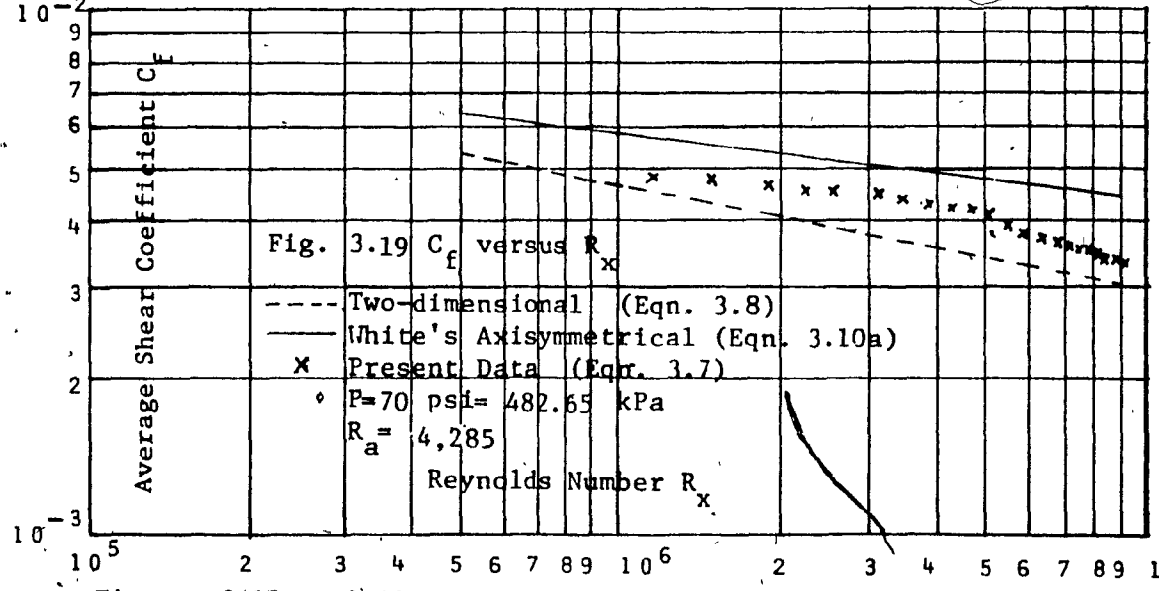

Fig. 3.19 C_f versus R_x

---- Two-dimensional (Eqn. 3.8)
——— White's Axisymmetrical (Eqn. 3.10a)
x Present Data (Eqn. 3.7)
◊ P=70 psi= 482.65 kPa
R_a= 4,285

Figures 3.17 to 3.19 C_f versus R_x with P equal to 482.65 kPa

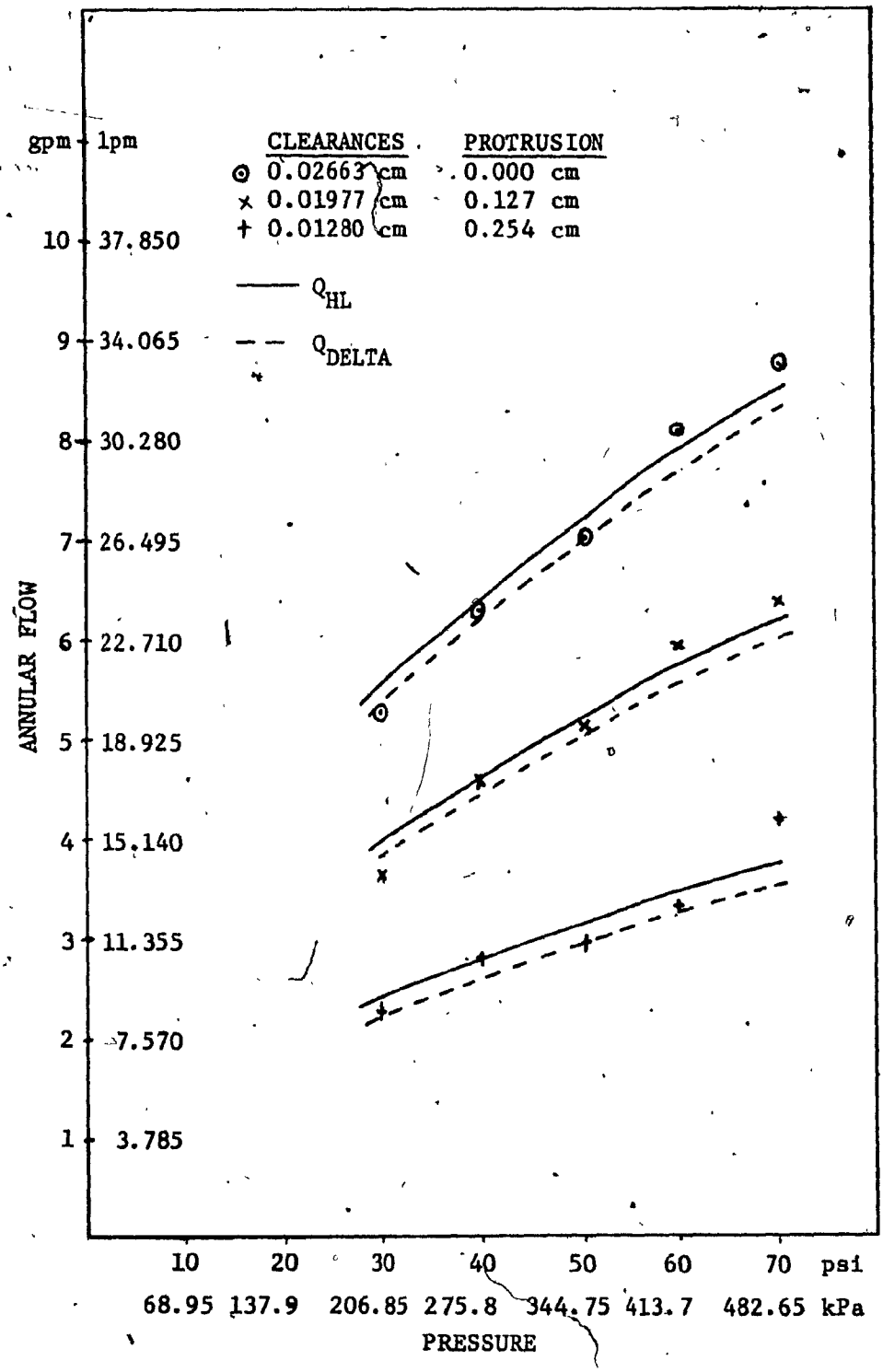

Fig. 3.20 Annular Flow versus Supply Pressure

protrusions for the same Reynolds number, R_x, but no consistent pattern to the variation could be observed that satisfied all supply pressure conditions. Although there was scattering for the points of the three protrusions, which can be partially attributed to the limitation of the accuracy of the force guage testing instrumentation utilized, the results were not affected to the extent as when the supply pressure parameter was changed.

The graphs of shear coefficient, C_f versus R_x showed that the plots of the experimentally based C_f values shifted downward with increased supply pressure. Although with increased supply pressure for the same protrusion the shear coefficient was found to decrease, it should be noted that the force increases as seen in Tables 3.2 and 3.3. As the supply pressure was increased for the same protrusion, this resulted in the flow and consequently the velocity also being increased. In Eqn. 3.7 representing the experimentally based C_f, even though the value of τ in the numerator increased, the denominator contained a velocity squared term which was the dominant factor in that equation.

As well as the experimentally based C_f from Eqn. 3.7, two theoretical curves were drawn; the two-dimensional average shear coefficient using Eqn. 3.8, and White's average axisymmetrical shear coefficient using Eqn. 3.10. For all the pressure readings, the experimentally based C_f values were greater than the two-dimensional plot. They were closer in value to White's coefficients for lower pressures while tending to the two-dimensional for higher pressure. Neither of the two theoretical plots fully represented the experimental values

as this study based on the assumption of a zero pressure gradient and only studied the transverse curvature effect. A further study to verify the experimentally based readings would have to take the pressure gradient into account.

3.5.0 DISCUSSION OF THE VARIOUS PARAMETERS AFFECTING NOZZLE PERFORMANCE

It has been previously shown in section 3.4.1 that the parameter which most substantially affects nozzle performance is the water supply pressure. This discussion centers on the effect of pressure on the other performance parameters while concentrating on the intial flow region.

3.5.1 Creation of a Air Pocket

3.5.1.a Effect of Nozzle Angle

At the end of the nozzle protrusion an air pocket exists around the initial length of thread having a diameter, a, before the annular water jet from the nozzle comes in contact with the thread. This is shown in Fig. 3.21 and 3.22. This point of contact is dependent on the angle α at which the water jet leaves the nozzle and the water pressure used. In Fig. 3.21 one can see the hypothetical case if the water jet continued at the same angle α as that leaving the nozzle and was unaffected by any external influences, then the maximum length from the end of the nozzle protrusion of the air pocket without thread would be x_{WT}. For the same conditions but having the thread would be x_T. Therefore, if these conditions existed in the real case, there would be no shear force on the thread due to the water jet for the length of thread x_T. With angle α equal to 3.1218 , the distance x_{WT} would be 1.886 cm. and

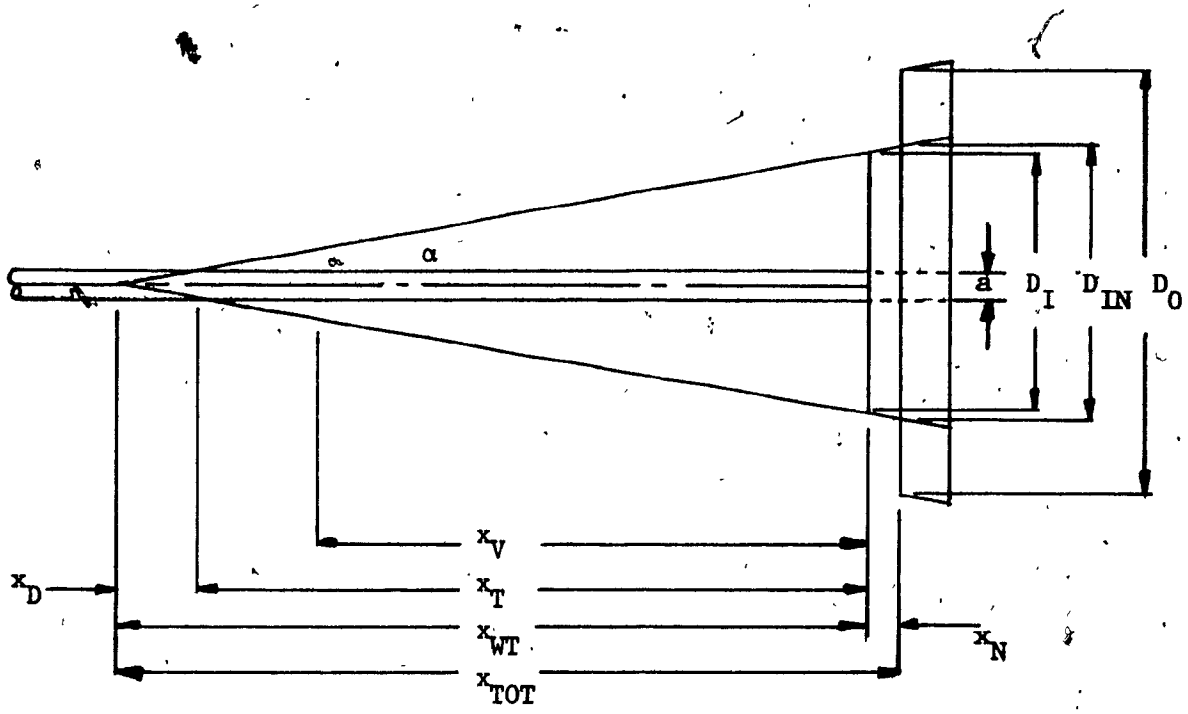

Fig. 3.21 Air Pocket Surrounding Thread

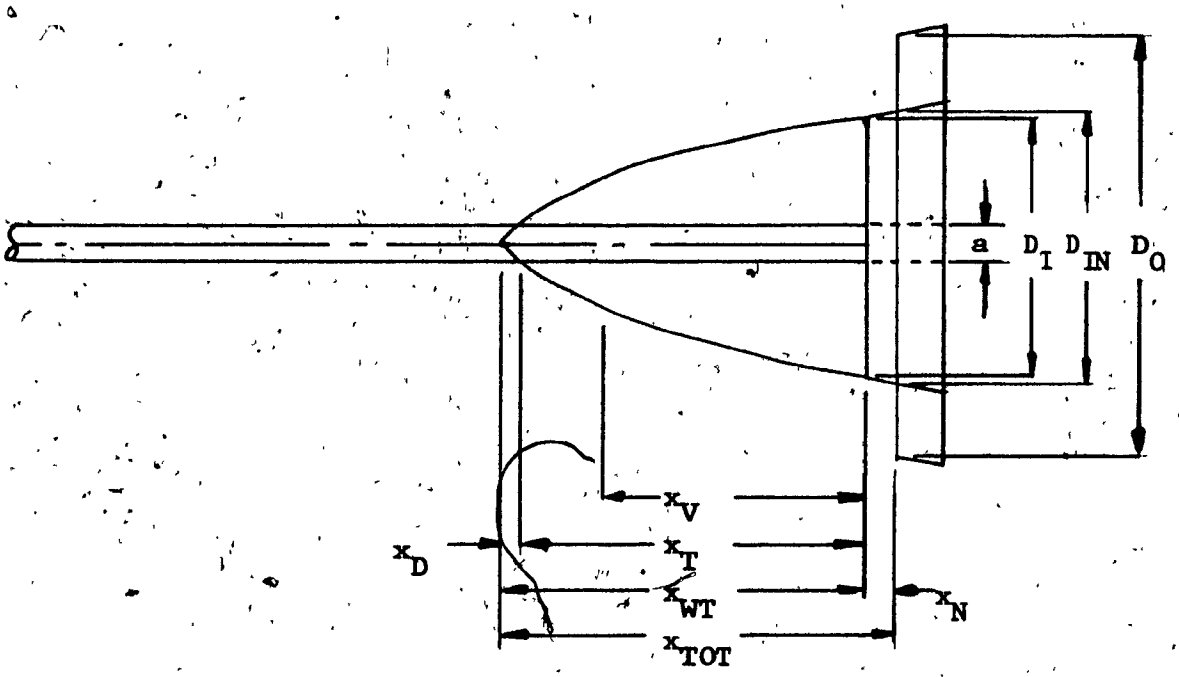

Fig. 3.22 Air Pocket Surrounding Thread At Lower Pressure

x_T would be 1.63 cm.. Experimentally, it was found that there was shear forces at thread lengths smaller than 1.27 cm., which is less than x_T in Fig. 3.21. Therefore, some external factors must exist and be taken into consideration.

3.5.1.b Effect of Water Vortices and Air Pocket Shape

In the air pocket region close to the point of contact, x_T, in Fig. 3.21 water vortices are initiated, thereby creating shear forces on the thread within that region and reducing the maximum length of the air pocket to x_V. It was experimentally noted that the size of the air pocket and therefore the point of contact of the water jet with the thread, x_T, was a function of the operating pressure. A parabolic decay with decreasing operating pressure was noted (see Fig. 3.22). The values of x_D, x_T, x_{WT}, x_{TOT}, and x_V, which are shown to be smaller in Fig. 3.22 than in Fig. 3.21, are reduced further with decreasing pressure. As the operating pressure is increased, the water jet is projected further and the size of the air pocket is increased as more air is drawn through the open central section having the diameter D_I, which runs the entire length of the nozzle.

3.5.2 Entrainment of Air

Another factor invovled is the entrainment of air across the boundaries of the annular water jet. The rate of entrainment of gases from the surroundings into a jet is due to friction and is dependent upon the density and velocity differences between the jet and its surroundings. When jet densities are made higher than those of the surrounding gases, the effects of entrainment is reduced in importance. For the present experiment, the density of the water jet, ρ_w, is signi-

ficantly greater than the density of the stationary surrounding air ρ_A.

3.5.2.a Effect of Nozzle Protrusion

The entrainment is also dependent on the nozzle protrusion. The thickness of the annular water jet is equal to the clearance, c, between the inner and outer nozzle. As the length of the protrusion, x_N, is increased, the clearance is decreased (see Appendix A.2). If the flow is maintained constant as the clearance is reduced, the water jet velocity is increased since it passes through a smaller annular area and the rate of entrainment is changed.

3.5.3 Choice of Coordinate Axis

The effect of pressure on the experimentally based shear coefficients can be partially explained through examination of the choice of the coordinate axis. The point of origin of the horizontal axis for the measurement of the thread length, x, was at the end of the nozzle protrusion. This length was used in Eqns. 3.5 and 3.7 for the experimentally based shear stress, τ, and average shear coefficient, C_f, respectively.

From Fig. 3.22 , it can be seen that if a thread of length x_v was inserted within the nozzle, there would be no force exerted by the water jet on it. Therefore, if the origin of the axis was shifted to the point where the water jet exerts a direct force on the thread, Eqn. 3.5 would be changed and the shifted shear stress would be

$$\tau_s = \frac{F}{a\,(x - x_v)} \tag{3.31}$$

Since the force, F, remains the same and the denominator is reduced, the value of τ_s would be greater than τ for the same length, x. Similarly

Eqn. 3.7 would be modified and the shifted average shear coefficient would be

$$C_{fs} = \frac{\tau_s}{\frac{\rho_w U_{jet}^2}{2}} \tag{3.32}$$

which would be greater than C_f for the same value of x at the same pressure. As discussed previously, when the supply pressre was increased, so were the values of x_v. Substituting larger values of x_v in the above equation would increase the difference between C_f and C_{fs}. This difference is therefore greater for higher supply pressures than lower ones.

When comparing the graphs for 206.85 kPa (see Fig. 3.5 to 3.7) with those for 482.65 kPa (see Fig. 3.17 to 3.19), the experimentally based C_f values shifted noticeably downward with increased supply pressure. This downward shift can be partially explained if the C_f values were replaced with those for C_{fs}. Although all the C_{fs} values would be greater than the C_f values, the higher supply pressure C_{fs} values are increased more than the lower pressure C_{fs} values. Therefore, the downward shift when comparing graphs of 206.85 kPa and 482.65 kPa would be reduced.

Although a theoretical value for x_v was not obtained, it was experimentally observed that it was less than 1.27 cm over the supply pressure range utilized. Precise experimental values of x_v could not be obtained due to the difficulty in observing exactly where the air-water interface occured due to water jet turbulence. The values of x varied from 1.27 to 30.48 cm. Therefore, in Eqn. 3.32 for the same value of x_v, the values of C_{fs} would be affected more when the values of x were

close to the values of x_v than if x was much greater than x_v. Therefore, a graph of C_{fs} versus R_x would not have the plot curving downward to the same extent at low R_x values as shown in the graphs of Fig. 3.5 to 3.19 when plotting C_f versus R_x.

3.6.0 CONCLUSIONS AND SUGGESTIONS FOR FURTHER WORK

3.6.1 Conclusions

This chapter has dealt with the experimental and theoretical analysis of shear coefficients of a thread subjected to a steady jet of water discharging from the conical annulus nozzle utilized in a shuttleless fluid jet loom. The various parameters affecting nozzle performance were examined (i.e.: consideration of changes in supply pressure, the length of nozzle protrusion, the entrainment of air by the water jet, the shape of the water jet, the point of contact of the water jet with the thread, and the water vortices created).

In the graphs of C_f versus R_x the plots of the experimentally based C_f, obtained from Eqn. 3.7, shifted downward with increased supply pressure while the force for the same protrusion increased. This can be partially explained by the dominance of the U_{jet}^2 term in Eqn. 3.7 which increased greatly with greater supply pressures.

White's axisymmetrical average shear coefficients obtained from Eqn. 3.10 were found to be closer in value to the experimentally based values than the theoretical two-dimensional values from Eqn. 3.8 for the lower supply pressures. For higher pressures the experimental C_f values tended towards the theoretical two-dimensional plot. The most influencal performance parameter was the supply pressure, with the nozzle protrusion length having only a minor effect. Therefore, the necessity of an adjustable protrusion for industrial purposes is questionable. A fixed protru-

sion length would simplify the design, thereby facilitating the production of a thread shooting conical annulus jet nozzle and importantly reducing costs per unit.

3.6.2 Suggestions For Further Work

The first additional study should take the pressure gradient into account as well as the present effect of transverse curvature discussed within this chapter. Further investigation could be directed into taking into account the velocity decay of the water jet along the length of the thread in shear coefficient calculations, retesting the effect of the protrusions with more accurate testing instrumentation to obtain optimum protrusion dimensions, and examination of the effect of modifying the nozzle angle.

Another additional study which could be performed would be with threads having different surface roughness values. Schlichting (73) has stated that for two-dimensional flow with the same R_x value, the average shear coefficient would increase in value with increasing surface roughness. For axisymmetrical flows a corresponding increase would occur. Therefore, substitution of a rough thread would increase the values of the average shear coefficients which were obtained in the present experiments which used a smooth thread. A series of tests with various threads utilized in the textile industry could be performed.

GENERAL CONCLUSIONS

The previous axisymmetrical studies for the law of the wall were classified according to six hypotheses. The first reported hypothesis, based on the assumption of a power law velocity profile, has long been abandoned due to limited Reynolds number range application and its inaccuracy. Of the remaining five modern hypotheses, three (the two-dimensional, the streamline, and derivative) can be recommended for application only if the radius, a, is large and for smaller values of y/a. The local similarity and Rao's hypotheses have been found superior to the preceeding three in describing the experimental profiles for the entire range of values of a and y/a examined. All the hypotheses have been found inaccurate in predicting the velocity distribution in comparision with experimental results for low values of a . Patel (24) postulated that this was the result of relaminarsation of the turbulent boundary layer due to transverse curvature effects and proposed a a^+ value of approximately 28. Rao and Keshaven (20) suggested that relaminarisation occured for R_a values less than 15,000.

The previous axisymmetrical studies for the velocity defect laws were classified according to four hypotheses. Three (Chin et al's (11), Yu's(10), and Afzal et al's (12)) are based on modification of the classical two-dimensional velocity defect law with respect to variation in empirical constants, B_1 and B_2. All three had B_2 constants dependent on the cylinder radius, in terms of a, R_a, and δ /a respectively. Each method's velocity defect plots in two-dimensional coordinates of $(U-u)/u_*$ versus y/δ coincided closely with experimental results, with the only difference being that of presentation. In the

fourth approach, Rao and Keshaven (20) found that the velocity defect plots with the two-dimensional coordinates did not reveal any similarity for their experimental data. Their data did not collapse into a single curve for the same R_a and δ/a values. Afzal and Narasimha (12) attributed the discrepency to the slow recovery of the boundary layer from the tripping devices used, which invalidated the experimental results at the initial data reading stations. When Rao and Keshaven (20) plotted the velocity defect against a local Reynolds number, r_*, similarity was found for each individual value of R_a. Agreement exists between the various reports that the traditional division of the mean flow properties into wall and wake regions may be invalid when there is a large transverse curvature effect, for conditions where a is very small or δ/a is extremely large. Presently there is insufficient documented data to specific exact a and δ/a transition point values where the traditional division ceases to hold.

Experimentally based axisymmetrical shear coefficients were obtained for a circular thread subjected to a series of tests with a steady jet of water discharging from a conical annular nozzle. For the same R_x, the Reynolds number based on thread length, the experimentally based axisymmetrical shear coefficients decreased in value for increasing supply pressure but still remained greater in value than the two-dimensional average shear coefficients. White's (21) theoretical axisymmetrical average shear coefficient represented the experimentally based coefficients more closely for the tests at the lower supply pressures. At the higher pressures and the resulting higher values of R_a, the Reynolds number based on the cylinder radius,

the experimentally based coefficients tended towards the theoretical two-dimensional coefficient values. With the exception of one data point, the experimental average exit velocity at the end of the conical annular nozzle varied by less than 10% from the theoretical values obtained using an integral momentum method and a macroscopic energy balance method. The major parameter affecting nozzle performance was found to be the supply pressure.

BIBLIOGRAPHY

1. Deissler, R.G., "Investigation of Turbulent Flow and Heat Transfer In Smooth Tubes, Including the Effects of Variable Fluid Properties ". Trans. of the ASME, Feb. 1951, pp. 101-107.

2. Driest, E.R. Van, "On Turbulent Flow Near a Wall". Journal of the Aeronautical Sciences, Nov. 1956, pp. 1007-1011.

3. Patel, V.C., "A Unified View of the Law of the Wall Using Mixing Length Theory". Aeronautical Quaterly, Aug. 1976, pp. 217-228.

4. Millikan, C.B., "The Boundary Layer and Skin Friction for a Figure of Revolution". Journal of Applied Mechanics, Trans. of ASME, Vol. 54, 1932, pp. 29-43.

5. Landweber, L., "Effect of Transverse Curvature on Frictional Resistance". David Taylor Model Bain Report No. 689, Mar. 1949.

6. Eckert, H.V., "Simplified Treatment of the Turbulent Boundary Layer Along a Cylinder In Compressible Flow". Journal of Aeronautical Sciences, Jan. 1952, pp. 23-38.

7. Karhan, K., "The Axial Frictional Resistance of Long Cylinders In Turbulent Flow". Journal of Ship Research, Vol. 4, Oct. 1959, pp. 24-28.

8. Sakiadis, B.C., "Boundary Layer Behaviour on Continuous Solid Surfaces: III. The Boundary Layer on a Continuous Cylindrical Surface" . AIChE Journal, Vol.7, No. 3, 1961, pp. 467-470.

9. Chase, D.M., "Mean Velocity Profile of a Thick Turbulent Boundary Layer Along a Circular Cylinder". AIAA Journal, Vol. 10, July 1972, pp. 849-850.

10. Yu, Y.S., "Effect of Transverse Curvature on Turbulent Boundary Layer Characteristics". Journal of Ship Research, Vol. 3, 1958, p. 33.

11. Chin, Y.T., Hulesbos, J. and Hunnicult, G.H., 1967 Proc. Heat & Mass Transfer Fluid Mech. Inst..

12. Afzal, N. and Narasimha, R., "Axisymmetric Turbulent Boundary Layer Along a Circular Cylinder At Constant Pressure". Journal of Fluid Mechanics, Vol. 74, 1976, pp. 113-128.

13. Afzal, N. and Singh, K.P., "Measurements in an Axisymmetric Turbulent Boundary Layer Along a Circular Cylinder". Aeronautical Quaterly, Aug. 1976, pp.217-228.

14. Willmarth, W.W., Winkel, R.E. and Sharma, L.K. and Bogav, T.J., " Axially Symmetric Turbulent Boundary Layers on Cylinders: Mean

Velocity Profiles and Wall Pressure Fluctuations". Journal of Fluid Mechanics, Vol. 76, Part 1, 1976, pp. 35-64.

15. Richmond, R.L., "Experimental Investigation of Thick Axially Symmetric Boundary Layers on Cylinders at Subsonic and Hypersonic Speeds". Ph.D. Thesis, Calif. Inst. of Technology, 1957.

16. Yasuhara, M., "Experiments of Axisymmetric Boundary Layers Along a Cylinder In Incompressible Flow". Trans. Japan Society of Aerospace Sciences, Vol. 2, 1959, pp. 33-38.

17. Willmarth, W.W. and Yang, C.S., "Wall Pressure Fluctuations Beneath Turbulent Boundary Layers on a Flat Plate and a Cylinder". Journal of Fluid Mechanics, Vol. 41, Part 1, 1970, pp. 47-80.

18. Huffman, G.D. and Bradshaw, P., "A Note on Von Karman's Constant In Low Reynolds Number Turbulent Flows". Journal of Fluid Mechanics, Vol. 53, Part 1, pp. 45-60.

19. Rao, G.N.V., "The Law of the Wall in a Thick Axisymmetric Turbulent Boundary Layer". Journal of Applied Mechanics, Mar. 1967, pp. 237-238.

20. Rao, G.N.V., and Keshaven, N.R., "Axisymmetric Turbulent Boundary Layers in Zero Pressure Gradient Flow". Journal of Applied Mechanics, Trans. of the ASME, Vol. 94, 1972, pp. 25-32.

21. White, F.M., "An Analysis of Axisymmetric Turbulent Flow Past a Long Cylinder". Journal of Basic Engineering, Trans. of the ASME, Mar. 1972, pp. 200-206.

22. White, F.M., Lessmann, R.C. and Christoph, G.H., "Analysis of Turbulent Skin Friction on Thick Axisymmetric Boundary Layers". AIAA Journal, Vol. 11, No. 6, June 1973, pp. 821-825.

23. Chase, D.M., "Reply to Author to P. Bradshaw and V.C. Patel". AIAA Journal, Vol. 11, No. 6, June 1973, pp. 894-895.

24. Patel, V.C., "A Unifified View of the Law of the Wall Using Mixing Length Theory". Aeronautical Quaterly, Feb. 1973, pp. 55-70.

25. Patel, V.C. and Bradshaw, P., "Comment on Mean Velocity Profile of Thick Turbulent Boundary Layer Along a Circular Cylinder". AIAA Journal, June 1973, pp. 893-895.

26. Sparrow, E.M., Eckert, E.R.G. and Minkowyez, W.J., "Heat Transfer and Skin Friction for Turbulent Boundary Layer Flow Longitudinal to a Circular Cylinder". Journal of Applied Mechanics, Trans. of the ASME, Mar. 1963, pp. 37-43.

27. Ginevski, A.S. and Solodkin, E.E., "The Effect of Lateral Surface Curvature on the Characteristics of Axially Symmetric Turbulent Boundary Layers". Journal of Applied Mathematics and Mechanics,

Vol. 22, 1958, pp. 1168-1179.

28. Cebeci, T., "Laminar and Turbulent Incompressible Boundary Layer on Slender Bodies of Revolutions in Axial Flow". Journal of Basic Engineering, Trans. of the ASME, Sept. 1970, pp. 545-554.

29. Reichardt, H.Z., Zeitschrift Math. & Mech., Vol. 31, 1951, p. 208.

30. Laufer, J., Natl. Adviory Comm. Aeronaut. Tech. Report 1174, 1954.

31. Stokes, G., "On the Effect of the Internal Friction of Fluids on the Motion of Pendulums". Trans. Cambridge Philos. Soc., Vol. 9, 1851.

32. Coles, D.E., Rand Corp. Report R-403-PR, 1962.

33. Townsend, A.A., "Equilibrium Layers and Wall Turbulence", Journal of Fluid Mechanics, Vol. 11, 1961, pp. 97-120.

34. Rao, G.N.V., "Comment on Mean Velocity Prpfile of a Thick Turbulent Boundary Layer Along a Circular Cylinder". AIAA Journal, Vol. 12, No. 4, 1974, pp. 574-575.

35. Cebeci, T., "Eddy Viscosity Distribution in Thick Axisymmetric Turbulent Boundary Layers". J. Fluids Eng., Vol. 95, pp. 319-326.

36. Cebeci, T. and Mosinskis, G.J., Proc. ASME Space Technology and Heat Transfer Conference, Part 2, 1970.

37. Patel, V.C. and Head, M.R., "Reversion of Turbulent to Laminar Flow ". Journal of Fluid Mechanics, Vol. 34, 1968, p. 371.

38. Rao, G.N.V., "Hydrodynamic Stability of a Laminar Boundary Layer with Tranverse Curvature Effect". Zeitschrift fur angewandte Mathematik and Mechanik, Vol. 47, 1967, p. 427.

39. Glauret, M.B. and Lighthill, M.J., "Axisymmetric Boundary Layer on a Long Thin Cylinder". Proc. Roy. Soc. A203, 1955, p. 188.

40. Willmarth, W.W., "Structure of Turbulence in Boundary Layers". Adv. Appl. Mech., Vol.15, 1975, p. 159.

41. Simpson, R.L., "Characteristics of Turbulent Boundary Layers at Low Reynolds Numbers With and Without Transpiration". Journal of Fluid Mechanics, Vol. 42, 1970, pp.769-802.

42. Herring, H.J. and Mellor, G.L., NASA Contractor Report CR-1144, 1968.

43. Kline, S.J., Reynolds, W.C., Schraub, F.A. and Runstadler, P.W., Journal of Fluid Mechanics, Vol. 30, 1967, p. 741.

44. Gupta, A.K., Laufer, J., and Kaplan, R.E., Journal of Fluid Mechanics, Vol. 50, 1971, p.193.

45. Coles, D., "The Law of the Wake in the Turbulent Boundary Layer". Journal of Fluid Mech., 1956, Vol. 1, pp. 191-226.

46. Cebeci, T., and Smith, A.M.O., "Analysis of Turbulent Boundary Layers". Academic Press Inc., New York, 1974.

47. Daily, J.W., and Harleman, D.R.F., "Fluid Dynamics" . Addison-Wesley Publishing Company Inc., 1966.

48. Hinze, J.O., "Turbulence". McGraw-Hill Book Company, 1959.

49. Bushnell, D.M., and Morris, D.J., "Shear-Stress, Eddy-Viscosity, and Mixing-Length Distributions in Hypersonic Turbulent Boundary Layers". NASA TMX-2310, Aug. 1971.

50. Cebeci, T., and Mosinskis, G.J., "Computations of Incompressible Turbulent Boundary Layer at Low Reynolds Numbers". AIAA Journal, Vol. 9, No. 8, Aug. 1971, pp. 1632-1634.

51. Cebeci, T., "Kinematic Eddy Viscosity at Low Reynolds Number". AIAA Journal, Vol. 11, No. 1, Jan. 1973, pp. 102-104.

52. Kwok, C.K., and Lee, P.M., "A Simple Method for Calculating the Turbulent Jet Velocity in a Conical Annulus". Journal of Fluids Engineering, Transaction ASME, Dec. 1976.

53. Bernard, Q., "Design and Application of Shuttleless Weaving Machines", 14th Canadian Textile Seminar, May 1974.

54. Suchy, L., "A Weft Yarn Filling Arrangement for Fluid Jet Loom". FCC Internal Report, Concordia University, Montreal, 1976.

55. Brighton, J.A., and Jones, J.B., "Fully-Developed Turbulent Flow In Annuli", Journal of Basic Engineering, Transaction ASME, Series D, Vol. 88, No. 2, Dec. 1964, pp. 835-844.

56. Fredrickson, A.G., and Bird, R.B., "Friction Factors in Non-Newtonian Annular Flow". Industrial and Engineering Chemistry, Vol. 50, 1958, p. 1599.

57. Okiishi, T.H., and Servoy, G.K., "An Experimental Study of the Turbulent Flow Boundary Layer Development in Smooth Annuli". Journal of Basic Engineering, Tranaction ASME' Dec. 1967, pp.823-836.

58. Rothfus, R.R., "Isothermal Skin Friction in Flow Through Annular Section". Industrial and Engineering Chemistry, Vol. 47, 1945.

59. Rothfus, R.R., "Velocity Distribution and Fluid Friction in Concen

tric Annuli", Ph.D. Thesis, Caregie Institute of Technology, 1948.

60. Sparrow, E.M., and Lin, S.H., "The Developing Laminar Flow and Pressure Drop in the Entrance Region of Annular Ducts". Journal of Basic Engineering, Transaction ASME, Dec. 1964, pp. 827-834.

61. Kempf, G., "Flachenwiderstand". Werft-ReedereiHafen, 1924, pp. 521-528.

62. Telfer, E.V., "Frictional Resistance and Ship Similarity". TINA, Vol. 92, 1950, p. 1.

63. Hughes, G., "Friction and Form Resistance in Turbulent Flow and a Proposed Formulation for Use in Model and Ship Correlation". Trans. of the Institute of Naval Architects, Vol. 96, 1954, p. 314.

64. Selwood, A., "The Axial Drag of Monofilaments". Letters to the Editor, Trans. of the Journal of the Textile Industry, Vol. 9, 1962, p. 20.

65. Landweber, L., and Siao, T.T., Journal of Ship Research, Vol. 2, 1958, p. 52.

66. Patel, V.C., Journal of Fluid Mechanics, 1965, Vol. 23, p. 185.

67. Head, M.R., Entrainment in the Turbulent Boundary Layers, ARC R and M Report 3152, 1958.

68. Patel, V.C., A Simple Integral Method for the Calculation of Thick Axisymmetric Turbulent Boundary Layers, Aeronautical Quaterly, Feb. 1974, pp. 47-58.

69. Shanebrook, J.R., and Summer, W.J., "Entrainment Theory for Axisymmetric Turbulent Incompressible Boundary Layers, Journal of Hydronautics, Vol. 4, 1970, p. 159.

70. Clauser, F.H., "The Turbulent Boundary Layers", Advances in Applied Mechanics, Vol. 4, 1956, p. 1.

71. Prandtl, L., "Essentials of Fluid Dynamics". Blackie and Son Ltd., 1954, pp. 105-145.

72. Streeter, V.L., and Wylie, E.B., "Fluid Mechanics". Sixth Edition, McGraw-Hill Book Company, 1975.

73. Schlichting, H., "Boundary Layer Theory", McGraw-Hill Book Company Inc., 1968, pp. 610-611.

APPENDIX A CALCULATION OF ANGLE α

In Fig. 3.21

$$\frac{D_I}{2} = 0.0405 \text{ in.} = 0.10287 \text{ cm} \tag{A.1}$$

$$\frac{D_O}{2} = 0.0510 \text{ in.} = 0.12954 \text{ cm} \tag{A.2}$$

When $\frac{D_{IN}}{2}$ equals $\frac{D_O}{2}$, then x_N is at x_{Nmax}

If $\alpha = 3^o$ as in the specifications of the nozzle and $x_N = x_{Nmax}$

Therefore,

$$\tan\alpha = \frac{D_{IN}}{2x_{TOT}} = \frac{D_O}{2x_{TOT}} \tag{A.3}$$

$$x_{TOT} = \frac{D_O}{2\tan\alpha} \tag{A.4}$$

$$x_{WT} = \frac{D_I}{2\tan\alpha} \tag{A.5}$$

$$x_{Nmax} = x_{TOT} - x_{WT} = \frac{D_O - D_I}{2\tan\alpha} = \frac{0.12954 - 0.10287}{\tan 3^o} = 0.5089 \text{ cm} \tag{A.6}$$

but experimentally x_{Nmax} was measured to be 0.1925in.= 0.48895 cm

Therefore,

$$\tan\alpha = \frac{D_O - D_I}{x_{Nmax}} = \frac{0.12954 - 0.10287}{0.48895} = 0.05454 \tag{A.7}$$

$$\alpha = 3.1218^o$$

APPENDIX B CALCULATION OF CLEARANCE c

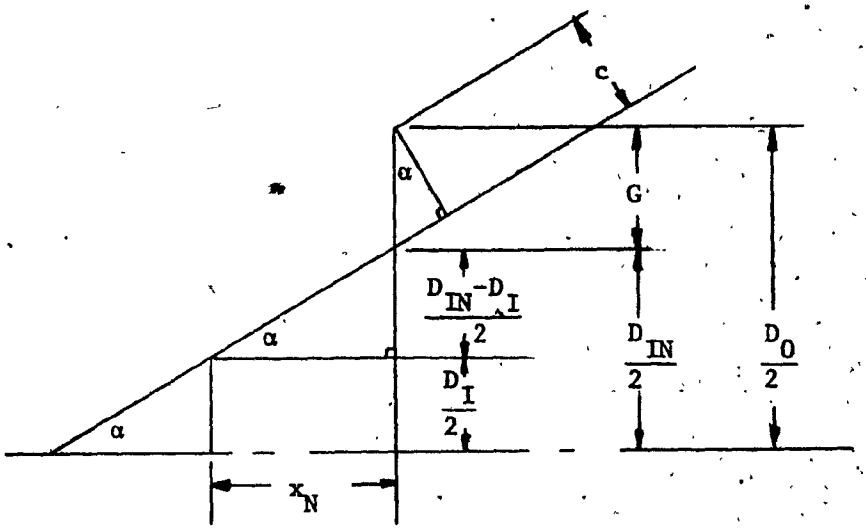

Fig. B.1 Protrusion-Clearance Relationships

$$\tan\alpha = \frac{D_{IN} - D_I}{2x_N} \qquad (B.1)$$

$$\frac{D_{IN}}{2} = x_N \tan\alpha + \frac{D_I}{2} \qquad (B.2)$$

$$G = \frac{D_O - D_{IN}}{2} \qquad (B.3)$$

$$\cos\alpha = \frac{c}{G} \qquad (B.4)$$

$$c = G\cos\alpha \qquad (B.5)$$

APPENDIX C CALCULATION OF D_H

In Fig. 3.2

$$D_H = 4\left(\frac{\text{cross-sectional flow area}}{\text{wetted perimeter}}\right) \qquad (C.1)$$

$$D_H = 4\,\frac{\frac{\pi}{2}(D_1\ D_1\ 2c\ \cos\alpha)c}{\pi(D_1\ D_1\ 2c\ \cos\alpha)} \qquad (C.2)$$

$$D_H = 2c \qquad (C.3)$$